Mineralogical, geochemical and palaeoclimatic characterisation of the Thar desert playas, Rajasthan (India)

Zur Erlangung des akademischen Grades eines
Doktors der Naturwissenschaften
an der Fakultät für Bauingenieur-, Geo- und Umweltwissenschaften
der
Universität Karlsruhe
vorgelegte
DISSERTATION

von

Priyadarsi Debajyoti Roy

aus Rourkela/Sundargarh (Orissa)

2003

Tag der mündlichen Prüfung: 04. 02. 2004
Referent: Prof. Dr. Werner Smykatz-Kloss
Korreferent: Prof. Dr. Udo Haack

Hiermit bestätige ich, dass ich die vorliegende Arbeit selbstständig angefertigt habe und nur die angegebenen Hilfsmittel verwendet habe

Priyadarsi Debajyoti Roy

Acknowledgements

I am grateful to my supervisor Prof. Dr. Werner Smykatz-Kloss, for giving me the opportunity to do this Ph.D study at Institut für Mineralogie und Geochemie, Universität Karlsruhe. His vast experience of the subject, valuable guidance and suggestions were the key in improving the quality of this research. He was completely involved in my Ph.D project, starting from its formulation, field works to finally its completion. His company in the field was very helpful in understanding some of minor details of the playas and desert morphology. I am thankful to him for providing me all the necessary facilities for geochemical and mineralogical investigations. I am thankful to Prof. Dr. Udo Haack of Institut für Geowissenschaften und Lithosphärenforschung, Universität Gießen, for accepting to be my 2nd examiner and providing some of his valuable time to review my work. The financial help from Landesgraduiertenförderung (Universität Karlsruhe) is generously acknowledged. I would like to thank the scientists (Dr. Utz Kramar, Dr. Georg Istrate, Dr. Ekkehard Karotke), technical assistants (Mrs. Claudia Mößner, Miss Gesine Preuß, Mrs. Beate Oetzel, Mr. Kristian Nikoloski, Mr. Predrag Zrinjscak) and secretaries (Mrs. Bender, Mrs. Tannhäuser, Mrs. Nytz) of Institut für Mineralogie und Geochemie, for their scientific and official help during my stay here. The cooperation from Dr. Nilesh Bhatt of Baroda University (India) during the filed visit is thankfully acknowledged. The moral and scientific support from my friends (Prasanjit Dash, Frederic Pujol, Katharina Knabe, Kirstin Fuhlberg, Birgit Scheibner) was very helpful during the final stages of thesis writing. For this study some of the data are taken from Indian Institute of Meteorology (Pune), Indian Meteorological Division (Delhi), USGS and NASA (USA). Finally, I would like to thank my family, whose prayers and blessings always strengthened my confidence and make me capable to complete the work smoothly.

This dissertation is dedicated to my friend and brother late Mr.Vinay Chauhan, who died in an accident on 1st of January, 2004.

List of contents

1. Introduction

Population on the earth is increasing dramatically. The need of land for living and agriculture is also growing. The only possibility for land expansion is to offer the regions with low or no population and make them suitable for agriculture and living. These are the steppes or (semi) deserts, where nature makes the cultivation and existence of civilisation difficult. Deserts are the regions very sensitive to climatic and ecological changes. The studies and understanding of the (hydro) geology and (palaeo) ecology of the arid regions are the principal keys for preventing the processes of desertification and for improving the quality and quantity of desert soils and regional water resources. Morphological and sedimentological features indicate that the deserts of the world have experienced significant episodic expansions and contractions during the Quaternary period. The geological records further show that the positions of deserts have changed in response to major global tectonics and climatic developments throughout the history of the earth. Various criteria may be used to identify sediment with a former arid zone origin. The utility of these criteria is dependent upon the application of results from studies of today's arid zone phenomena. The sedimentological record of arid zone expansion and contraction is often complemented by different morphological evidences (fossil sand dunes, alluvial fans and saline lakes).

A number of geoscientific studies have been focused on the saline lakes and their hydrogeochemical evolutions (Eugster, 1970; Hardie & Eugster, 1970; Lerman, 1970; Eugster & Jones, 1979; Rettig et al., 1980), on sedimentology (Last, 1983; Ordo´nez et al., 1991; Schreiber et al., 1998; Rouchy et al., 2001), on geology (Ordo´nez & Es Garciá Del Cura, 1994; Mayayo et al., 1996; Ingles et al., 1998), and on the deposits of evaporites and their mineralogical and (isotope) geochemical characterisation (Longmore et al., 1986; Risacher & Fritz, 1991; Möller & Bau, 1993; Camur & Mutlu, 1996; Liu et al., 1997; Ingebritsen et al., 1998; Volkova, 1998; Dutkiewicz et al., 2000). Several geomorphologists and other geoscientists tried to reconstruct the palaeoclimate and palaeoecology of arid regions e.g., Thomas, 1997; Magee & Miller, 1998; Schütt, 1998, 2000; Giralt et al., 1999; Reinhardt & Ricken, 2000; Abbott et al., 2003; Grosjean et al., 2003; Eitel et al., 2003; Felix-Henningsen, 2003; Heine, 2003; Rögner et al., 2003; Leuschner et al., 2003; Smykatz-Kloss et al., 2003. But there is still a great scope for further mineralogical and geochemical research in deserts.

The (semi-) arid zone of the north-western Indian sub-continent, the *Thar desert*, stretches from the flood plains of the perennial Indus river in the west to the Aravalli mountains in the east. A major part of the desert is situated in the north-western Indian state of Rajasthan. The climate of this region is neither identical to, nor as harsh as climate of other arid belts occurring in the same lattitude, such as northern Arabia, parts of Egypt, Sahara and parts of Mexico (Mensching, 1979; Kajale & Deotare, 1997). The climate of the region is witness of the dynamics of the south-western monsoon, which is the only source of the rainfall of the region and affects the economy in the sub-continent. The presence of closed basins and their associated salt deposits (Wasson et al., 1984) situated more specifically to the western side of the Aravalli mountain range, fossilised sand dunes (Dhir et al., 1992) in the relatively humid parts, and dramatic shifting of the perennial rivers once flowing through the region (Bakliwal & Grover, 1999), act as indicators of the climatic changes in the region. The saline lakes of the region are economically important, as thousands of tons of salts are produced from evaporation of the brine (e.g., brines from Sambhar, Didwana and Pachapadra playas). The lakes vary in size from tens of square meters (occurring in the inter-dunal corridors) to hundreds of square km (tectonic basins). But all of them are very shallow (<1 m average depth) and mostly dry, so they are named as palaeo or playa lakes. The physical and chemical evolution of these lakes have been studied since few decades (Godbole, 1952; Bhattacharya et al., 1982; Kar, 1990; Ramesh et al., 1993; Yadav, 1997; Roy, 1999). The studies led to a number of theories regarding the origin of the playas. Recently, the Holocene and late Pleistocene south-western monsoon has been reconstructed using organic rich black layers from deep sea (Rossignol-Strick et al., 1998), continental deposits (Khadkikar et al., 1999), Himalayan ice core (Thompson et al., 2000), stalagmite records in caves (Wang et al., 2001), ice cores from Tibetan plateau (Shi et al., 2001), and the terrigenous material from Indian ocean (Anderson et al., 2002; Gupta et al., 2003). The sediments deposited on the lake floors show Pleistocene stratigraphy, with alternations of aeolian, fluvial, and hypersaline lacustrine material. Though the origin of the Thar desert is relatively unknown, the pioneering works of Singh et al. (1990) on palynology, Wasson et al. (1984) and Enzel et al. (1999) on mineralogy and geochemistry of the two eastern lakes (e.g. Didwana and Kuchaman) give some insight in to the Holocene climatic change of one part of the region.

The aim of the present study is to reconstruct the mineralogical and geochemical evolution of the different parts of the Thar desert, depending on the (palaeo-) climatic differences and changes.

In detail the objectives of the study are outlined as follows:

1. The detailed mineralogical and (isotope) geochemical composition of the sediments of the different playas, of the evaporites as well as of the detrital components, and down to a depth of few meters.

2. The hydrogeochemical composition of the saline waters of the playa surface and shallow depths.

3. The chemical and mineralogical characterisation and differentiation between the eastern and western part of the Thar desert.

4. The determination of the source of the saline and detrital material.

5. The reconstruction of the palaeo-ecology (climate) of the region and the outlining of the systematics of the regional desertification process.

To obtain these objectives, the sediments of ten playas, five from the semi-arid to semi-humid steppe region at the eastern margin (e.g., Sambhar, Phulera, Sargot, Kuchaman, and Didwana playas) and five from the arid region of the west (e.g., Bap-Malar, Pokhran, Pachapadra, That and Thob playas) and waters from three playas have been studied. The investigations have been made by X-ray diffraction, X-ray fluorescence, electron microprobe analysis, thermal analysis, carbon analyser, ion chromatography, and inductively coupled plasma mass spectrometric methods respectively.

2. Previous work

The first report on the (semi-) arid Thar region and the presence of the saline lakes was given by Humes (1867-1868). Later, Holland and Christie (1909) published a hydrological study of some surface and rain waters in and around the Pachapadra playa and concluded that the salinity of the region was caused by aeolian processes and the salts were transported by the south-western winds from the Rann of Kutch. But this hypothesis could not explain the diversity of the composition of the evaporites of the different playas. The existence of a real fresh water lake (e.g., Pushkar) between several saline lakes convinced Godbole (1952) to reject the hypothesis of Holland and Christie. On the contrary, Godbole (1972) thought the saline lakes being relicts of the former Tethys sea. He interpreted the hydrogeochemical differences between several lakes as being due to biochemical activity of algae and bacteria. Saxena and Seshadri (1966) related the salinity of the Thar playa lakes to sub-surface percolation of saline waters from the elevated Indo-Gangetic plains from the north-western part of India. Khandelwal (1975) and Bhattacharya (1982) saw the origin of the saline waters in a sub-surface halite bed. The Precambrian metamorphic terrain forming the basement of the playas and absence of any saline horizon in the deep bore holes ruled out both the theories (Godbole, 1972).

The later investigations on the chemical evolution of the playa lakes mainly confined to geochemical and mineralogical studies of the larger and economically important lakes like Sambhar and Didwana (Misra, 1982; Sinha & Raymahashay, 2000; Roy et al., 2001). Rai & Absar (1996) found high silica and boron contents and their inverse behaviour with halogenide anions (Cl^-) in the waters of Kuchaman and Sargot. They interpretated these relationship as indicator of hydrothermal contributions to the lake water. Ramesh et al. (1993) measured the stable isotopes of fresh and saline waters of the region. They discarded the "Tethys relict" theory of Godbole (1972) and explained the playas as being hydrologically closed basins, where evaporation during the summer months compensates the inflow of the monsoon season. Yadav (1997) studied the evolution of oxygen isotope composition during a complete (annual) cycle of precipitation and evaporation in the Sambhar lake (playa).

The physical evolution of the playas, in this part of the world, sustained the curiosity of the investigators for more than one century. Some of the workers reported the presence of a dynamic fluvial system in the region before the onset of aridity, which later blocked the

course of the rivers and led to the formation of the playas (Singh et al., 1972; Biswas et al., 1982). The theories explaining the formation of saline lakes range from aeolian erosion of rocky terrains creating depressions (Kar, 1989; Kar, 1993; Roy, 1999), to segmentation of palaeo-channels by sand dunes and excessive siltation at the confluence (Agarwal, 1957), to the stream trap theory of Kar (1990), which explains the longitudinal dunes guiding the streams flowing away to feed the basins forming in between. The main theories explaining the physical evolution of the playas are summarised in Table 1.

Table 1 Theories explaining the physical evolution of Thar playas

Theory	Features	Example (playas)	References
Deflation of sand bodies	local depressions in underlying limestones, caused by wind erosion	playas of the Jaisalmer region	Kar, 1989; Kar, 1993
Segmentation of palaeochannels	transverse barriers formed by (a) mobile dunes (b) excessive siltation at river confluences	(a) Kharari rann, Kanod rann, Khara rann and Mitha rann (b) Pachapadra	(a) Agarwal, 1957; Singhvi & Kar, 1992 (b) Ghosh, 1964, 1965; Ghosh et al., 1977
Stream trap	formation of saline lakes between parallel (longitudinal) dunes	Didwana and Degana	Kar, 1990
Tectonism	(a) tectonic formations of lineaments, horst and grabens (b) pull-apart structures due to strike-slip faulting	(a) Pokhran, Didwana, Kuchaman, Sargot, Chapar and Lunkaransar (b) Sambhar	(a) Sinha-Roy, 1986; Roy, 1999 (b) Roy, 1999

The eastern playas, Sambhar, Didwana, and Lunkaransar have been investigated for palynology and isotope geochemistry, including some C^{14} and OSL dating (Singh et al., 1972, 1974, 1990; Wasson et al., 1984; Kajale & Deotare, 1997; Deotare et al., 1998; Enzel et al., 1999). Sedimentological studies were made at the playas of Kuchaman (Rai & Sinha, 1990), Pokhran (Rai, 1990) and Sambhar (Sundaram & Pareek, 1995). Based on the pollen analysis, sedimentological, geochemical and mineralogical data a fairly clear palaeo-climatic history of the region is emerging. A hyper-saline (arid) condition (19,000 yr to 10,000 yr B.P.) was followed by a fluctuating phase till 6,000 yr B.P. An increased precipitation during next 1,500 to 2,000 yr led to the intermittent filling of the lakes. Aridity set in around 5,500 yr B.P. in the

western arid core (Bap-Malar, Kanod), around 4,800 yr B.P. in the north-western desert margin (Lunkaransar) and finally around 3,000 yr B.P in the eastern desert margin (Didwana, Sambhar). The laminated sediments of Arabian Sea off Pakistan and other tropical and sub-tropical belts of Africa, as well as Middle East have also recorded the same humid phase from 5,000 yr B.P. to 3,000 yr B.P. (Lückge et al., 2001). But they divided this humid phase into a phase of strong summer and a phase of strong winter monsoon. The phase between 5,000 yr B.P. and 3,900 yr B.P. was a phase of strong summer monsoon and the next phase up to 3,000 yr B.P. was recognised as a strong winter monsoon phase. A summarised overview of the palaeoclimatic interpretations of these authors is given in Table 2 (a & b).

Table 2 Palaeoclimatic developement of some Thar playas

(a) after Singh et al., 1972 [1], Wasson et al., 1984 [2], and Rai & Sinha, 1990 [3].

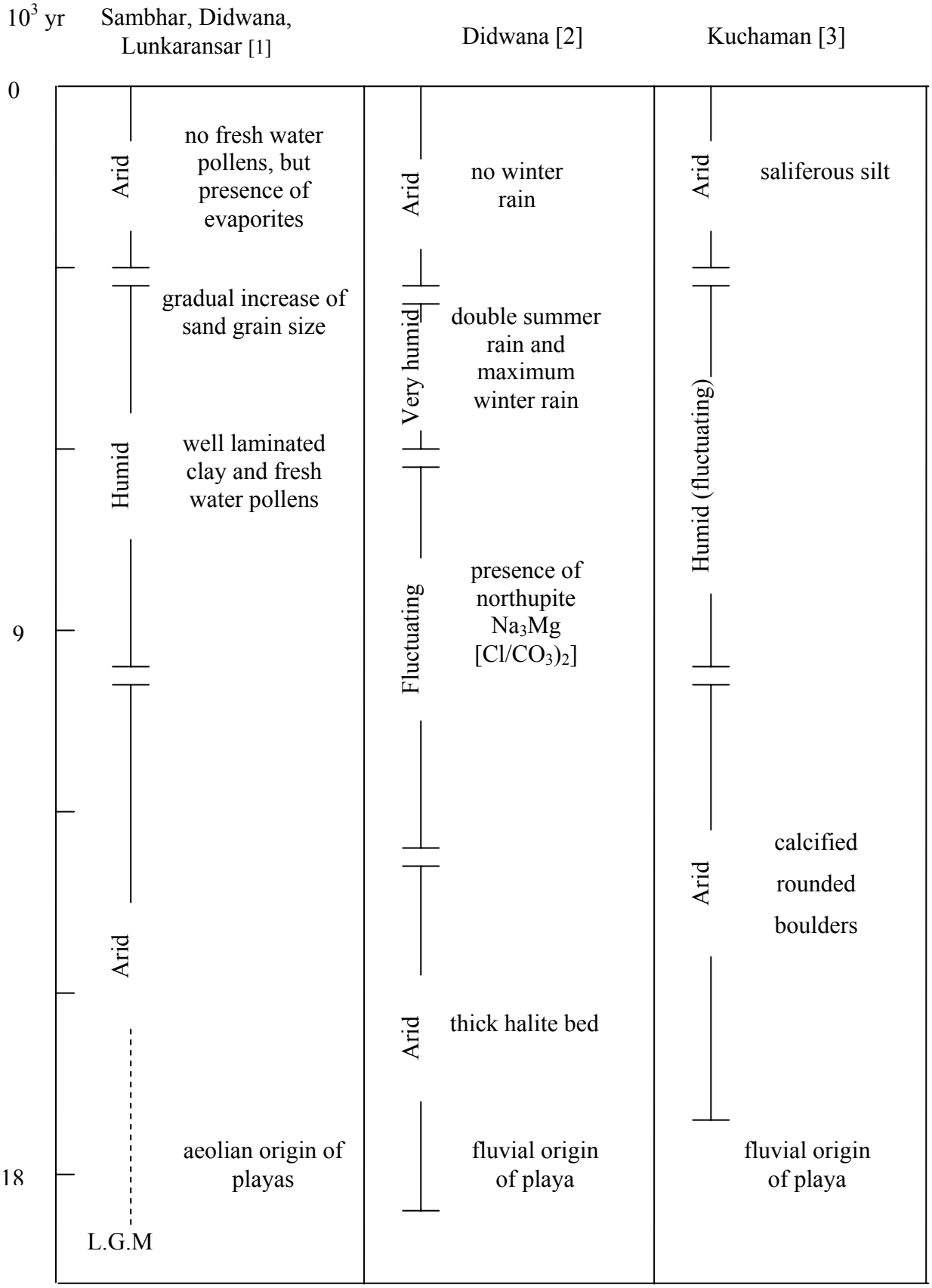

(b) after Deotare et al., 1998 [4], Deotare et al., 2003 [5], Enzel et al., 1999 [6].

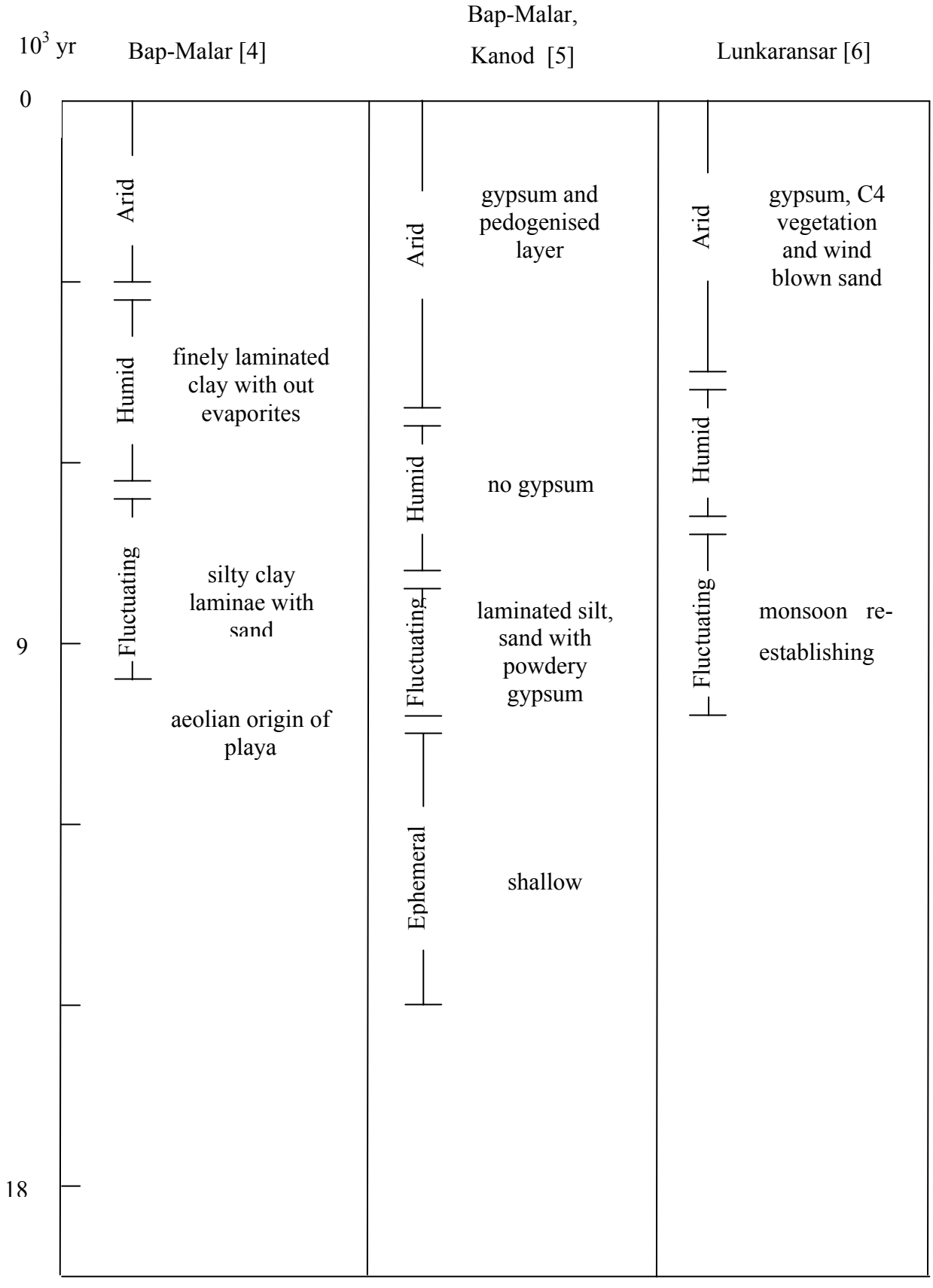

3. Geography, geomorphology and geology of the region

The Great Indian Sand Desert (Thar) covers an area of ca ~ 450,000 km^2. It belongs partly to the Rajasthan state of India and the Sindh province of Pakistan. The origin of the Thar desert is one of the most debated topics of Quaternary Geology of India (Singh, 1988; Pant, 1993). In the east the desert is limited by the Aravalli range of mountains (Figure 1), which divides Rajasthan into two parts; the semi humid eastern and the semi arid to arid western part. The flood plains of the Indus river forms the western margin, the Rann of Kutch the southern and the sub-Himalayan plains the northern boundary of the Thar desert. The USGS GTOPO30 DEM (digital elevation model) image over the study area indicates a regional slope from east to west: the eastern Aravalli hilly tracts showing a maximum elevation of 500 to 600 m and the western arid part covered by sand dunes has an elevation of 100 to 200 m above m.s.l. (Figure 2).

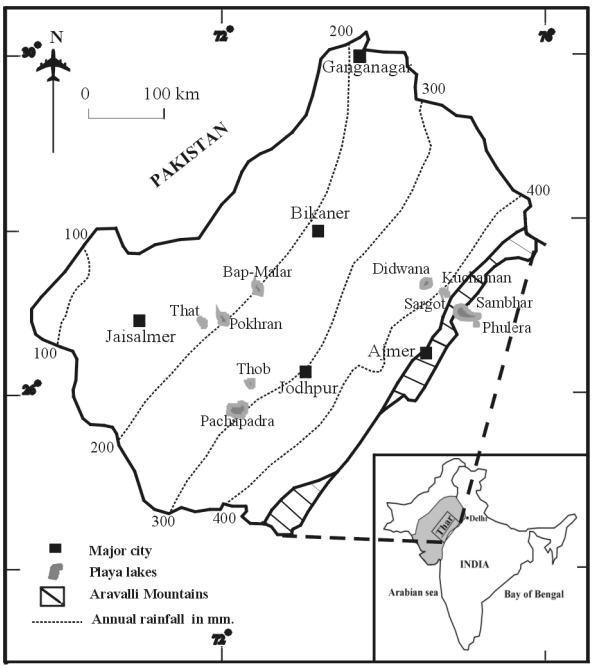

Figure 1 Location map of Thar desert, India. The (sampled) playa lakes are scattered in the region west of Aravalli mountains

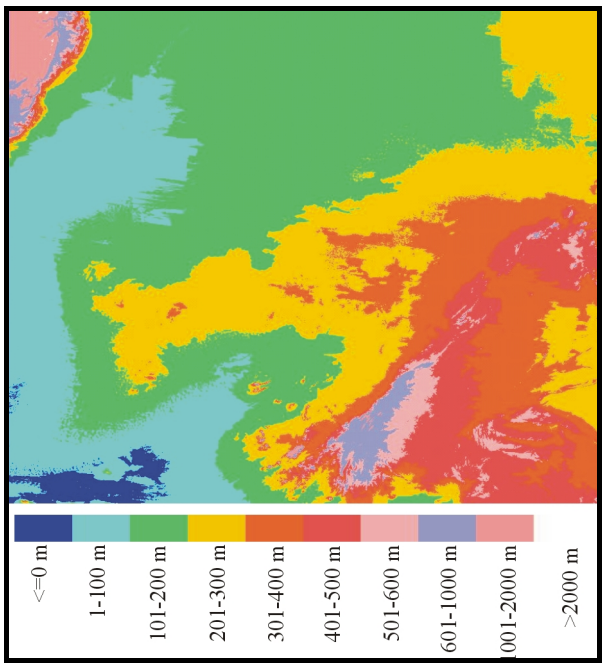

Figure 2 USGS GTOPO30 DEM (digital elevation model) of the study area (69.63º, 30.80º: 76, 90º, 23, 90º). The blue pixels are sea surface and the elevations are in meter.

The climate of the region is influenced strongly by the southwestern summer monsoons. During the summer months, the heating of the Tibetan Plateau creates a zone of low pressure

and causes moist winds to blow from the southern Indian ocean towards the Tibetan Plateau. Like many other deserts, the Thar is characterised by very sparse but variable rainfall, and by extreme variation of diurnal and annual temperatures. The variability of the monsoon rainfall has been linked to expanding of the Eurasian/Tibetan snow cover, which leads to changes in albedo and weakening of monsoonal circulation (Dickson, 1984; Meehl, 1994). The meteorological data from 1871 to 2001 show a highly fluctuating annual rainfall record of the desert (Figure 3). This temporal precipitation pattern, ranging between 30 mm to 500 mm, is very similar to the all India average. Figure 1 shows the spatial distribution of the average precipitation in different parts of the desert. The precipitation of the region varies from 500 mm, in the eastern margin to 100 mm, in the western margin. In the Thar, the mean maximum temperature during the summer months ranges between 40 and 45 ^{0}C, and the mean minimum temperature during the winter months fluctuates between 3 to 10 ^{0}C. Figure 4 shows the minimum and maximum temperature of different months during a year (1990) in N-W India. The evapo-transpiration of the region ranges from three to twenty fold higher than the precipitation, indicating a negative water balance. Around ninety percent of the rainfall is received during the four monsoonal months of the year (between June to September) and the winter rainfall constitutes less than 10 % of the total. The Luni river forms the only integrated drainage network within the desert. During the periods of flood, the ephemeral Luni originates in the western slopes of the Aravallis, drains through the south-eastern desert and finds its way to the Rann of Kutch. Compared to the relatively better drained southern part, the central and northern parts are almost devoid of any streams. The water from the yearly precipitation in the region has practically no outlet and gets accumulated in the various large and small natural depressions (playas).

Owing to the highly variable rainfall, lack of proper drainage and high evaporation losses, the western Rajasthan has a large number of saline lakes (Figure 1). Except the saline lakes (playas), the other characteristic geomorphological features of the Thar are palaeochannels, active and stabilised sand dunes. The present day exogenic processes are dominated by the aeolian agents. The radio carbon dates and thermoluminescence ages suggest aeolian processes were very dominant in the region from 20 kyr to 6 kyr B.P. (Khadkikar et al., 1999). Presently, they are active only in the western margin and the relatively higher rainfall of the eastern part subdues their effects. Features like stabilised and vegetated longitudinal sand dunes are very common in the surroundings of the eastern playa lakes. The active

transverse dune fields are characteristics for the western Thar whereas parabolic dunes are characteristic for the central Thar.

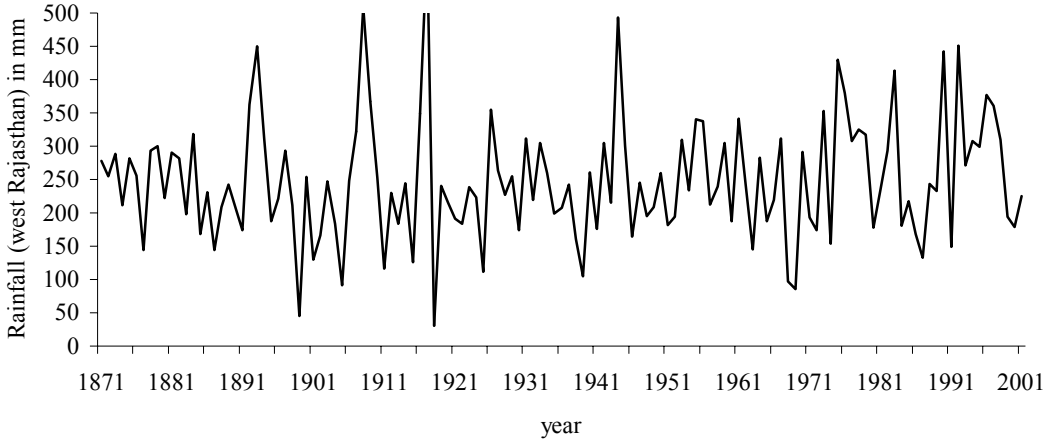

Figure 3 The average yearly precipitation in the Thar desert from 1871 to 2001. The temporal variation in rainfall is characteristic of the deserts all over the world. (source: Indian Institute of Tropical Meteorology, Pune)

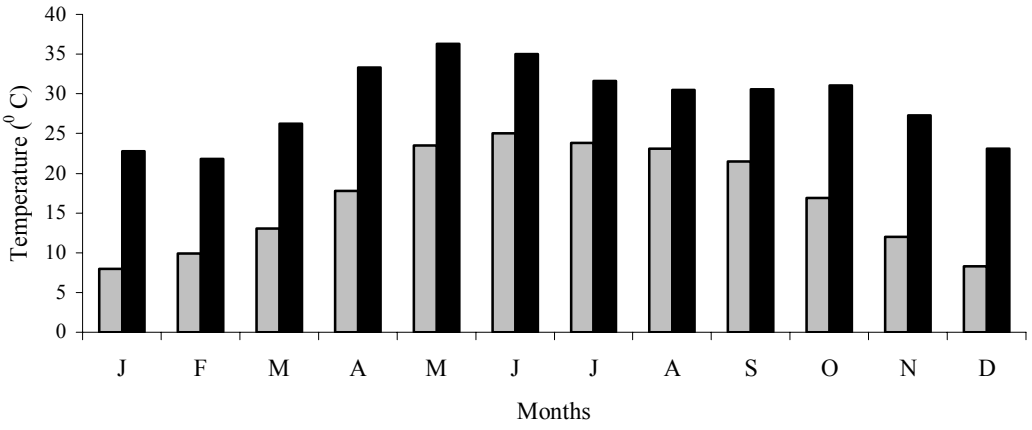

Figure 4 Average maximum (dark shade) and average minimum (light grey shade) temperature of different months during a year (1990) for north-western India. (source: Indian Institute of Tropical Meteorology, Pune)

The GeoCover mosaic of Landsat Thematic Mapper (TM), obtained from National Aeronautics and Space Administration (NASA), USA, gives an overview of the study area (Figure 5). The specifications of the data used are listed below the figure. In the mosaic, band 2 is displayed in blue, band 4 is displayed in green and band 7 is displayed in red. Each band is sensitive to a different part of the solar energy reflected by the earth's surface, and clearly distinguishes water, vegetation and bare soil (Lillesand & Kiefer, 1994). Clear water absorbs

relatively little energy in the wave lengths range less than 0.6 µm. So the band 2 (0.52-0.60µm, green) of the TM receives maximum energy from the water bodies which

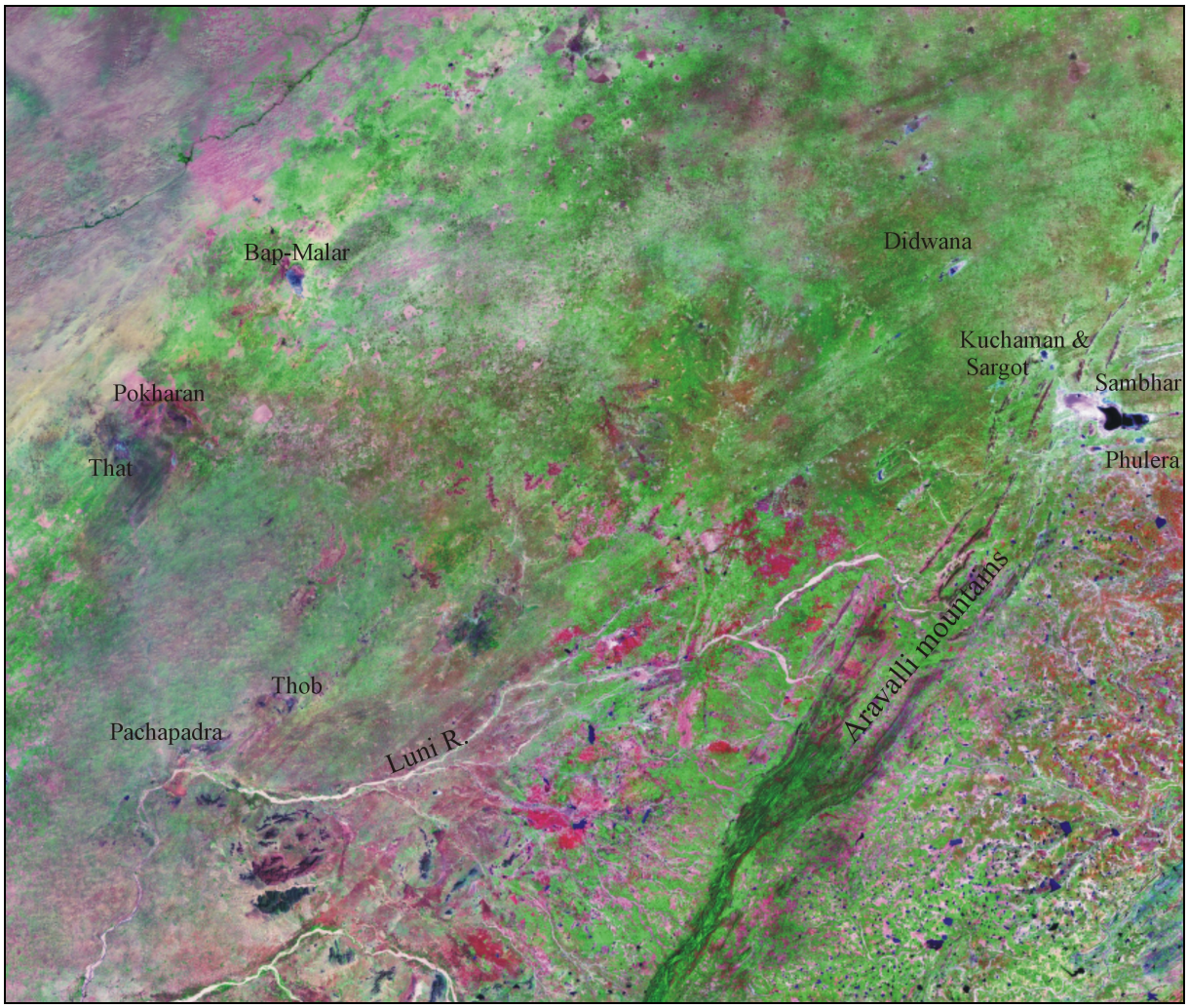

Figure 5 GeoCover mosaic over the study area (71º 25' 14.2", 28º 05' 54.3": 75º 19' 13.1", 25º 12' 59.2"), using band 2, 4 and 7 of Landsat TM. (Scale: 1cm = 25.5 km)

Specification of the data used: satellite- Landsat 4 & 5, sensor- thematic mapper, mosaic scene- N-43-25, pixel size-28.5 m, date of coverage-1990 +/- 3. (source: National Aeronautics and Space Administration, USA)

appear blue in the mosaic. In the wavelength range 0.7 to 1.3 µm (near infrared), plant leaf reflects up to 50 percent of the solar energy incident upon it and water bodies absorb the maximum energy. So band 4 (0.76-0.90 µm, NIR) of TM sensor is very sensitive to the vegetation present and shows the vegetation in shades of green. The soil reflectance is influenced by a number of factors like, surface roughness, moisture content, presence of organic matter and iron oxide. The increasing of the above mentioned factors cause a decrease in the soil reflectance. In the wavelength range above 1.4 µm (short wavelength infrared) the reflectance of soil is higher and it is distinctly more than that of the vegetation and water. In

the band 7 (2.08-2.35 µm, SWIR) of Landsat, bare soil and urban areas are characteristically distinguished from vegetation and water. The sand dunes present in the western arid part of Thar desert are distinctly visible because of their characteristic forms and appears in shades of red. The Aravalli mountain range is visible in shades of green or red, depending upon whether it is vegetated or bare. But the folding structure of the mountain range is the characteristic feature which distinguishes it from the other features present in the mosaic. Three different types of sand dunes are visible according to their shape and size. The former courses of many extinct rivers, now buried under thick sand cover, are also visible (upper left corner of Figure 5) owing to their moisture content and presence of vegetation all along them.

The characteristics of the geology of the region is the presence of several groups of rocks belonging to the Archaean (3.3 Ga) and Proterozoic (0.75 Ga) ages (Sen & Sen, 1983; Dassarma, 1988; Bakker & Mamtani, 2000; Abu-Hamatteh, 2002). They form the Aravalli mountain system, which runs across the region for 700 km, having a variable width of 30-200 km and forming the eastern boundary of the desert. Aligned in a NE-SW direction, the mountain system stretches from northern Gujarat to Delhi. The stratigraphy suggested by Heron (1935, 1953) remained the basis for subsequent stratigraphic revisions (Gupta et al., 1980; Roy, 1988; Sinha-Roy, 1988). The Archaean granitic and gneissic rocks represent the oldest rock sequences in Rajasthan. They are overlain by the rocks of the Aravalli supergroup, Delhi supergroup, Vindhyan supergroup, the younger Pleistocene sand alluvium, blown sand and lacustrine sediments (Table 3). The Archaean supergroup consists of the Bundelkhand gneiss and the banded gneissic complex. The early Proterozoic Aravalli supergroup overlies the Archean supergroup unconformably. It consists of basal quartzites, shales, conglomerates, composite gneisses and slates. The Aravalli rocks are overlain unconformably by the mid to late Proterozoic Delhi supergroup. The highly folded and metamorphosed rocks of Delhi supergroup forms the main part of Aravalli mountains and is divided into lower Alwar group and upper Ajabgarh group. The Alwar group consists of arkose, quartzite, conglomerate and mafic volcanics. The Ajabgarh consists of calc-schist, and calc-gneiss. The Delhi rocks have been extensively intruded by the Erinpura granitic plutons. The Vindhyan supergroup consists of conglomerate, sandstone, limestone and shales. These rocks are exposed along the eastern margin of the desert. A widespread acidic volcanism at the end of the Proterozoic is marked by the Malani Igneous suite and is present in the western Rajasthan. The suit consists of tuffs and rhyolites. The igneous suit is overlain by the sandstone and limestone of the Marwar supergroup. The Palaeozoic Bap boulder bed along with dolomite and minor shale overlie the

Marwar rocks. The Malani group, the Marwar sediments and the Palaeozoic rocks are exposed in the western Rajasthan. The Mesozoic sandstones overlie the Palaeozoic rocks and exposed along the Ganganagar-Jaisalmer-Barmer shelf. The Quaternary continental sediments, consisting of fluvial, lacustrine and aeolian deposits, form a 300 m sequence. For details see Dhir et al. (1992) and Table 3.

Table 3 Generalised geological succession in Rajasthan

Geological Era	Divisions	Lithologies
Cenozoic	Recent sediments	Sand, silt and clay, limestone, sandstone
Mesozoic		Decan trap, sedimentary sequence of Jaisalmer-Barmer-Ganganagar shelf
Palaeozoic	Bap boulder bed	Pebbles, cobbles and boulders, dolomites and minor shale
Proterozoic	Marwar supergroup	Sandstone, limestone and conglomerates
	Malani volcanics	Tuffs, rhyolite, mafic dikes, and granites
	Vindhyan supergroup	Conglomerates, sandstones, grits and shales
	Delhi supergroup	Arkosic schists, quarzites, biotitic schists, calc-schists and calc-gneisses
	Aravalli supergroup	Phyllites, schists, limestones, ortho quazites and meta volcanics
Archaean	Banded Gneissic Complex	Granites, gneisses, amphibolites, migmatites and pegmatites, dolomite and marble etc.

Concerning the provenance of the detrital material of the Thar playas, the publications of Singh et al. (1972), Sen & Ramalingam (1976), Biswas et al. (1982), Misra (1982), Wasson et al. (1984), Rai & Sinha (1990), Rai (1990), Sundaram & Pareek (1995), Rai & Absar (1996), and Deotare et al. (2003) indicate that the different parts of the Thar may be related to several catchment areas, depending on the former fluvial and aeolian system. Thus, it seems that at least two distinct source regions existed, e.g., an eastern bound system and a western bound one.

4. Field work

The saline lakes are scattered all across the western Rajasthan, more specifically to the western side of the Aravalli mountain range. Figure 6 shows the location of the sampled playa lakes.

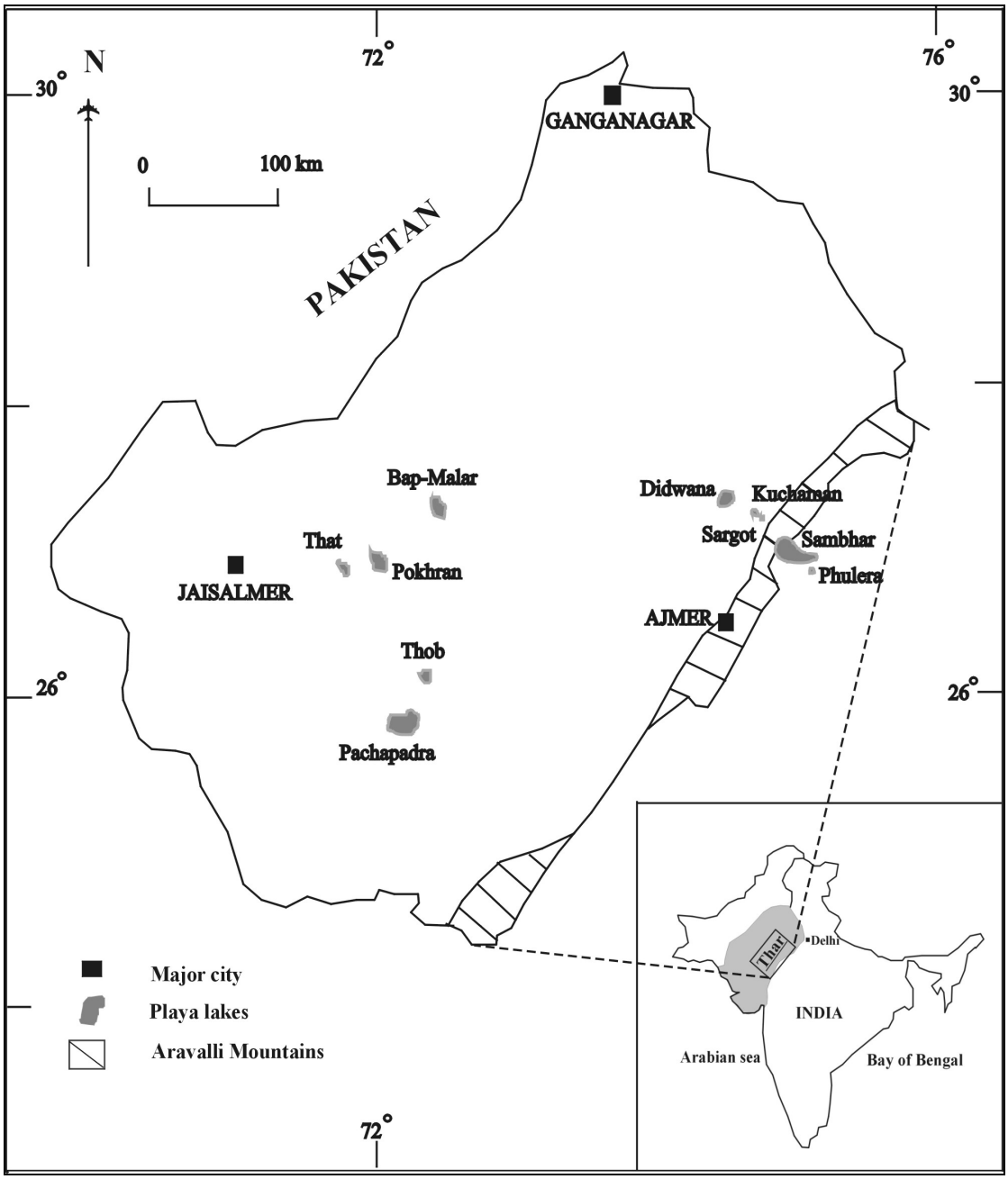

Figure 6 The studied playa lakes of the Thar desert

They are locally known as *ranns*, and are characterised by centripetal drainage of ephemeral type with absolutely no outflow, alkaline brine, and efflorescent duri-crust. During the months

of monsoon, these terminal lakes are mainly fed by periodic rivers flowing in the region, rain and groundwater and for the rest of the year they remain dry. In recent times, the dry lake surface is being extensively used as salt pans for commercial salt production, by evaporating the saline ground water. The saline lakes at eastern desert margin (Phulera, Sambhar, Sargot, Kuchaman, and Didwana) are present in a narrow belt bound by two sets of NW-SE trending lineament: Raisinnagar-Tonk lineament in the north and Sakhi-Khatu-Kishangarh-Bundi lineament in the south (Roy, 1999). Their origin is linked to the neotectonic movement along the NE-SW and NW-SE trending lineaments, which led to the series of rhomb-shaped horsts and grabens. Figure 6 shows the studied playas. Additionally to some of the materials from the Sambhar lake, which had been collected for a previous study (Roy, 2001), this largest playa lake of the whole region was the location of detailed field and laboratory studies. Surface samples from 25 locations of this playa were taken during two field trips (Figure 7). Location 2 was chosen for profile studies down to 125 cm depth.

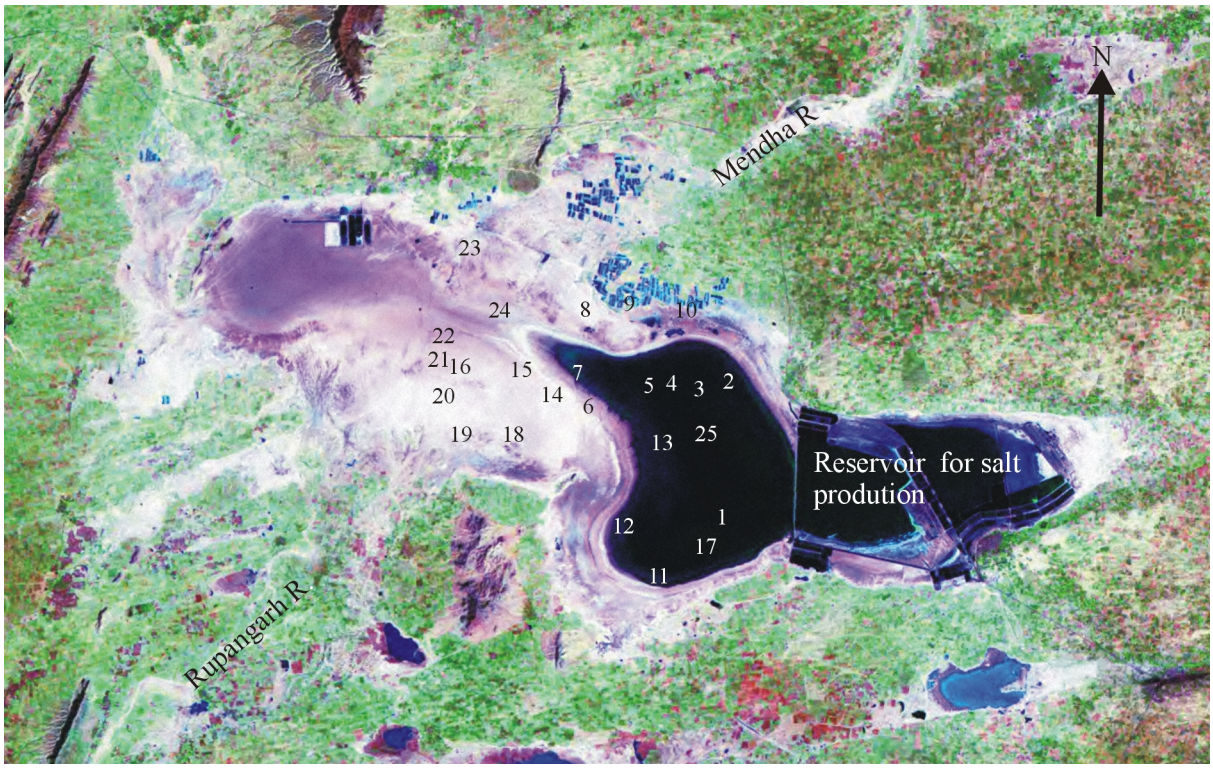

Figure 7 GeoCover mosaic of Landsat TM showing SAMBHAR lake (playa) and its surroundings. The sampling points spread all across the playa surface are also shown. (The mosaic area 74º 52' 4.5", 27º 04' 0.7": 75º 15' 19.8", 26º 50' 52.6", scale 1cm = 1.6 km)

Sambhar lake is located within the wind gaps of the Aravalli mountains. It is the most extensive and economically most important lake of the region. It holds a unique distinction of having maximum thickness of Quaternary deposits. It is situated at an altitude of 350 m above

the m.s.l. The lake is 28 km in length and its width ranges from 3 to 10 km, with the main axis along the NW-SE direction (Figure 7). It is bordered by the vegetated stabilised sand dunes and rocks of Delhi supergroup. The origin of the Sambhar basin is thought to be linked to the pull-apart structural depression, due to the strike-slip faulting along curvilinear planes (Roy, 1999). It is a shallow basin with a maximum depth of 3 m (eastern side) and an average depth of 0.6 m. The lake receives an average annual precipitation of 500 mm. Fed by periodic rivers like Rupangarh and Mendha, it remains partially filled even during the dry summer months. The man made dam divides the lake into two parts: a reservoir part and a natural part. The reservoir part (east) is used to store the brine and later used for salt production. The lithostratigraphic studies in the proximity of the Sambhar revealed three sedimentary cycles, each commenced with fluvial phase, going through a transitional lacustrine phase, culminated with an aeolian phase (Raghav, 1992).

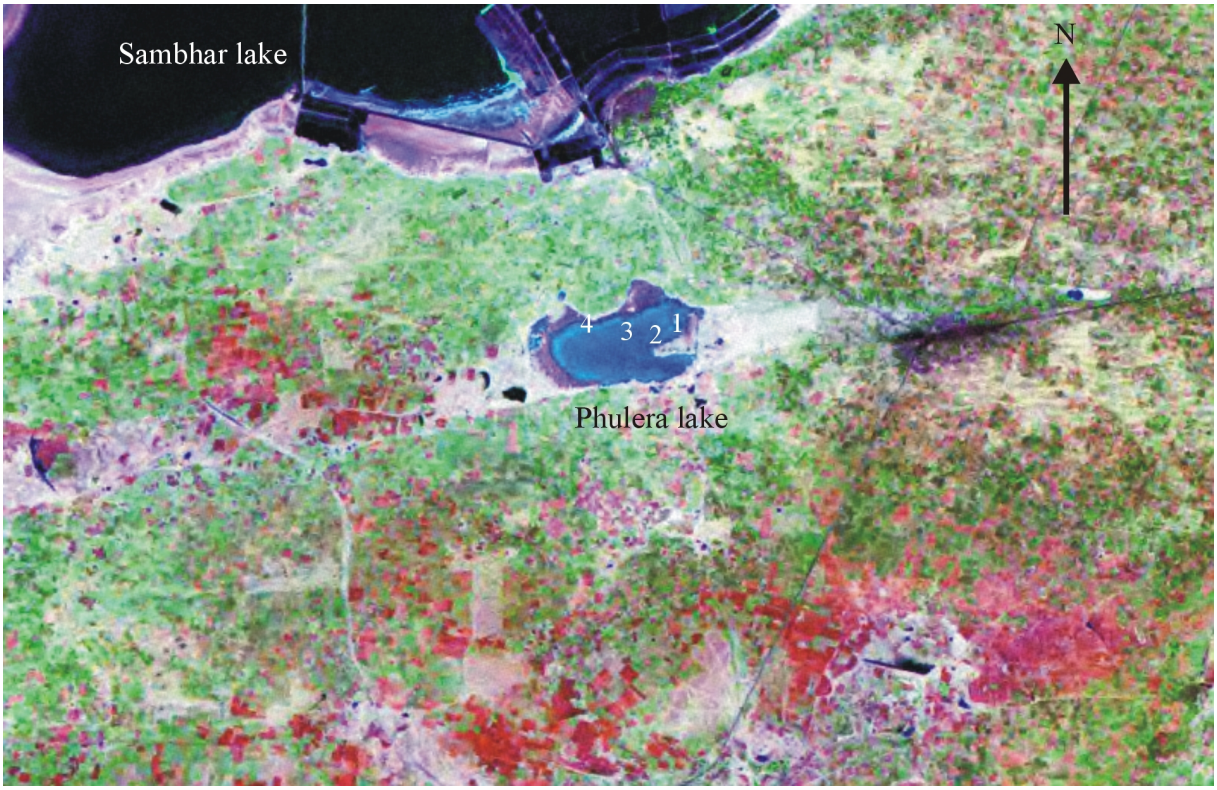

Figure 8 GeoCover mosaic of Landsat TM showing PHULERA lake (playa), its surroundings and the sampling points (marked in numbers). (The mosaic area 75º 03' 55.2", 26º 55' 42.4" : 75º 17' 38.8", 26º 47' 44.3", scale 1cm = 1.12 km)

Phulera is a small and dry playa located at 3 km south of the Sambhar lake, to the east of the Aravalli mountain range. The lake is 3.3 km in length and 1.9 km (average) in width, with its major axis oriented along east-west (Figure 8). The lake receives average annual precipitation

of more than 500 mm and is mainly fed by rain water. Because of the present day dry conditions, the playa surface exhibit distinct desiccation polygonal cracks.

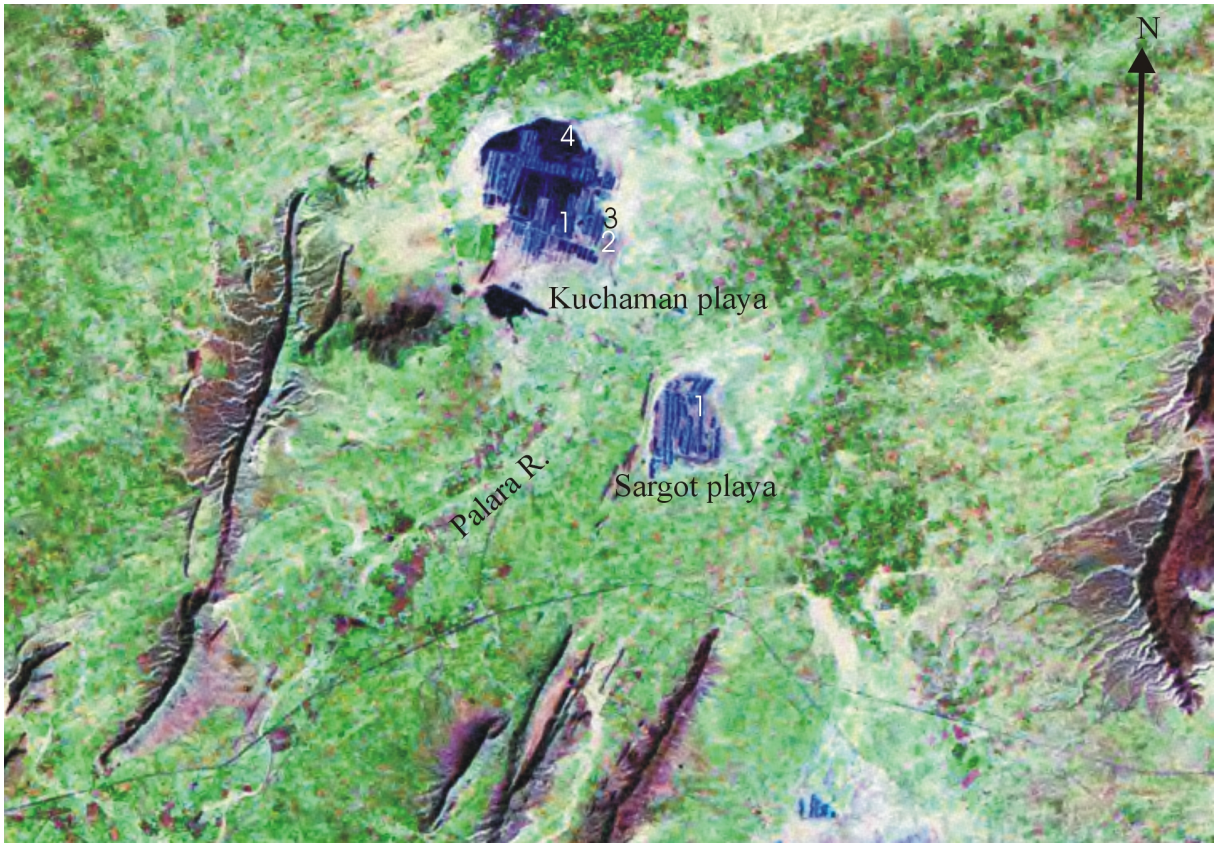

Figure 9 GeoCover Landsat TM mosaic showing KUCHAMAN and SARGOT lakes (playas), its surroundings and sampling points (marked in number). Like Sambhar, they are also located with in the wind gaps of Aravalli mountain. (the mosaic area 74º 46' 5.8", 27º 09' 9.6" : 74º 59' 10.9", 27º 01' 3.9", scale 1cm = 1.12 km)

Kuchaman and Sargot are two continental saline lakes, located around Kuchaman city, around 10 km north-west of the Sambhar playa, within the gaps of the Aravalli mountains (Figure 9). The Kuchaman is a bigger lake with an average length of 2.7 km and width of 2 km. The Sargot is the smaller lake, 1.6 km long and 1.5 km wide. Both the lakes are rounded in shape, and receive average annual precipitation of 400 mm. The evolution of the basin is related to the rhomb shaped grabens formed due to the neotectonic movements along the NE-SW and NW-SE lineaments. The Kuchaman is fed by the Palara river from the south and the Sargot is fed by the narrow streams and gullies coming from the surrounding Delhi ridges. Rai & Absar (1996) reported possible hydrothermal inputs to the lake brines.

Didwana playa lake lies 50 km north-west of the Sambhar lake. It is the second largest playa in the eastern part of the desert and is used extensively for the commercial salt production. This oval shaped lake is 5.6 km long and 2.4 km wide, with its longest dimension orientated

NE-SW, confirmable to the prevailing wind direction (Figure 10). In the south-western margin, it is flanked by hills of quartzite and slate. Stable longitudinal dunes are present along the north-western and south-eastern margins. The lake receives average summer rainfall of 330 mm (Wasson et al., 1984). Temperature of the region varies from 17º C to 31º C. There is no major river feeding the lake, it is mainly fed by rainwater during the summer months but remains dry during the winter. The two dams are constructed in the northern and the southern end of the lake to protect the salt pans from the excessive inflow during the monsoon season. The lake, which is located at the wind shadow zone of the quartzite hills, gets the inflow from a pirated ephemeral stream. The stream is guided by the longitudinal dunes along the interdunal corridor and ends up in the lake basin (Kar, 1990).

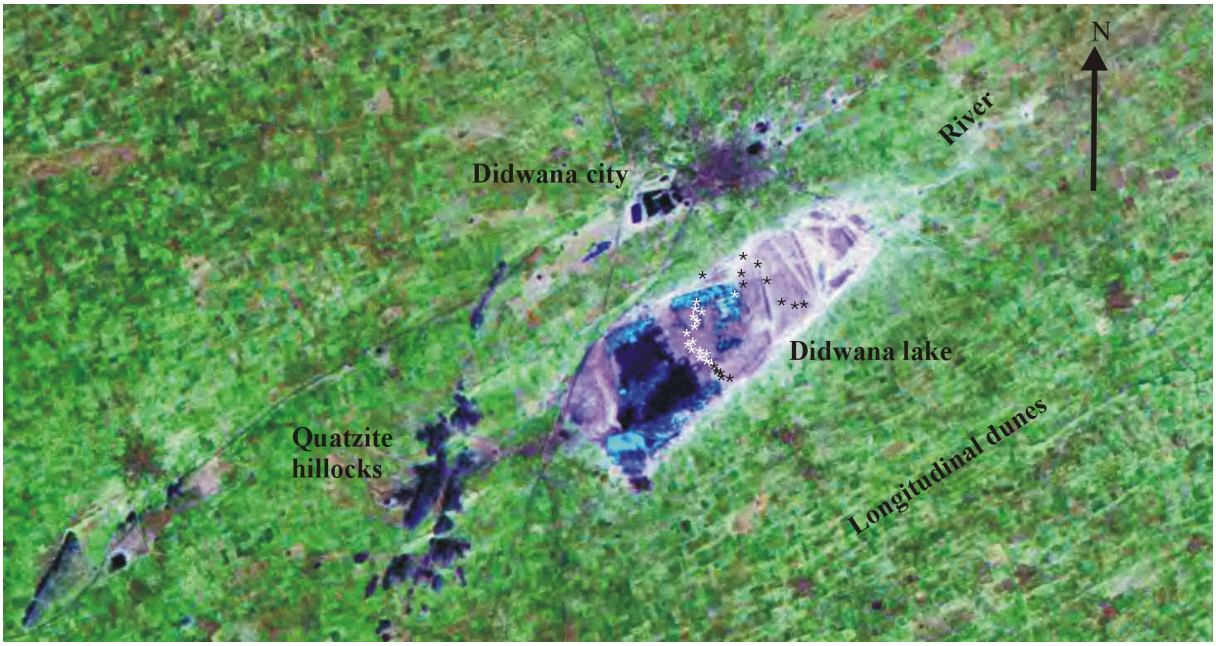

Figure 10 GeoCover mosaic of Landsat TM showing DIDWANA lake (playa), located in the wind shadow zone of the quartzite hillocks. The sampling points (*) are scattered all across the playa surface. (The mosaic area 74º 27' 4.9", 27º 25' 32.1" : 74º 39' 43.9", 27º 19' 38.8", scale 1cm = 1.12 km)

The following five playas are located in the western part of the Thar. Bap-Malar playa lake is situated 160 km north-east of Jaisalmer city, in the arid core of western Rajasthan. The lake receives a mean annual rainfall of ~200 mm and mean annual evapo-transpiration of the region is ~2000 mm (Deotare et al., 1998). The N-S elongated lake (~ 45 km^2) is 10 km long and its width ranges from 1.0 to 6.0 km (Figure 11). A few significant ephemeral streams feed the lake on the south-western side, but the major source of water to the basin is rainfall and ground water. The lacustrine deposits do not exceed 7 m in average.

Pokhran playa lake is located about 60 km south-west of Bap-Malar, on the 200 mm isohyet line. It is an elongated basin, orientated in the NNE-SSW direction (Figure 12). The lake is 6.0 km long and the average width is 2.2 km. The lacustrine deposits have their maximum (5.2 m) in the northern part of the basin. Their thickness decreases to 2.0 m in the southern part (Rai, 1990). During the rainy season, the lake collects water from the surrounding hills through small gullies and streams.

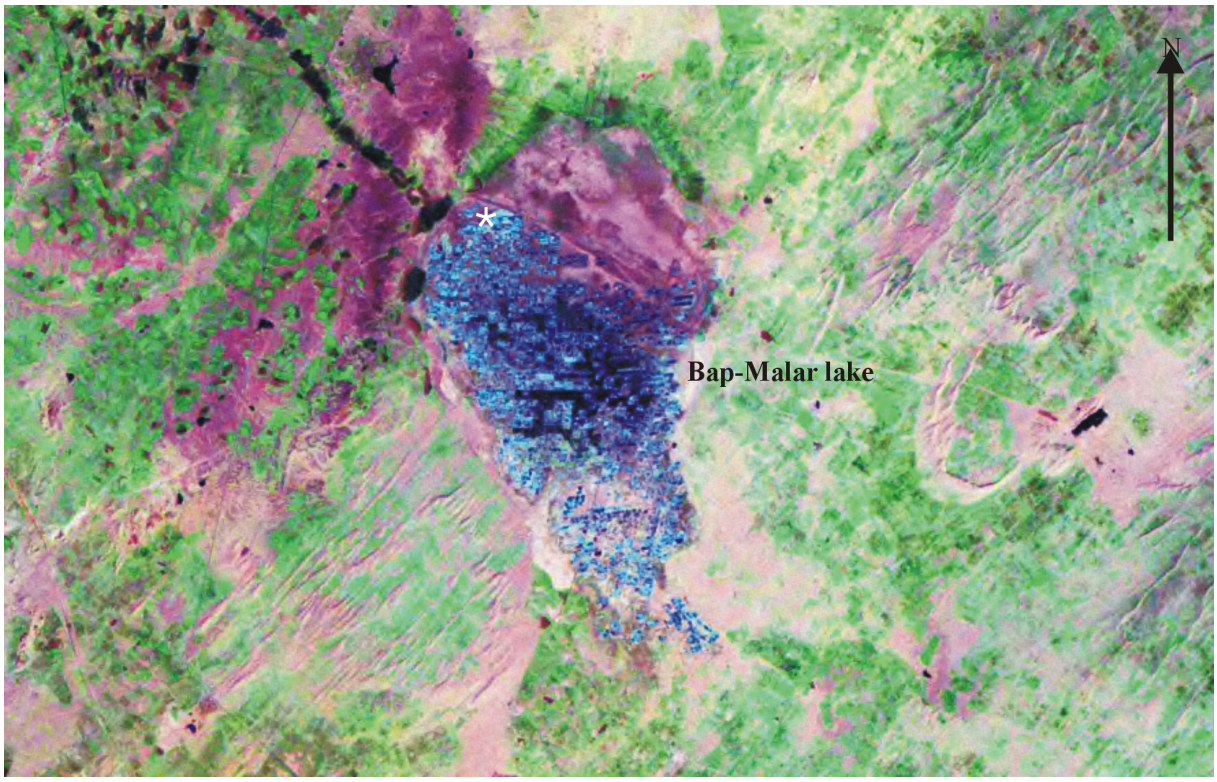

Figure 11 GeoCover mosaic showing the location and surroundings of BAP-MALAR lake (playa). The sample location (*) is marked. (The mosaic area 72º 16' 39.7", 27º 22' 59.2" : 72º 32' 8.8", 27º 14' 34.3", scale 1cm = 1.12 km)

That is a shallow playa lake (17 km^2), located 13 km south-west of the Pokhran playa lake. It is rectangular in shape, 6 km long and 2.5 km (average) wide, with its major axis along the NNW-SSE direction (Figure 13). It receives average annual precipitation of less than 200 mm. The basin is a hollow in sand and is surrounded by sand dunes. A very thin (~ 4 mm) crust of halite is present throughout the lake surface. Like many other saline lakes present in the region, the lake is extensively used for commercial salt production.

Pachapadra playa lake is located 170 km south-east of Jaisalmer city, at the confluence of two periodic streams. The lake is 5 km long and 2 km wide, with its major axis along NE-SW (figure 14). It receives an average annual precipitation of ~300 mm and is surrounded by parabolic sand dunes.

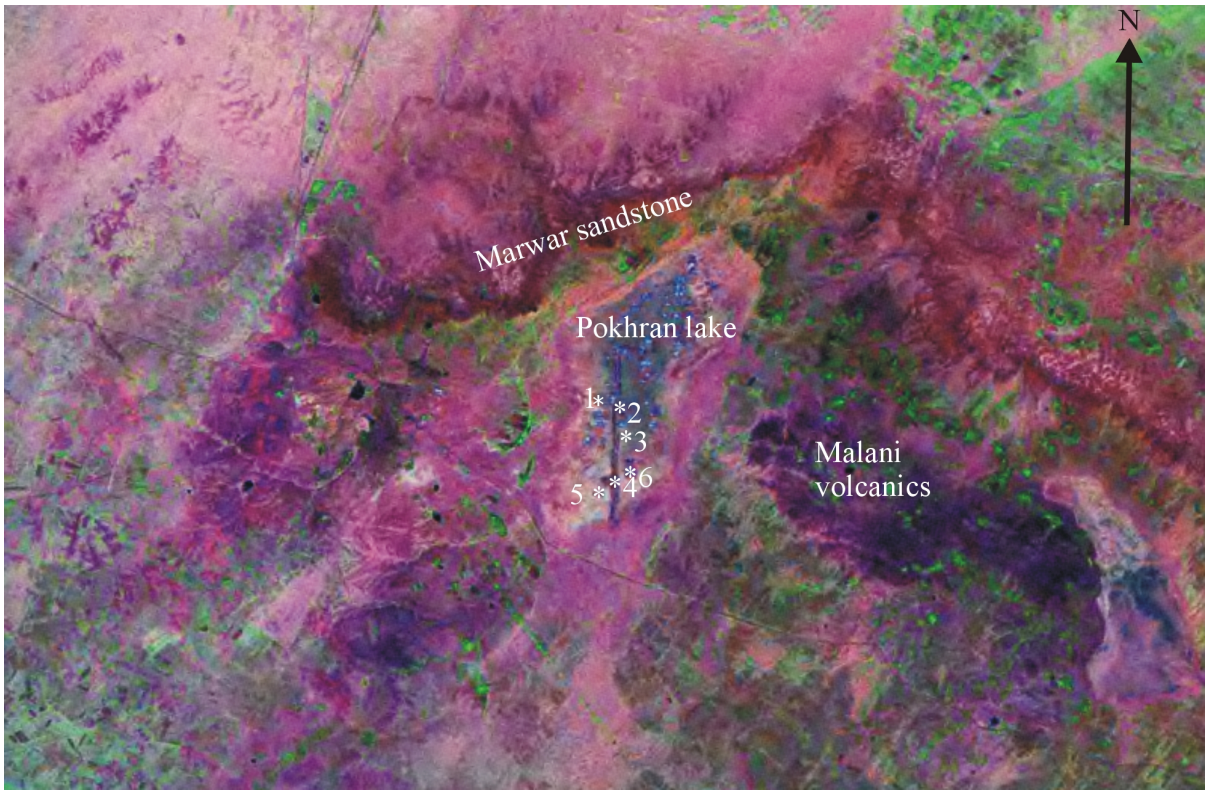

Figure 12 GeoCover mosaic showing the location and surroundings of POKHRAN lake (playa). The sampling points (*) are confined to the southern end of the playa. (The mosaic area 71º 50' 33.4", 26º 59' 23.4" : 72º 04' 27.9", 26º 51' 40.0", scale 1cm = 1.12 km)

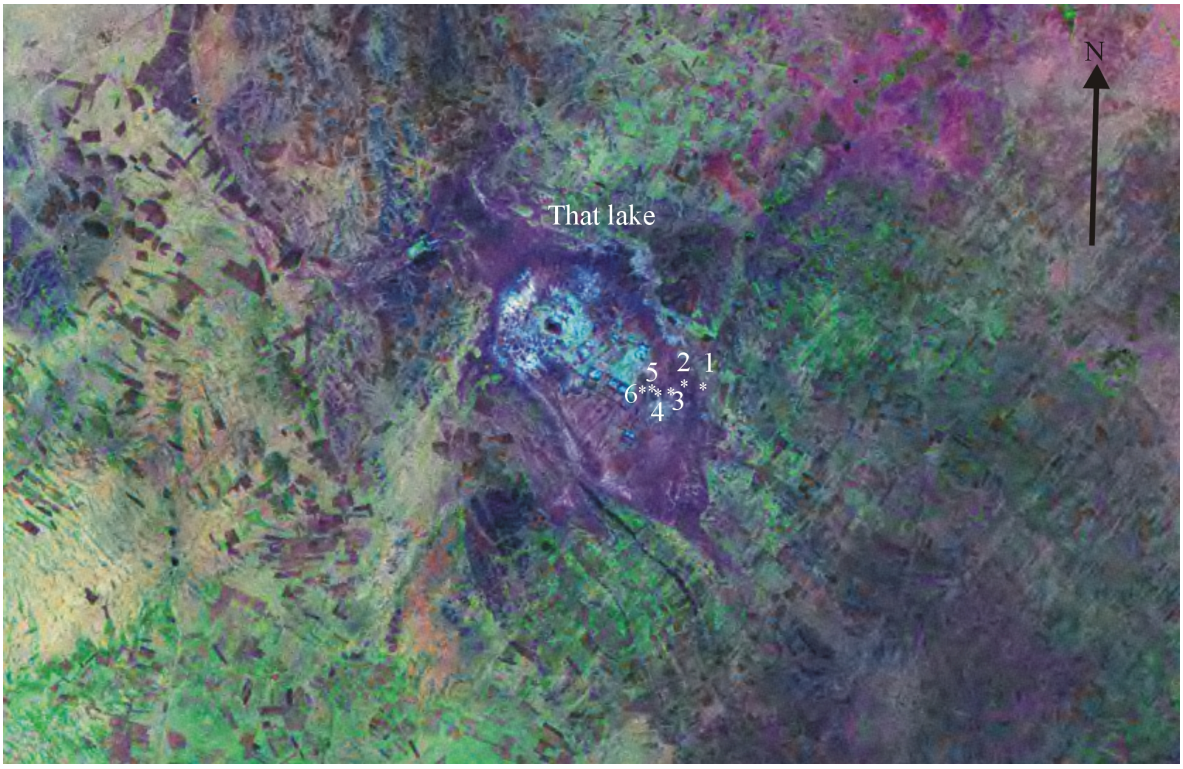

Figure 13 GeoCover mosaic showing the location and surroundings of THAT lake (playa). The sampling points are marked on the lake surface. (The study area 71º 43' 13.1, 26º 52' 20.5, 71º 57' 45.6, 26º 44' 22.9, scale 1cm = 1.12 km)

Figure 14 GeoCover mosaic showing the location, surroundings and sampling points (*) in and around PACHAPADRA lake (playa). The NE-SW trending parabolic sand dunes are present in the surroundings of the lake. (The mosaic area 71º 57' 16.9", 25º 57' 56.0" : 72º 11' 14.5", 25º 50' 10.6", scale 1cm = 1.12 km)

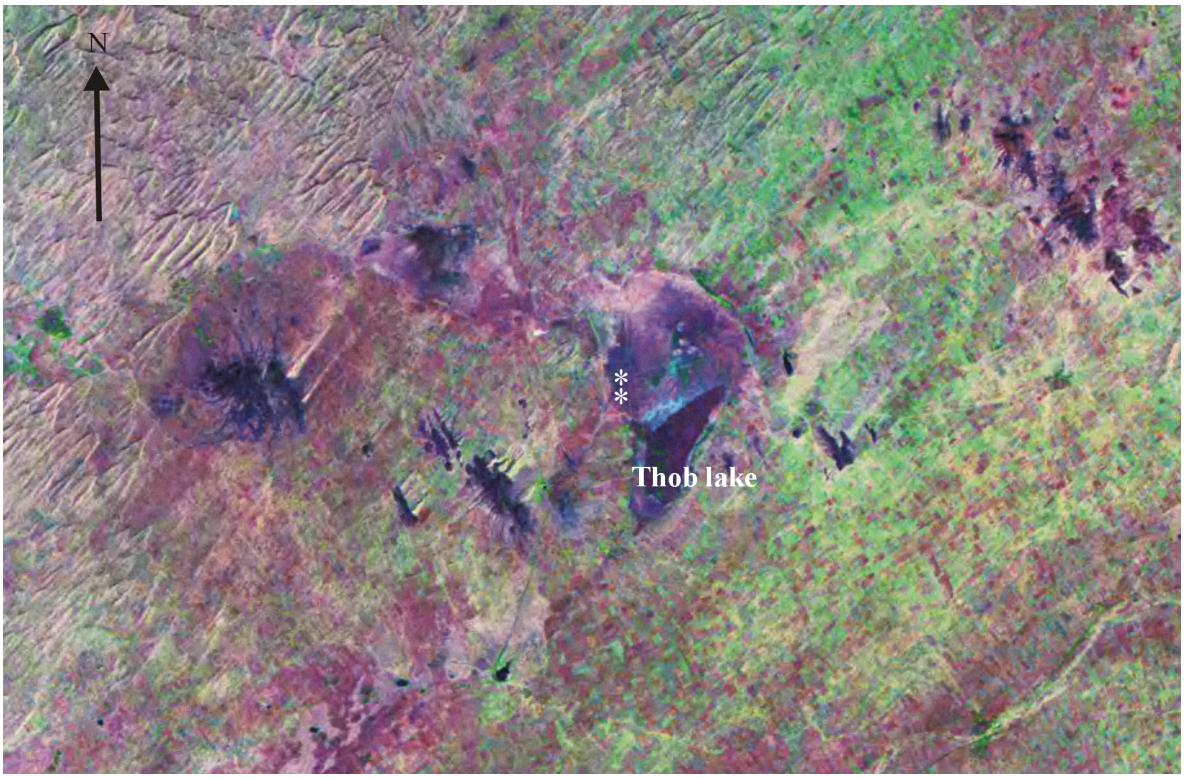

Figure 15 GeoCover mosaic of Landsat TM showing THOB lake (playa), its surroundings and sampling points (*). (The mosaic area 72º 15' 42.3", 26º 08' 46.8" : 72º 31' 31.2", 25º 59' 52.0", scale 1cm = 1.12 km)

Thob playa (11 km^2) is present around 30 km north-east of the Pachapadra playa lake. This shallow playa is a hollow in the sand and fed by rain water during the monsoon months (200-300 mm). The lake is 5.5 km long and 2.5 km wide, with the major axis oriented in N-S (Figure 15).

Sediment samples were collected from the eastern desert margin playas (Sambhar, Didwana, Kuchaman, Sargot, and the Phulera) in May 2001 and from the western arid core playas (Bap, Pokhran, That, Pachapadra, and Thob) in October 2002. Surface samples were collected either along profiles or from scattered locations throughout the lake surface from all ten playas. The locations of the sampling points were fixed with hand held Global Positioning System (GPS) and are shown on the location maps (figure 7 to 15). The deeper profile samples were collected from some selected playas to understand the mineralogical and geochemical variations with depth. Samples were collected from an augured hole in the Phulera playa (110 cm) at an interval of 10 cm, from an augured hole in the Sambhar playa (125 cm) at an interval of 25 cm, from an augured hole in the Didwana playa (120 cm) at an interval of 15 cm and from Bap-Malar playa (75 cm) at an interval of 25 cm. To understand the late Pleistocene lacustrine records samples were collected from the dug pits at Pokhran (190 cm) and Pachapadra (150 cm) playas at an interval of 10 cm. Samples could not be collected beyond the mentioned depths, as saline ground water flushed in to the pits in large amounts and disturbed the sampling process. A brine sample was collected from Pachapadra playa and saline ground water samples were collected from Sambhar (200 cm), Pokhran (210 cm) and Pachapadra (150 cm) playas. The information regarding locations and collected samples of the studied playas are summarised in Table 4.

Table 4 Summarised features of investigated playas of the Thar

Playa lakes	Average annual precipitation (mm)	Extension (km)	Distance from Aravalli mountains	Figure No.	Number of samples
Phulera	> 500	Length : 3.3 Width : 1.9 (average) Orientation: E-W	28 km east	8	4 surface and 10 depth samples
Sambhar	500	Length : 28 Width : 3 to 10 Orientation: NW-SE	Within the mountain gaps	7	25 surface and 5 depth samples
Sargot	400	Length : 1.6 Width : 1.5	Within the mountain gaps	9	One surface sample
Kuchaman	400	Length: 2.7 Width: 2.0	11 km west	9	3 surface samples
Didwana	330	Length: 5.6 Width: 2.4 Orientation: NE-SW	50 km west	10	31 surface and 8 depth samples
Pachapadra	300	Length: 5.0 Width: 2.0 Orientation: NE-SW	180 km west	14	10 surface and 15 depth samples
Thob	~250	Length: 5.5 Width: 2.5 Orientation: N-S	150 km west	15	2 surface samples
Bap-Malar	200	Length: 10 Width: 1.0 to 6.0	230 km west	11	One surface and 3 depth samples
Pokhran	200	Length: 6.0 Width: 2.2 (average) Orientation: NNE-SSW	260 km west	12	5 surface and 19 depth samples
That	< 200	Length: 6.0 Width: 2.5 (average) Orientation: NNW-SSE	240 km west	13	6 surface and and 5 shallow depth samples

5. Methods

Samples collected from the surface and the deeper profiles were packed in plastic bags and numbered in the field. The sediment characteristics and textures were properly noted down. The brine and ground water samples were measured for pH and temperature in the field and packed in air tight cleaned plastic bottles. Each of the sediment samples was divided into two equal halves. One half of each sample was used for mineralogical and geochemical analysis and the other half was preserved as reference material. The samples for mineralogical and geochemical analysis were undergone some pre-analysis preparations like, air drying at 50 ºC, homogenising and grinding them to -200 mesh size in an agate mortar. The powdered samples were used to identify and quantify the minerals present by XRD (X-ray diffraction), DTA-TG (differential thermal analysis and thermogravimetry) and microprobe, the major and trace elements by XRF (X-ray fluorescence), total carbon by CWA (carbon and water analyser), sulphates and inorganic carbonates by CSA (carbon and sulphur analyser), C and O isotopic ratios by gas ion mass spectrometer, rare earth elements by ICP-MS (inductively coupled plasma-mass spectrometer) and cations and anions present in the brine by IC (ion chromatography). The details of sample preparation and analysis are given below.

5.1 X-ray diffraction (XRD)

Three different types of samples were prepared for XRD analysis. For the (i) bulk analysis, a very small amount of the sample was dried in an oven at a temperature of 50 °C. Heating at higher temperature was avoided as many of the evaporites (saline minerals) could disappear. The sample was then crushed manually with caution to fine particle size. With the help of a glass slide it was smeared into a plastic sample holder, so that most of the crystals would have a preferred orientation. For the (ii) salt free analysis, the salts were removed by dissolving in distilled water. For the salt removal, 5 g of bulk sample was dissolved in 500 ml distilled water and shaken for 48 hrs. The residues were then filtered using cellulose nitrate filter paper and later dried. The salt free analysis helps in better identification of the silicates. For the (iii) clay mineral analysis, fractions smaller than 2 μm in diameter were separated by the commonly used dispersion and gravity settling procedure, on the principles of Stokes' law. Under gravity the particle size of 2 μm (density 2.65g/cm^3) takes ~ 3 hrs and 50 minutes to

settle 5 cm in water at 20 °C, but particles of size 5 μm take 37 minutes 30 seconds to settle the same height (Grim, 1953; Brown, 1961; Brindley & Brown, 1980). The clay particles were properly dispersed by vigorously shaking in water. For proper dispersion the samples were made salt free, as salts caused flocculation of clay particles. The particles larger than 2 μm (quartz, feldspars and carbonates) settled down quickly leaving the lighter clay fractions in suspension, which were poured on to a glass slide with the help of a pipette and allowed to dry slowly. For clay mineral identifications, three different samples were prepared for each sample, i.e., untreated (textured), glycol treated and heated. The glycol treated samples were put in a glycol chamber for 2 days, and the heated samples were burnt in an oven up to 550º C before measurements.

The bulk, the desalted and the textured samples were run on a Siemens (D500) diffractometer, using a Cu target (wavelength for the $K_{\alpha 1}$ radiation: 1.5418 Å). The bulk and desalted samples were measured from 3º to 63º at a speed of 0.5º / minute, with a step width of 0.01º. The textured, glycol treated and heated samples were measured from 2º to 22º at the above mentioned speed and step width. The minerals were identified from their 'd' spacings, using Bragg's law ($n\lambda = 2d \sin\theta$, where 'd' is the distance between successive atomic plane of a certain crystal, 'λ' is the monochromatic wavelength of the incident beam and 'θ' is the incident angle). Details see Brindley & Brown (1980).

5.2 Differential thermal analysis (DTA) and thermogravimetry (TG)

In differential thermal analysis (DTA), the temperature difference (ΔT) between the sample and thermally inert material was measured during heating of the sample. The DTA curve recorded these differences during reactions in the sample. The thermal effects were shown as deviations from the zero line. Conventionally, the DTA curve slopes upward for exothermic reactions and downward for endothermic reactions. In thermogravimetry (TG) the weight loss, due to dehydration or loss of CO_2, SO_3 etc., was recorded during heating. Together with the weight loss and the characteristic reaction at a particular temperature, individual clay minerals, carbonate minerals and silicates were identified.

For the present analysis, 100 mg of salt free dry and homogeneous sample was heated in an Al_2O_3 crucible in a standing air atmosphere, at a rate of 10º C/min, up to 1150º C, using $Pt/Pt_{90}Rh_{10}$ thermocouples (Smykatz-Kloss, 1974). DTA diagrams were plotted between ΔT (temperature difference between sample and inert material) vs sample temperature (both are

in °C) and TG diagrams are plotted between loss of weight in % vs sample temperature in °C. Sometimes, the slope of weight loss curve was very sharp due to loss of water from clay mineral or loss of CO_2 due to carbonate decomposition, but in other times there was a more gradual reduction of weight.

5.3 Microprobe analysis

Surface samples from the Didwana playa (0.125-0.250 mm fraction), one surface (0.250-0.350 mm fraction) and two deeper (30 cm) samples from the Pokhran playa (0.250-0.350 mm and 0.090-0.125 mm fractions) were selected from the sieved fractions by observing the minerals present under binocular microscope and then thin sections were prepared. The composition of individual grains were analysed with electron microprobe analyser (SX50 cameca) in the Laboratory of Electron Microscopy at the University of Karlsruhe.

5.4 X-Ray fluorescence analysis (XRF)

The major elements were measured by wavelength dispersive spectrometry (WDS), which use crystals to disperse the component wavelength of the X-ray spectrum emitted from the sample. The trace elements were measured by energy dispersive spectrometry (EDS), which achieves the same purpose by electronic sorting of pulses of different amplitude produced by X-ray photons of different energies (Williams, 1987).

Powder specimens were prepared for EDS analysis. For the better results the bulk samples were ground to fine powders in an agate mortar, and precautions were taken to avoid any contamination of the specimen. The specimens were kept at constant particle size to avoid the risk of variation in fluorescence intensities. The powder samples were put in plastic sample cups and were covered by thin plastic sheets very tightly with the help of plastic bands. The covered surface was kept very smooth to avoid scattering of X-rays. The samples were measured against the soil standard GXR-2 (Govindaraju, 1994) using Cu and Pd filters in Spectrace 5000 instrument.

The glass transformed specimens are favoured for the measurement of major element, as the decomposition of a portion of sample and flux produces a homogeneous glass and it eliminates the particle size and the mineralogical effects (Tertian and Claisse, 1982). Glass transformed specimens were prepared for WDS analysis by mixing 1 part of desalted dry sample with 4 parts of lithium tetraborate flux. After properly mixing, they were heated using

gas burners for a period of 30 minutes. Heating was done in platinum crucibles. During fusion the melt was agitated for the production of homogeneous glass. The ideal specimen shape for XRF measurement is a flat polished disc and this was obtained by casting the molten glass in a circular mould of required size. The samples were measured against the BE-N standard in the SRS 303 AS instrument.

The following table lists the standard deviation of the measured major and trace elements.

Na_2O	MgO	Al_2O_3	SiO_2	P_2O_5	CaO	K_2O	TiO_2	MnO	Fe_2O_3	Cu	Zn	Rb	Sr	Y	Zr	Nb	Ba	Ce
(mass %)										(ppm)								
0.01	0.04	0.01	0.70	0.02	0.01	0.01	0.01	0.01	0.03	3	9	2	2	0.5	4	1	50	3

5.5 Carbon water analysis (CWA)

Organic carbon in the sediments was estimated through measurement of inorganic carbon content by Leybold 5003 carbon water analyser (CWA) and then subtracting it from total carbon value. For inorganic carbon analysis, the instrument was calibrated with respect to $CaCO_3$ and for water analysis the instrument was calibrated with respect to $CaSO_4 \cdot 2H_2O$. Approximately 250 ml of salt free dry sample was used for the measurements. The sample was burnt with a steady flow of N_2 and the carbonates were converted into CO_2. The output was obtained in terms of percentage of CO_2 and H_2O.

5.6 Carbon sulphur analysis (CSA)

Leybold 5003 carbon sulphur analyser (CSA) was used to measure total carbon and sulphur in percentage. It was calibrated with respect to the 0.42 % carbon containing free cutting steels. The other constituents of the standard are sulphur (0.147 %), silica (0.46 %), phosphorous (0.031 %), and manganese (1.15 %). For the analysis, approximately 100 mg of salt free dry sample was added to approximately 500 mg of iron cheap accelerator. To this mixture tungsten (wolfram) was added such that the ratio between tungsten accelerator and iron cheap accelerator was 3:1. The instrument oxidises the carbon and sulphur present in the sample with a constant flow of O_2.

5.7 Gas ion mass spectrometer

Prior to the measurement, the samples (7 from Phulera and 8 from Pokhran playa along the depth profile) were desalted, dried and ground to fine powder. They were analysed for ^{18}O

and ^{13}C by introducing the carbonate phase as gas into the mass spectrometer, and calculated using the formulae

$$\delta^{18}O \text{ (per mille)} = \left(\frac{\left(18O/16O\right)sample}{\left(18O/16O\right)s\tan dard} - 1 \right) \times 1000$$

$$\delta^{13}C \text{ (per mille)} = \left(\frac{\left(13C/12C\right)sample}{\left(13C/12C\right)s\tan dard} - 1 \right) \times 1000$$

V-PDB (PeeDee formation Belemnite) was used for both ^{18}O and for ^{13}C analysis as the standard.

5.8 ICP-MS analysis

Selected trace elements (Cr, Ni, U, Th, and V) and rare earth elements were measured in 7 samples from the eastern desert margin playas (Sambhar, Phulera, Kuchaman, and Didwana) and 12 samples from the western arid core playas (Bap-Malar, Pokhran, That, Pachapadra and Thob), after digesting the samples completely with HF, HNO_3 and $HClO_4$ in Teflon crucibles. These crucibles were properly cleaned with a mixture of HCl and HNO_3 (3:1) before the treatments. For the digestion, 50 mg sample was heated and simultaneously treated with 1 ml of 65% HNO_3, for organic carbon removal, with 2 ml of 40% HF and 2 ml of 70% $HClO_4$, to dissolve silicates. This procedure was followed at least three times till the silica gel showed no trace of colour. Then the residues were dissolved with 1 N HCl and the volume is made to 50 ml. For a few samples total digestion were carried out on the carbonate leached fractions to find out the effect of carbonates on REE mobility. For the analysis of carbonate leached fractions, bulk samples were treated with 1 M cold dilute HCl before their digestion as prescribed by Tripathi and Rajamani (1999). The rare earth elements were measured against the ICP-MS multielemental standard B and the trace elements were measured against the P/N 4400-ICP-MSCS, certified by National Institute of Standard and Technology.

5.9 Ion-chromatography (IC)

Ions (cations and anions) were separated and quantified on the basis of their differential migration on an ion exchange column in Metrohm 690 Ion Chromatograph. For the high

performance separation of ions, a small sample was used with a chromatograph column of relatively small diameter containing packing of uniform and small packing size, and a constant effluent flow (Fritz et al., 1982). For the cations and anions, two different low conductance eluents were prepared before the analysis.

The eluent used for separation of chloride, sulphate and nitrate (anions) was prepared by adding 4.15 gm of pthalic acid, 10 ml of acetonitrile and 950 ml of distilled water. The pH was then adjusted to 3.8 so that the salt could ionise completely. Then distilled water was added to make the total volume to 1 litre. A sub sample of 100 ml was taken from this solution and 50 ml of acetonitrile was added and again made to 1 litre. The eluent used for separation of Na^{+}, K^{+}, Ca^{+2},and Mg^{+2} (cations) was prepared by adding 125.3 mg of 2,6 pyridine decarboxylic acid and 750 mg tartaric acid with 200 ml distilled water. It was then heated and diluted to 1 litre. Before injecting the sample into the chromatograph, the eluents were pumped through the ion exchange columns so that the resin exchange sites could contain the eluent ions. The samples were diluted 10 to 1000 times, depending upon the concentration of Na^{+} and Cl^{-}, to facilitate the measurement of other anions and cations present in lower concentrations.

6. Results

6.1 Mineralogy

6.1.1 Surface mineralogy

The sediment samples were analysed for bulk mineralogy using Siemens (D500) diffractometer and for the heavy (accessory) minerals by electron microprobe. The mineralogical distributions in the sediments of the ten investigated playas and the geochemical composition of some of the detrital fractions are presented in appendix (tables 1 to 17). Depending upon the environment of formation, the surface mineralogy is divided into two different groups, e.g., (a) the association of detrital minerals and (b) the in-situ formations in the playa sediments, i.e. evaporites precipitated from the saline lake brine.

6.1.1 (a) Detrital minerals

The detrital minerals, transported into the playas by rivers and wind, do not show any significant difference (Tables 1 to 10 in the appendix). Quartz is the most abundant mineral. The amount of quartz is more than 50 % of the bulk sediments. The optical studies (thin section and electron microscopic investigation) indicate a variable degree of roundness of this resistant mineral. In many cases it shows to be quite angular. Feldspars (potassium feldspar and plagioclases) constitute the next detrital component in abundance. In the bulk analysis, the amount of plagioclases is much more in comparison with K-feldspars (tables 1 to 10 in the appendix). Plagioclases constitute 10-30 % and K-feldspar 5-20 % of the bulk mineralogy. Figure 16 shows the characteristic feldspars from one eastern playa (e.g. Didwana) and one western playa (e.g. Pokhran). The positions of the feldspars in the Na_2O-K_2O-CaO ternary diagram indicate that K-feldspars are very similar in composition from both the regions of the Thar, whereas plagioclases vary between albite and CaO rich labradorite. The Ba feldspar, hyalophane is rarely found in Pokhran sediments. The electron microprobe analyses of the feldspars are included in the appendix (tables 11 and 12). Two different kinds of detrital layer silicates, e.g. micas and chlorites are present in minor amounts. The micas and chlorites together represent less than 10 % of the samples. The micas of the eastern playas are of the di-octahedral type (muscovite). The western playa sediments constitute both the muscovite and

biotite (for analysis see appendix). The X-ray data of chlorites do not show any characteristic difference. The chlorites of both the eastern and western playas are characterised by high intensities of the even-order reflections (002, 004), but weak intensities of the odd-order reflections (001, 003), which indicate it to be a Fe-rich type (Moore & Reynolds, 1997). The base reflections of both types of layer silicates are sharp and symmetrical, mirroring a well ordered structure.

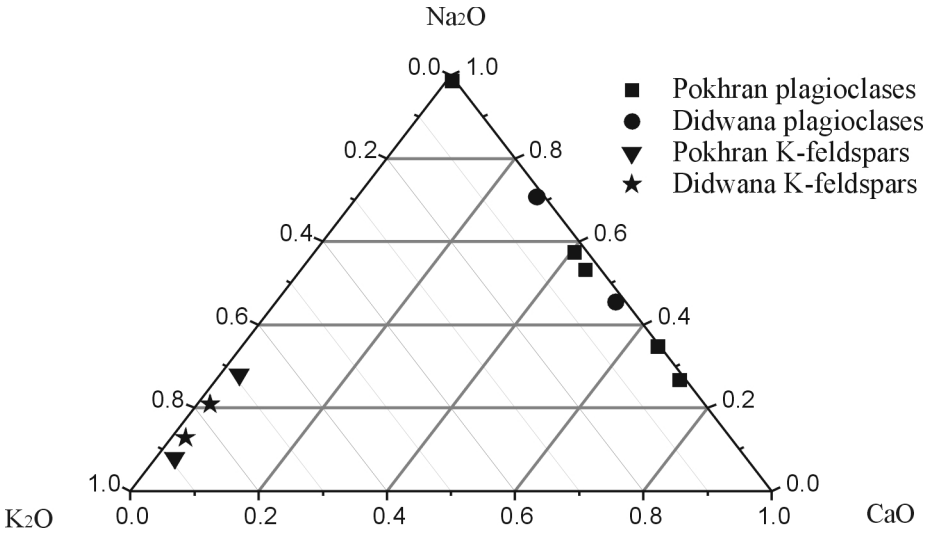

Figure 16 Na_2O-K_2O-CaO diagram showing the composition of the feldspars present in playa sediments

A further detrital type occurring in amounts between 3 and 5 % is the amphibole. The crystal chemical variation of amphiboles shows not to be large (Figure 17), with one (characteristic?) exception: a Pokhran amphibole is nearly Ca-free (compare Figure 17 and analysis in the appendix). Hematite is present in minor amounts (2 to 3 %) in the western playa sediments and could be detected in the XRD charts. The eastern playas are (nearly) free of hematite. Many of the western playa samples show the characteristic red colour due to the presence of the iron oxide mineral, while that of the eastern playa surfaces are brownish to grey. Under the electron microscope and with the help of electron-microprobe nearly ten trace minerals were identified, each in amounts of few tenths of percent. The number of trace minerals is remarkably larger in the western playas (e.g. Pokhran and Pachapadra). Some of the trace minerals, e.g. ilmenite, magnetite and titano-magnetite, are present in the western playas and absent in the eastern. The trace minerals, e.g. garnets, zircon, rutile, and titanite, are present in both the regions, though they show somewhat higher abundances in the western playas. The electron microprobe analysis of these minerals is presented in the appendix.

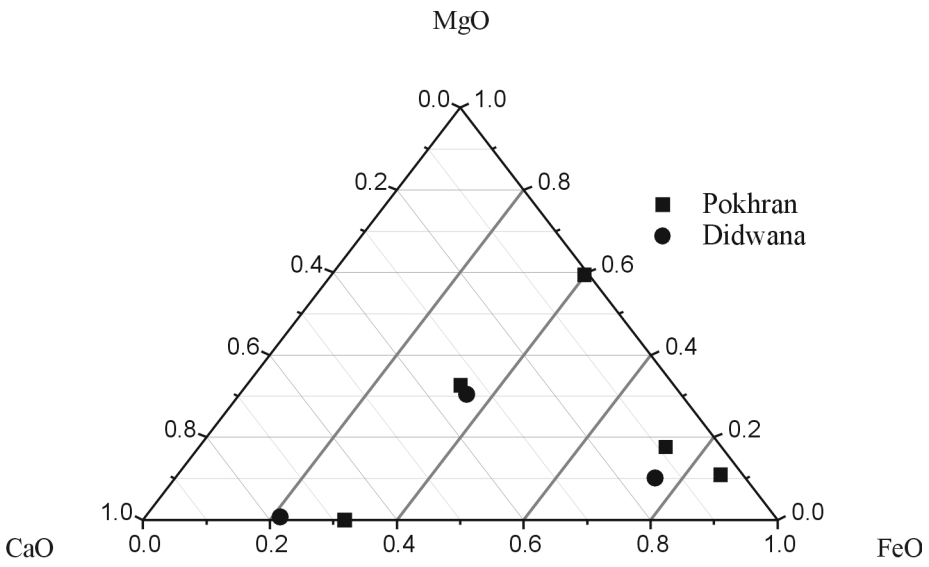

Figure 17 MgO-CaO-FeO diagram showing the composition of the amphiboles present in playa sediments

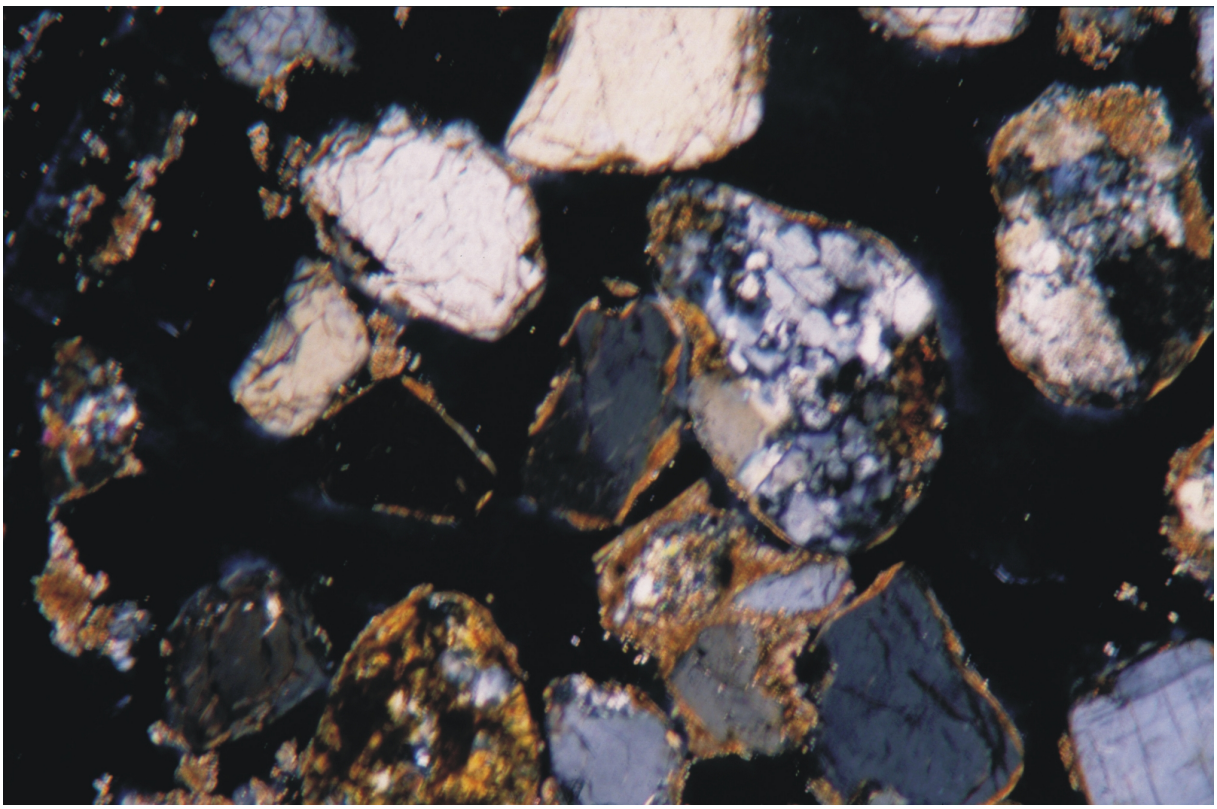

Figure 18 Rock fragment of (rounded) quartzite along with garnet, quartz and altered biotite schist. Scale : length of the picture = 1.4 mm)

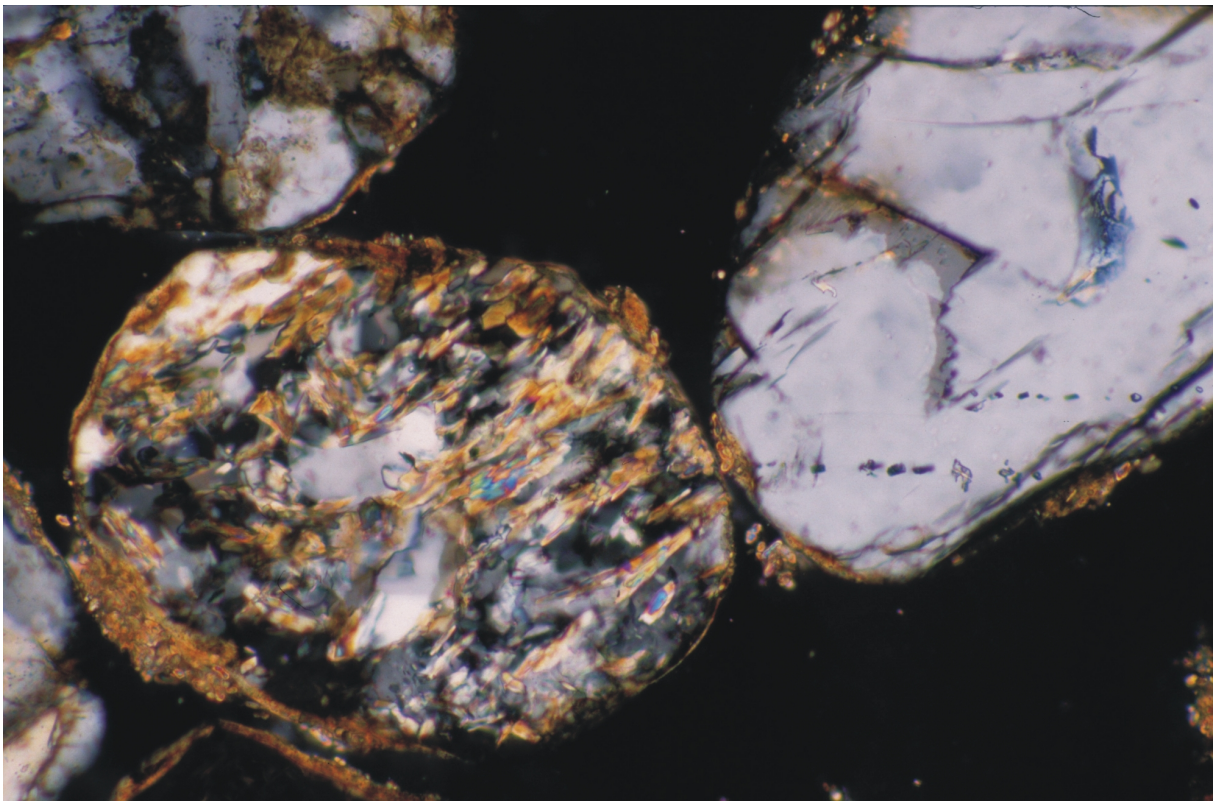

Figure 19 Rounded mica schist fragment and a quartz grain with secondary fluid inclusions. Scale : length of the picture = 0.6 mm)

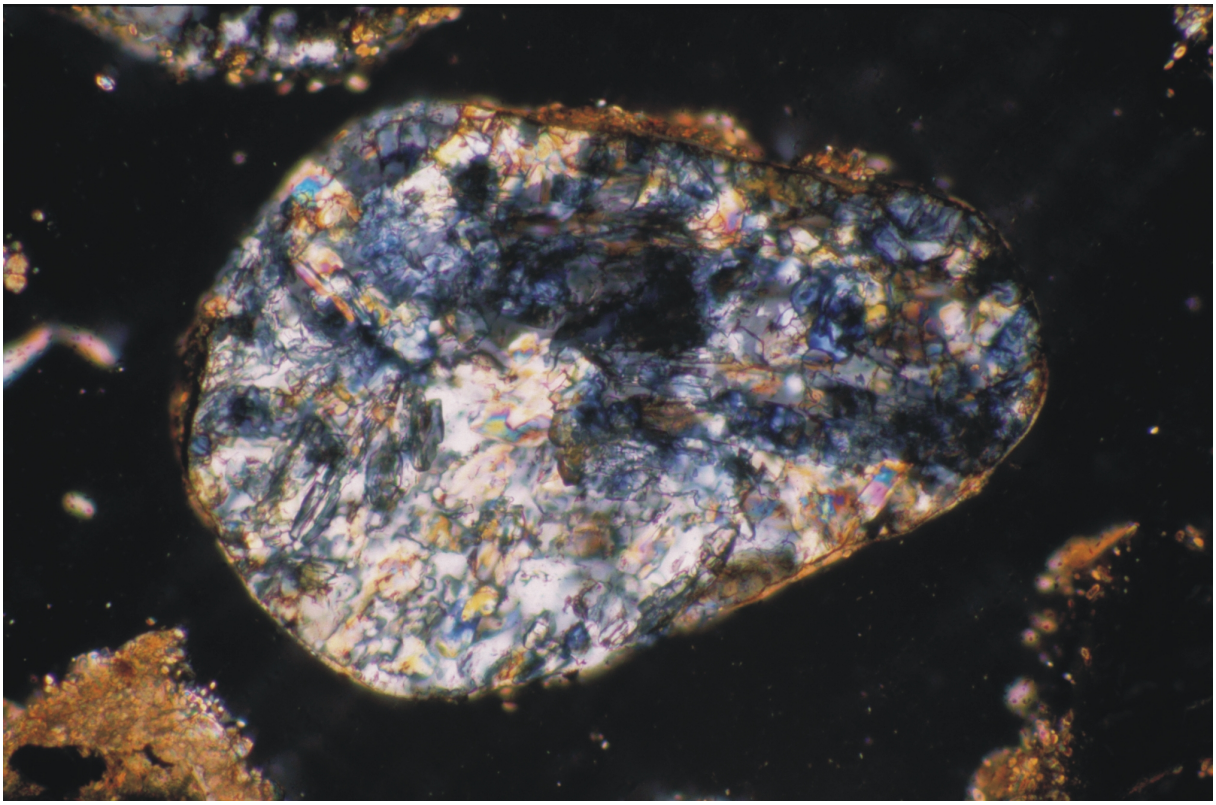

Figure 20 A metamorphic rock fragment with epidote-zoisite-muscovite. Scale : length of the picture = 0.6 mm)

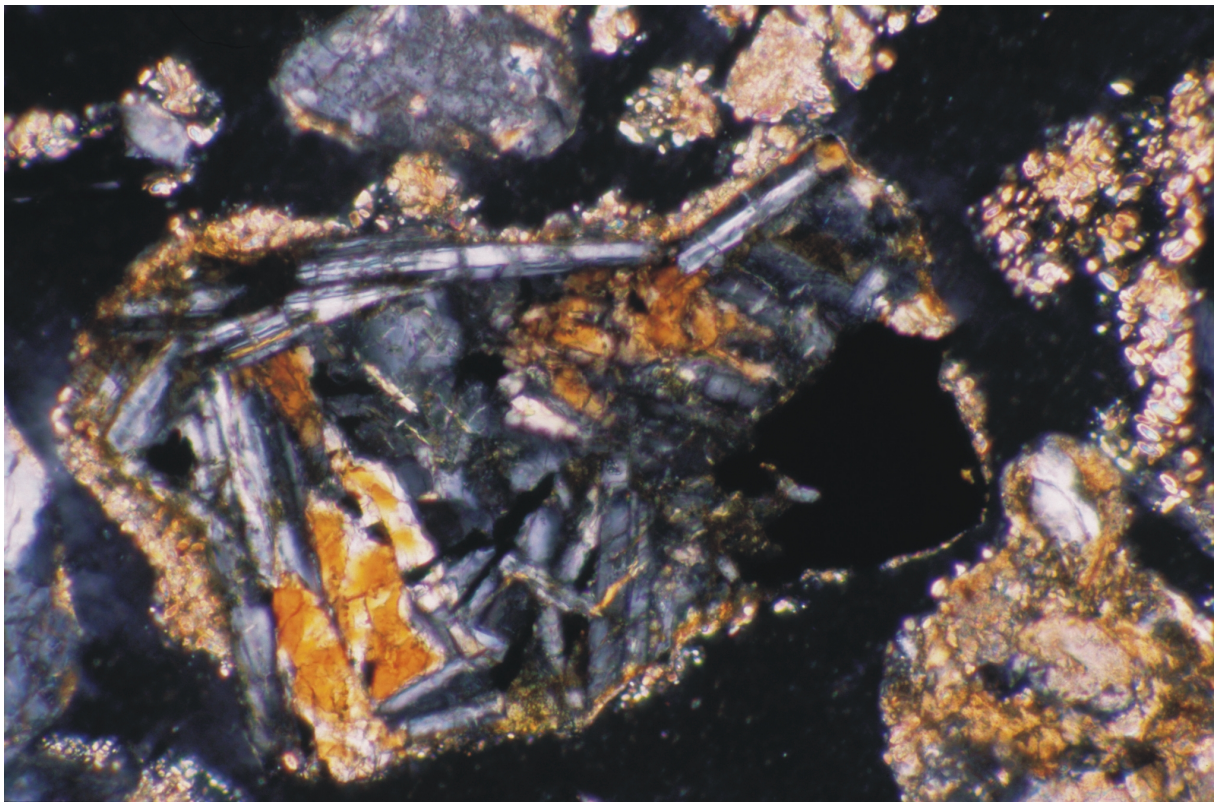

Figure 21 A fragment of basalt with labradorite, pyroxene and magnetite. Scale : length of the picture = 0.6 mm)

There are only some exceptions from this "rule", e.g. the soro-silicate lawsonite, $CaAl_2[(OH)_2Si_2O_7]$, the phosphate mineral xenotime, $Y[PO_4]$, monazite, $Ce[PO_4]$, epidote, pyroxenes, allanite, and the zeolite type mineral analcime, $Na[AlSi_2O_6] \cdot H_2O$. The first six minerals are detected in sediments of the Pokhran playa, whereas the latter two are found in the Didwana sediments. Both the regions show several types of trace garnets. The types pyrope, almandine, grossular and andradite (Ti-bearing $Ca_3Fe_2[SiO_4]_3$) are present in traces in the investigated playas (for composition see appendix). The crystal chemical composition of eastern playas and western playa garnets do not differ. Apart from the individual minerals, fragments of quartzite (Figure 18), mica schist (Figure 19), epidote-zoisite-muscovite schist (Figure 20), limestone, basalt (Figure 21), and rhyolite, are identified in the sediments of Pokhran.

6.1.1 (b) Evaporites

The evaporite minerals occurring in the surface samples consist of carbonates (calcite ($CaCO_3$), dolomite ($CaMg(CO_3)_2$), and trona ($Na_3H(CO_3)_2 \cdot 2H_2O$)), sulphates (gypsum ($Ca_2SO_4 \cdot 2H_2O$), anhydrite (CaSO4), and thenardite (Na_2SO_4), mirabilite ($Na_2SO_4 \cdot 10H_2O$),

polyhalite ($K_2MgCa_2(SO_4)_4 \cdot 2H_2O$), glauberite ($Na_2Ca(SO_4)_2$)) and chlorides (halite (NaCl), sylvite (KCl), and carnallite ($KMgCl_3 \cdot 6H_2O$)). Table 5 presents comparative surface evaporite mineralogy from the playas of the Thar desert. The (more humid) eastern playa sediments are showing more evaporite minerals than the western playas: the sulphates thenardite, mirabilite, polyhalite, glauberite, the Na-carbonate, trona, the K-Mg-chloride, carnallite and sylvite occur only in the eastern playas. The largest playa Sambhar is exhibiting the most complex varieties of evaporite minerals. The playas of the region remain partially filled only during 2-3 months of monsoon and remain dry for the rest of the year. This is valid for all the investigated playas, though the eastern playas receive more precipitation than the western playas (see chapter 3).

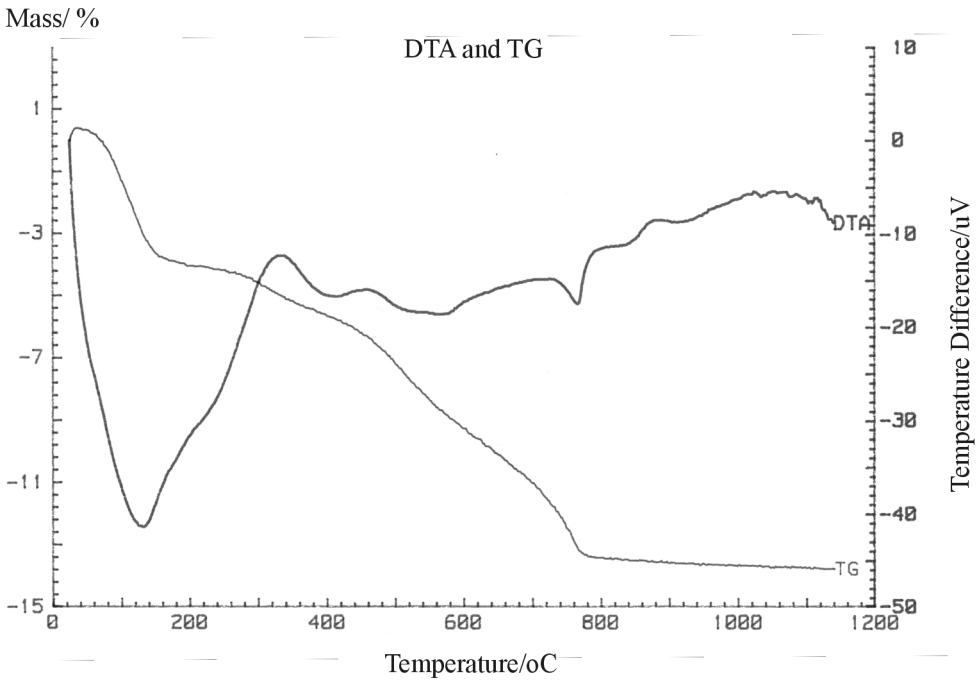

Figure 22 DTA/TG curve of a desalted surface sample from the Sambhar playa

Figure 22 shows the differential thermal analysis (DTA) and the thermogravimetric (TG) analytical curve of a desalted surface sample from the Sambhar playa. The first and strong endothermic effect between 100 and 150 °C mirrors the dehydration of water-bearing

Table 5 Comparative evaporate mineralogy from the surface sediments of the playa lakes

	Chlorides			Sulphates						Carbonates		
Playas	Halite ($NaCl$)	Sylvite (KCl)	Carnallite ($KMgCl_3 \cdot 6H_2O$)	Gypsum ($CaSO_4 \cdot 2H_2O$)	Anhydrite ($CaSO_4$)	Thenardite (Na_2SO_4)	Mirabilite ($Na_2SO_4 \cdot 10H_2O$)	Polyhalite ($K_2MgCa_2(SO_4)_4 \cdot 2H_2O$	Glauberite ($Na_2Ca(SO_4)_2$	Calcite ($CaCO_3$)	Dolomite ($CaMg(CO_3)_2$)	Trona ($Na_3H(CO_3)_2 \cdot 2H_2O$)
East												
Phulera	+				+	+				++++	+	
Sambhar	++++	++	+		+	+++	+	+		+++	+	
Sargot	++++			+	+	+			+	+		
Kuchaman	++++				+	+				+++	+	+
Didwana	++++				+	++				+++	+	++
West												
Bap-Malar	++++			+	+					+++	+	
Pokhran	++++			+	+					+++		
Pachapadra	++++			++	+					+++	+	
Thob	++++			+	+					+++		
That	++++				+					+	+	

(++++ = 20-30 %, +++ = 10-20 %, ++ = 5-10 %, + = < 5%)

(For the detail composition of the surface sediments see appendix table 1 to 10)

minerals (mixed layers and mirabilite). Between 500 and 600 °C the mixed layers dehydroxylate.This endothermic effect shows the mixed layers to be of the disordered smectite-illite type. The relatively sharp endothermic effect at 760 °C is caused by the decomposition of the calcite. Comparison of this peak decomposition temperature with the standard PA curves of Smykatz-Kloss (1974) indicates the amount of calcite to be around 4 %. The TG curve shows the amount of CO_2 released after the decomposition of $CaCO_3$ into CaO and CO_2 is around 1.6 mass % (Figure 22, left scale). This amount also corresponds to 3-4 % of $CaCO_3$. Another exothermic peak at 875 °C indicates the formation of a high temperature Mg-silicate phase after the (endothermic) decomposition of primary Mg-silicates. The most striking feature of this DTA curve is a remarkable exothermic effect at 325 °C, which is caused by the combustion of the organic carbon present in the sediments.

6.1.2 Depth profiles

Sediments samples were collected from six playas along the shallow depth profiles: three from the eastern (relatively humid) region and three from the western (relatively arid) region. The mineralogical distribution along these depth profiles are shown in tables 6 to 11.

Table 6 Mineralogy along the shallow depth profile of the Phulera playa

Depth (cm)	Quartz	Pl	KF	M	Ch	Am	Calcite $CaCO_3$	Dolomite $CaMg(CO_3)_2$	Huntite $CaMg_3(CO_3)_4$	Anhydrite $CaSO_4$	Glauberite $NaCa_2(SO_4)_2$	Halite NaCl
20	++++++	+++	+	+	+	+	+++	++	+			
30	++++++	++	+	+	+	+	++++	+++				
40	+++++	++	++	+	+	+	++++	+++				
50	+++++	++	+	+	+		++++	+++				
60	++++++	+		+	+	+	++++	+++				
70	++++	++	+	+	+		+++	+++++				+
80	+++++	++	+	+	+		++++	+++	+			
90	+++++	+++		+	+	+	++++	+++	+	+		
100	++++	+++	+	+	+	+	+++++	+++	+		+	
110	++++++	+++	+	+	+	+	++++	++				

(Pl= plagioclase, KF= K-feldspar, M= mica, Ch= chlorite, Am= amphibole)
(++++++ = >40%, +++++= 30-40%, ++++= 20-30%, +++= 10-20%, ++= 5-10%, += <5%)

The Phulera depth profile shows calcite, dolomite, quartz and and plagioclases as the main components. K-feldspars, mica, chlorite, amphibole and the evaporitic carbonate huntite, ($CaMg_3(CO_3)_4$) are present in minor components. Anhydrite, glauberite ($NaCa_2(SO_4)_2$) and halite are present in traces. These trace minerals are evaporitic and occur in one sample each (Table 6). Phulera is the only playa of this region with carbonates as the dominant evaporites.

The weight loss in TG curves shows the dolomite is occurring in amounts between 10 to 40 % (not included in Figure 23). The relatively sharp exothermic effect around 800 °C, caused by the oxidation of Fe^{2+} to Fe^{3+}, indicates the dolomite to be an iron-rich type. The large intensity of this oxidation effect prevents the occurrence of the endothermic decomposition effect of the carbonates (Emmerich & Smykatz-Kloss, 2002). Figure 23 shows the DTA curves of some of the Phulera samples from above to below with increasing depth.

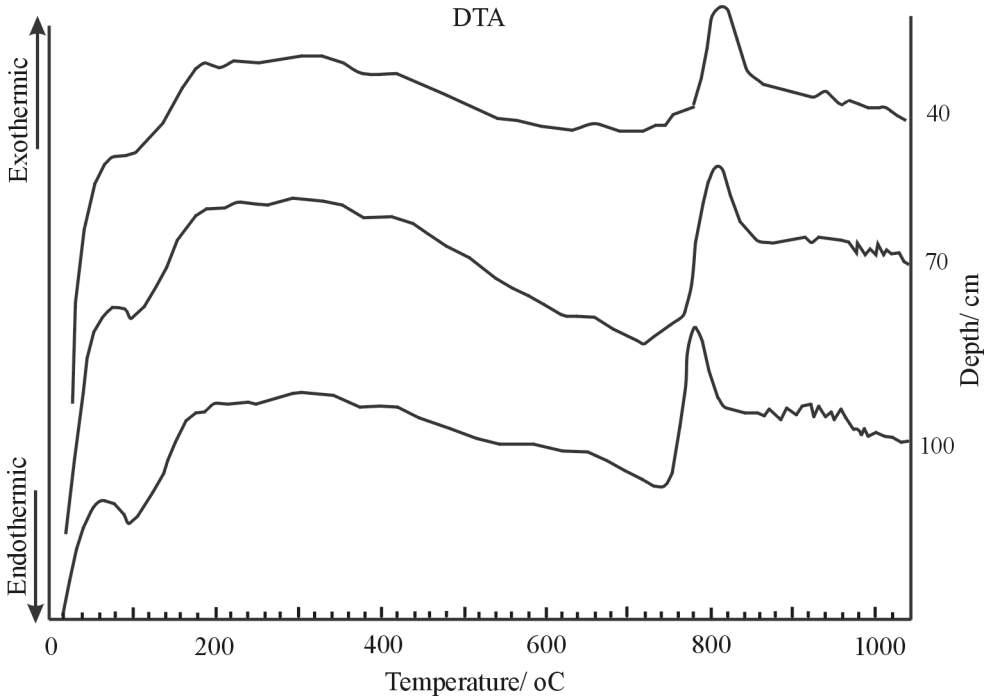

Figure 23 DTA curves of sediment samples of Phulera playa with increasing depth (right scale)

The profile of the Sambhar playa shows the similar mineralogical distribution as Phulera, with the exception of the presence of chlorides and sulphates. The chloride halite is present in traces in the Phulera, but occurs as a main component in the Sambhar profile (Table 7). Another chloride mineral, sylvite is occurring in trace amounts in one Sambhar sample. The sulphates are nearly absent in Phulera (Table 6), whereas they are commonly present in Sambhar (Table 7). Along the profiles of both the playas, the amount of dolomite is gradually increasing from surface to the depth of 70-75 cm (it shows a maximum, see Table 6, Table 7) and then decreasing again. The dolomite occurring in the Sambhar is iron-bearing and the sample shows to be rich in organic carbon as well (Figure 24). The combustion of organic carbon shows a very broad exothermic effect in the DTA curve of this Sambhar (75 cm depth) sample. The large weight loss occurring between 500 and 800 °C in the TG curve shows the dolomites to be strongly disordered.

Table 7 Mineralogy along the shallow depth profile of the Sambhar playa

Depth (cm)	Quartz	Pl	KF	M	Ch	Calcite $CaCO_3$	Dolomite $CaMg(CO_3)_2$	Anhydrite $CaSO_4$	Thenardite Na_2SO_4	Halite NaCl	Sylvite KCl
25	+++++	++	+	+	+	+++	+	+	+	+++	
50	+++++	++	+	+	+	++	+++	+	+	+++	+
75	+++	+	+	+	+	+	+++++	+	+	+++	
100	++++	+	+	+	+	+++	+++	+	+	++++	
125	++++	++	+	+	+	+++	+++	+	+	++++	

(Pl= plagioclase, KF= K-feldspar, M= mica, Ch= chlorite, Am= amphibole)
(++++++ = >40%, +++++= 30-40%, ++++= 20-30%, +++= 10-20%, ++= 5-10%, += <5%)

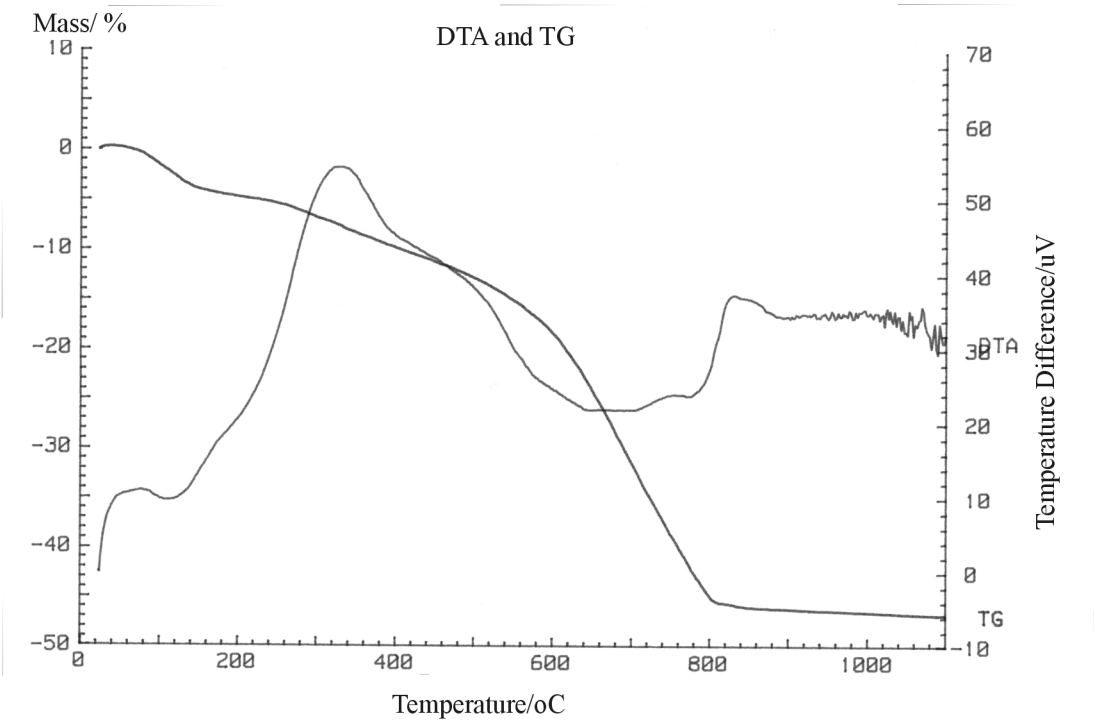

Figure 24. DTA/TG curve of a desalted Sambhar sample indicating the dolomite to be iron rich type

While dolomite is present as the dominant carbonate mineral in the Phulera and Sambhar profiles, in the neighbouring playa of Didwana calcite is occurring as the dominant evaporite in the depth profile of 120 cm. Here the carbonates dominate the sulphates and chlorides (Table 8). Dolomite is present in minor amounts from the depth of 60 cm to deeper horizons. The DTA curves of Didwana samples (e.g. from 60 cm and 105 cm depth respectively) do not show the iron oxide oxidation effect (Figure 25), but they show the oxidation of organic material (exothermic peak around 350 °C).

Table 8 Mineralogy of the Didwana playa along the depth profile

Depth (cm)	Quartz	Pl	KF	M	Ch	Am	An	Calcite ($CaCO_3$)	Dolomite $CaMg(CO_3)_2$	Anhydrite $CaSO_4$	Thenardite Na_2SO_4	Halite NaCl
15	++++++	+++	+	++	+	+	+	++		+	+	+
30	+++++	+++	+	+	+	+	+	+++	+	+	+	+++
45	+++++	++++	+	+	+	+	+	+++		+	+	++
60	+++++	+++	+	+	+		++	+++	++	+	+	++
75	++++++	+++	+	+	+	+	++	+++	++	+	+	++
90	++++++	+++	+	+	+		++	+++	++	+	+	++
105	+++++	+++	++	+	+		+	+++	++		+	++
120	+++++	+++	++	+	+		+	+++	++		+	+++

(Pl= plagioclase, KF= K-feldspar, M= mica, Ch= chlorite, Am= amphibole, An=analcime)
(++++++ = >40%, +++++= 30-40%, ++++= 20-30%, +++= 10-20%, ++= 5-10%, += <5%)

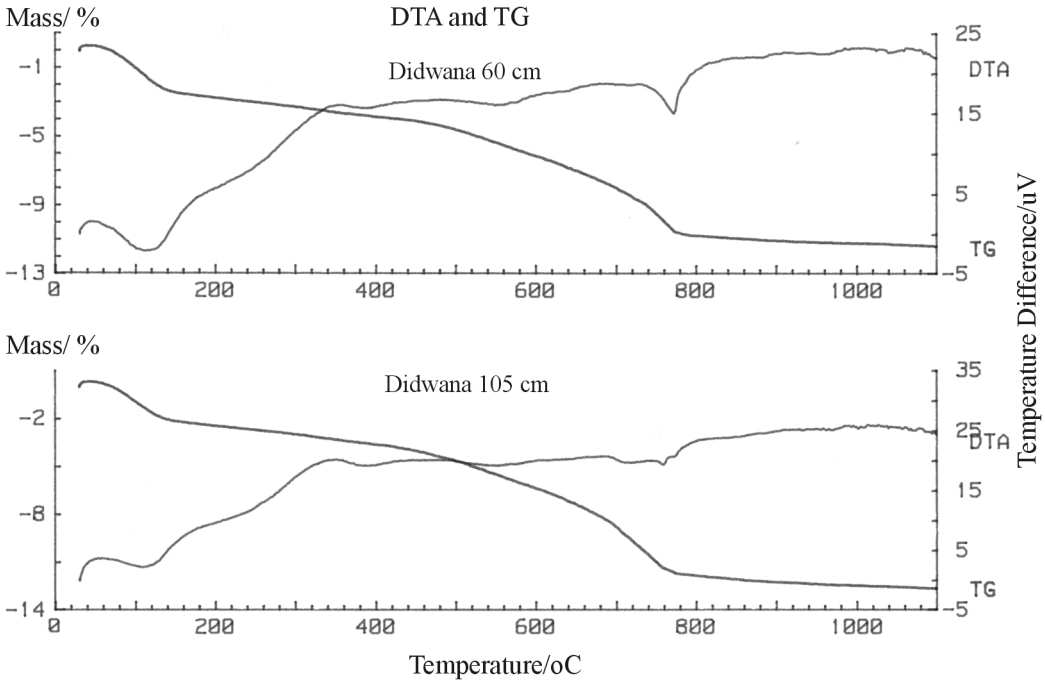

Figure 25 DTA/TG curves of desalted Didwana samples showing the combustion effect of organic matter (around 350 °C) and absence of Fe^{2+} oxidation peak

The remarkable endothermic effect around 550 °C mirrors the abundance of layer silicates (e.g. chlorite, mica). The profile is free of gypsum, but shows traces of sulphates free of water, e.g. anhydrite and thenardite (Table 8).

Calcite is the dominant carbonate in the western playa profiles (tables 9 to 11). Only Bap-Malar playa includes around 10 % of dolomite (Table 9), whereas this mineral is present in traces (< 5 %) in the Pokhran profile (Table 10) and absent in the Pachapadra profile (Table 11). The dolomite of Bap-Malar is iron rich as well (very sharp exothermic peak at 830 °C, see Figure 26). Bap-Malar is rich in halite. Detrital minerals like amphibole, hematite and the evaporate gypsum are present in traces (Table 9).

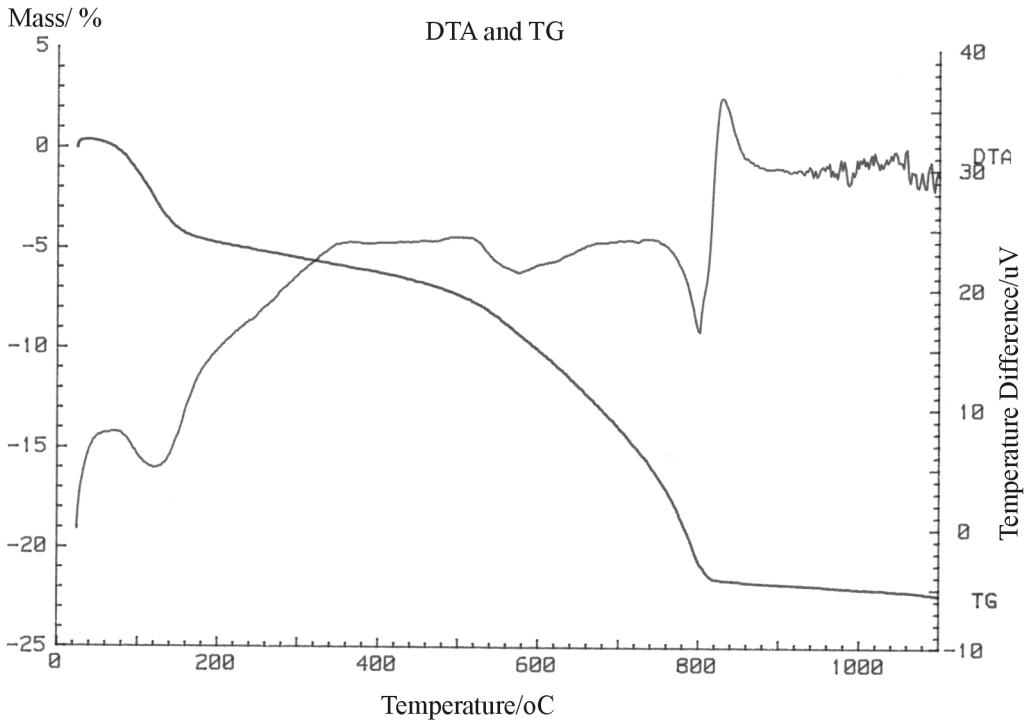

Figure 26 DTA/TG curve of a desalted Bap-Malar playa sample showing a very sharp exothermic Fe^{2+} oxidation peak

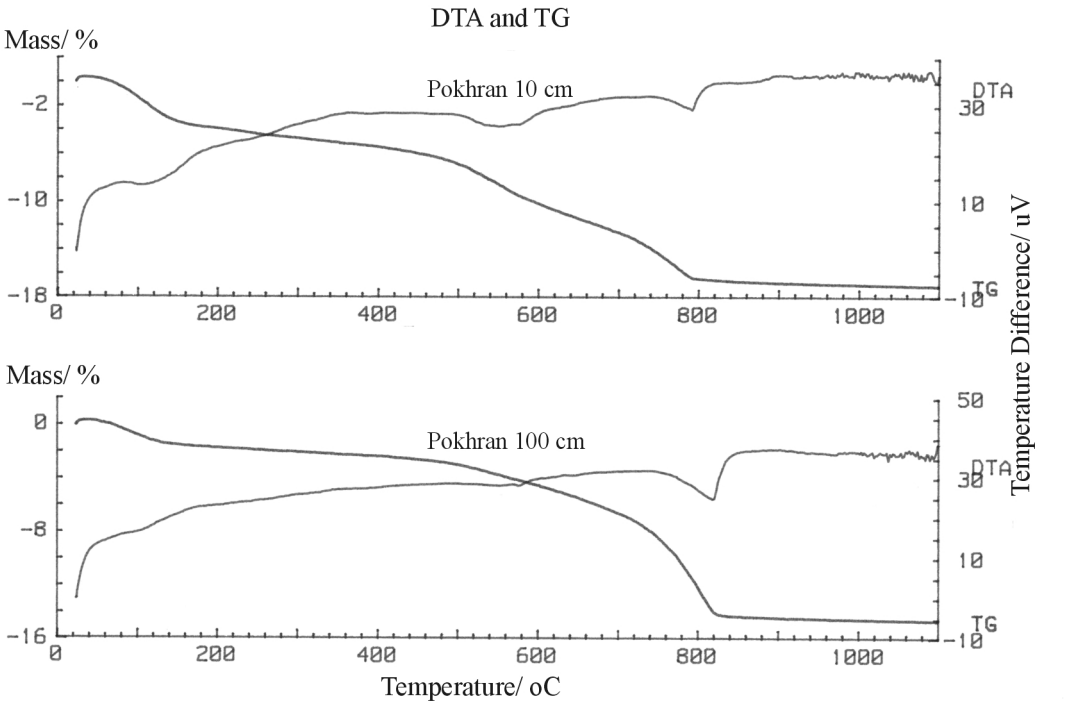

Figure 27 DTA/TG curves showing the thermal behaviour of two desalted samples from the Pokhran playa

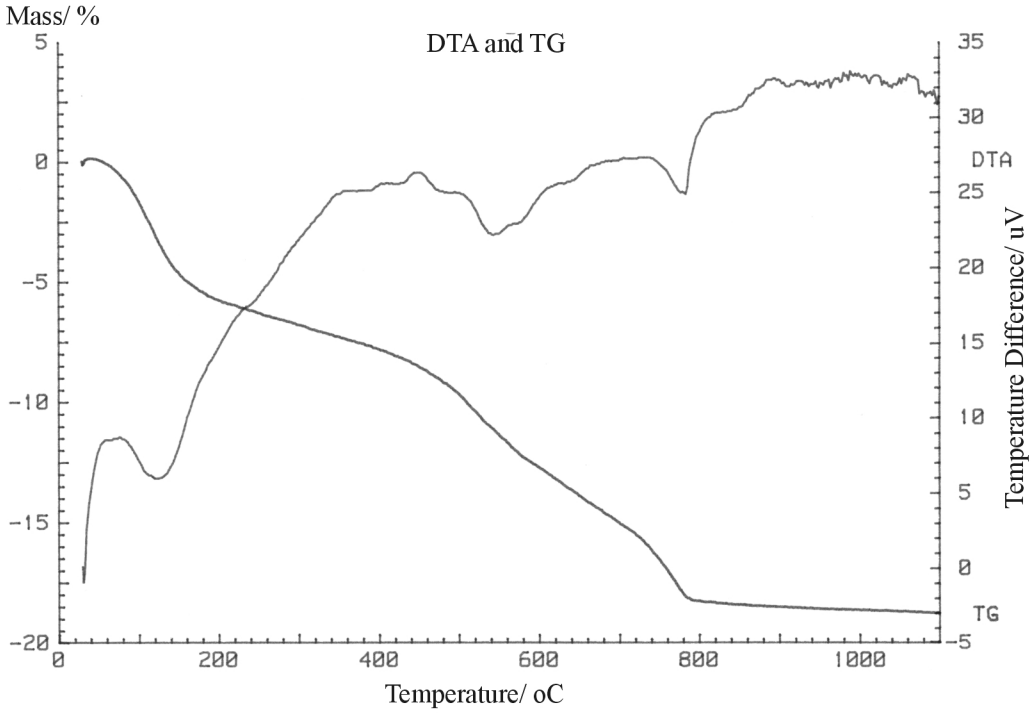

Figure 28 DTA/TG curve of a desalted sample from the Pachapadra playa

Table 9 Mineralogy along a shallow depth profile of the Bap-Malar playa

Depth (cm)	Quartz	Pl	KF	M	Ch	Am	Hematite	Calcite $CaCO_3$	Dolomite $CaMg(CO_3)_2$	Anhydrite $CaSO_4$	Gypsum $CaSO_4 \cdot 2H_2O$	Halite NaCl
25	++++	+	+	+	+			++++	++		+	++++
50	+++	+	+	+	+	+		+++++	++			+++++
70	+++	+	++	+	+		+	+++++	++		+	++++

Table 10 Mineralogy along the depth profile of the Pokhran playa

Depth (cm)	Quartz	Pl	KF	M	Ch	Am	Hematite	Palygorskite	Calcite $CaCO_3$	Dolomite $CaMg(CO_3)_2$	Anhydrite $CaSO_4$	Gypsum $CaSO_4 \cdot 2H_2O$	Halite NaCl
10	++++++	+++	+	+			+		+++				+
20	++++++	++	+	+	+		+		+++		+	+	+
30	++++++	+++		+	+		+		+++	+	+	+	+
40	++++	++		+	+							++++++	+
50	++++++	+++		+	+	+	+		+		+	+++	++
60	++++++	+++	+	+	+		+	+	+++	+	+	+	++
70	++++++	++		+	+		+		+++		+	+	+++
80	++++++	+++	+	+	+		+	+	+++		+	+	++
90	++++++	+++	++	+	+	+	+		+++	+	+	+	++
100	++++++	+++	+	+	+	+	+		+++	+	+		++
110	++++++	++	+	+	+				++	+	+		+
120	++++++	+++	+++	+	+	+			+++	+	+		+
130	++++++	+++	+	+	+	+			++	+	+		++
140	++++++	++	+			+			++++		+		+
150	++++++	++	+						++++		+		+
160	++++++	++	+						+++		+		+
170	++++++	+++	+	+	+		+		+	+	+		+
180	++++++	++	+	++	+		++		+	+	+		+
190	++++++	+++	+	++	+		++		+		+	+	+

(Pl= plagioclase, KF= K-feldspar, M= mica, Ch= chlorite, Am= amphibole) (++++++ = >40%, +++++= 30-40%, ++++= 20-30%, +++= 10-20%, ++= 5-10%, += <5%)

Gypsum is present in remarkable amounts in the profiles of Pokhran (Table 10) and Pachapadra (Table 11). It is confined to the uppermost 90 cm of Pokhran playa and occurs throughout the Pachapadra playa. Anhydrite is absent in Bap-Malar, whereas it is present in traces in the other two playas. Thenardite is occurring only in Pachapadra. Figure 27 shows the thermal behaviour of the Pokhran samples (at depths of 10 and 100 cm respectively) and Figure 28 shows that of a Pachapadra sample (100 cm depth). The Pokhran profile is the only one which exhibits traces of the Mg-silicate palygorskite. This mineral is occurring in the surface samples of the Sambhar playa as well. Recently, palygorskite has been reported from the aridic soils of Namibia (Eitel, 1993).

Table 11 Mineralogy along the depth profile of the Pachapadra playa

Depth (cm)	Quartz	Pl	KF	M	Ch	Am	Calcite CaCO3	Thenardite Na2SO4	Anhydrite CaSO4	Gypsum $CaSO_4.2H_2O$	Halite NaCl
10	++++++	++	+	+	+	+	+++		+	+	+++
20	++++++	++		+	+	+	++++	+		+	+++
30	+++++	++	+	+	+		++++			+	+++
40	+++++	++	+	+	+		++++	+		+	+++
50	++++++	++	+	+	+		+++		+	++	+++
60	++++++	++	+	+	+		+++		+	+	+++
70	+++++	++		+	+		++++			+	++++
80	+++++	+		+	+		++++			+	++++
90	++++++	++	+	+	+		+++			++	+++
100	+++++	++	+	+	+		++++			+	+++
110	+++++	+++	++	+	+		+++			+	+++
120	+++++	+++	+	+	+		+++			+	+++
130	++++++	+++	++	+	+	+	++	+	+	++	++
140	+++++	++		+	+		+++			+++++	+++
150	+++++	++		+	+	+	+++		+	+++	+++

(KF= K-feldspar, Pl= plagioclase, M= mica, Ch= chlorite, Am= amphibole)
(++++++ = >40%, +++++= 30-40%, ++++= 20-30%, +++= 10-20%, ++= 5-10%, += <5%)

6.2 Geochemistry

6.2.1 Surface samples

Table 12 and Table 13 present the chemical composition of the surface sediments of the studied playas. The contents of oxides of the most soluble cations, e.g. Na_2O, MgO, CaO, and of the cation Cu, are relatively higher in abundance in the western playas. The eastern playas on the other hand are showing higher concentration of less soluble hydrolysates, e.g. Al_2O_3, TiO_2, Fe_2O_3, SiO_2, Y, Zr, Ce, Ba and some soluble cations, e.g. Sr, Br, and Rb. Further the distribution of both the major and trace elements is more regular in the eastern playa sediments and random in the western.

Table 12 Major element concentration (in mass %) of the surface sediments of the studied playas

Playa (East)	Na_2O	MgO	Al_2O_3	SiO_2	P_2O_5	CaO	K_2O	TiO_2	MnO	Fe_2O_3
Phulera	3.62	2.51	8.70	67.94	0.15	5.87	1.62	0.40	0.05	2.55
Sambhar	2.55	3.16	12.99	50.84	0.15	5.53	2.26	0.55	0.09	5.27
Sargot	2.43	2.70	12.29	66.67	0.17	4.42	2.04	0.58	0.08	4.06
Kuchaman	1.70	3.12	13.00	63.72	0.16	4.27	2.29	0.55	0.09	4.66
Didwana	2.75	1.81	10.31	77.70	0.14	5.15	1.92	0.50	0.06	2.52
Average	2.61	2.66	11.46	65.37	0.15	5.05	2.03	0.52	0.08	3.81

Playa (West)	Na_2O	MgO	Al_2O_3	SiO_2	P_2O_5	CaO	K_2O	TiO_2	MnO	Fe_2O_3
Bap-Malar	1.82	5.17	11.09	71.03	0.15	4.61	2.36	0.52	0.08	3.99
Thob	17.10	1.49	7.51	54.77	0.07	5.59	1.07	0.39	0.04	2.11
That	4.02	2.62	11.27	69.18	0.13	4.78	1.66	0.26	0.03	1.60
Pachapadra	8.77	3.28	12.30	56.58	0.14	8.41	1.27	0.58	0.09	4.77
Pokhran						1.97		0.11	0.02	1.06
Average	7.93	3.14	10.54	62.89	0.12	5.07	1.59	0.37	0.05	2.70

Table 13 Trace element composition (in ppm) of the surface sediments of the studied playas

Playa (East)	Cu	Zn	Br	Rb	Sr	Y	Zr	Ba	La	Ce	Pb
Phulera	16	35	10	69	449	18	197	523	33	70	10
Sambhar	23	55	110	75	257	15	171	262	20	46	11
Sargot	22	48	81	88	412	20	173	360	31	58	16
Kuchaman	28	61	55	98	347	23	162	363	30	68	14
Didwana	15	29	48	60	367	20	228	313	35	70	9
Average	21	46	61	78	366	19	186	364	30	62	12

Playa (West)	Cu	Zn	Br	Rb	Sr	Y	Zr	Ba	La	Ce	Pb
Bap-Malar	24	53	2	73	168	22	199	398	33	68	17
Thob	78	36	28	47	204	17	179	218	34	65	9
That	18	27	11	35	278	11	100	169		38	2
Pachapadra	34	76	63	113	192	25	109	304	36	79	15
Pokhran	50	27	2	24	111	7	60	107	20	23	7
Average	41	44	21	59	191	16	129	239	34	55	10

Apart from these general observations on playa surfaces, some of the playas, e.g. Sambhar and Didwana, from the eastern desert margin show characteristic geochemical zones. On the basis of the major and trace elements concentration, the Sambhar playa is divided in three zones, e.g. A to C, (Figure 29) from western margin to the eastern margin. Table 14 presents the distribution of major and trace elements into the three geochemical zones of the Sambhar playa. The western-most zone A, situated at the mouth of the two rivers feeding the lake, is showing the highest concentration of hydrolysates, e.g. SiO_2, TiO_2, La, Ce, Y, Zr, Nb (Table 14). The eastern-most zone C is having the highest concentration of the major oxides, e.g. Na_2O, MgO, CaO, K_2O, MnO, Fe_2O_3, and trace elements, e.g. Cu, Zn, Br, Rb, and Sr. The intermediate zone B is showing lowest concentration of TiO_2, intermediate concentrations of all other major elements and the highest concentration of Ba (Table 14).

The Didwana playa, situated in the neighbourhood of the Sambhar playa, is also showing three characteristic geochemical zones, e.g. A to C (Figure 30), from the northern and southern margins to the lake centre. Table 15 shows the distribution of different major and trace elements present into the three different geochemical zones on the Didwana lake surface. Zone A, situated in the northern and southern marginal zones of the lake, is showing the highest concentration of SiO_2 along with Br. The Zone C, situated approximately in the centre of the lake, is having the highest concentration of Na_2O, MgO, CaO, Al_2O_3, K_2O, TiO_2, MnO, Fe_2O_3, Cu, Zn, Rb, and Sr. The intermediate zone B is showing intermediate concentrations of all the major elements and the highest concentration of Y, Zr, Nb, La, Ce, Pb, and Ba.

Table 14 Major and trace element distribution in the three geochemical zones of the Sambhar playa surface

Zone	Na_2O	MgO	Al_2O_3	SiO_2	P_2O_5	CaO	K_2O	TiO_2	MnO	Fe_2O_3	Trace elements (ppm)
	(mass %)										
A	1.95	1.80	9.80	74.23	0.11	4.58	1.87	0.71	0.07	2.87	La, Ce, Y, Zr, Nb
B	2.12	3.00	10.69	61.28	0.13	5.42	1.90	0.49	0.07	3.56	Ba
C	2.39	3.63	14.87	44.86	0.19	5.71	2.57	0.60	0.11	6.55	Cu, Zn, Br, Rb, Sr,

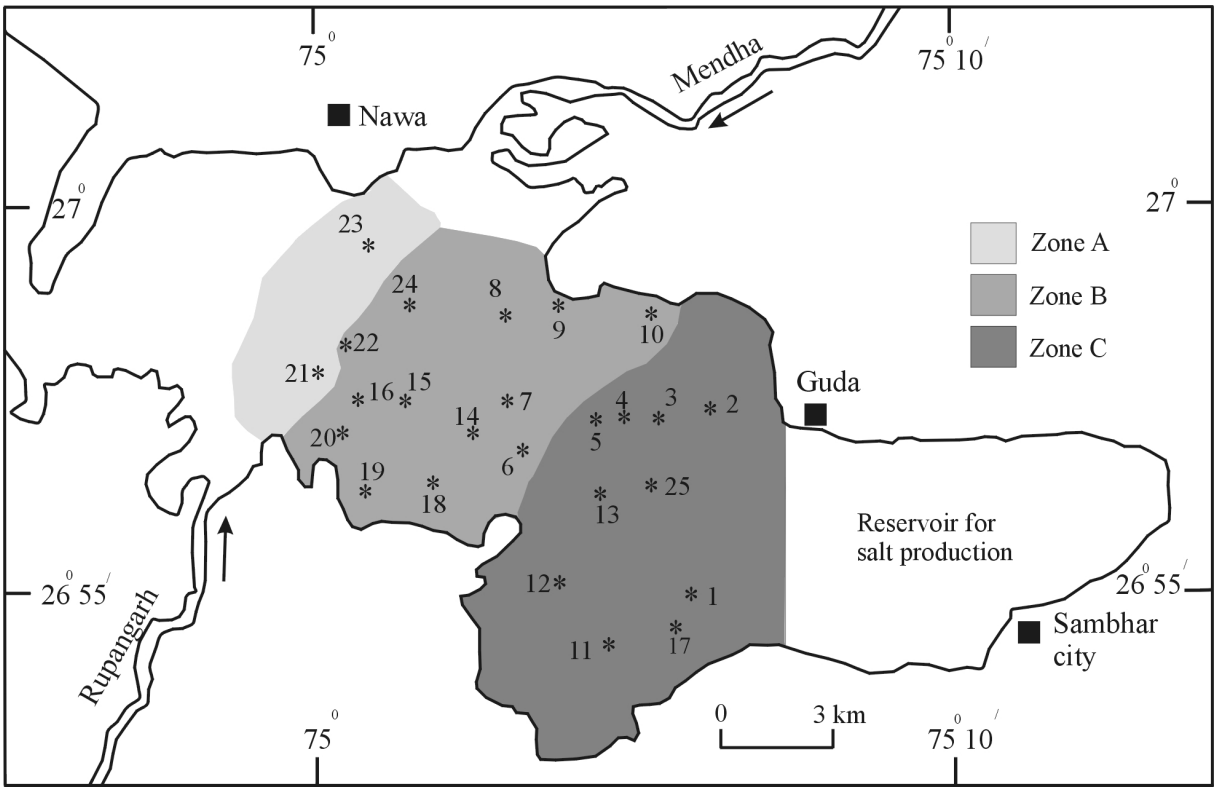

Figure 29 Map showing the geochemical zones due to the major and trace element concentrations in the Sambhar playa

The zonal pattern is comparable for the surfaces of both the eastern playas (table 16), except for the hydrolysate TiO_2. Comparing the average contents of major and trace elements for both regions (east and west), it is evident that the hydrolysates (e.g. Al_2O_3, Fe_2O_3, TiO_2, SiO_2, P_2O_5, MnO, and Zr) and those trace elements which exhibit very low solubility in the presence of HCO_3^- and SO_4^{2-} are enriched in the eastern playas. This is also valid for the large (soluble) cations. Inspite of their high solubility, K^+ and Rb^+ tend to be adsorbed by fine grained material (clay, organic matter). In contrast, very soluble cations, e.g. Na^+, Mg^{2+}, Ca^{2+}, are enriched in the western playas (Table 12).

Table 15 Major and trace element distribution into the three geochemical zones of the Didwana playa surface

Zone	Na_2O	MgO	Al_2O_3	SiO_2	P_2O_5	CaO	K_2O	TiO_2	MnO	Fe_2O_3	Trace elements (ppm)
	(mass %)										
A	2.35	1.32	8.70	77.73	0.10	4.56	1.71	0.34	0.04	1.64	Br, Sr
B	2.57	1.47	9.58	75.08	0.13	4.71	1.76	0.49	0.05	2.25	Y, Zr, La, Ce, Pb, Ba
C	2.87	2.51	11.05	67.55	0.16	5.49	2.06	0.55	0.07	3.27	Cu, Zn, Rb, Sr

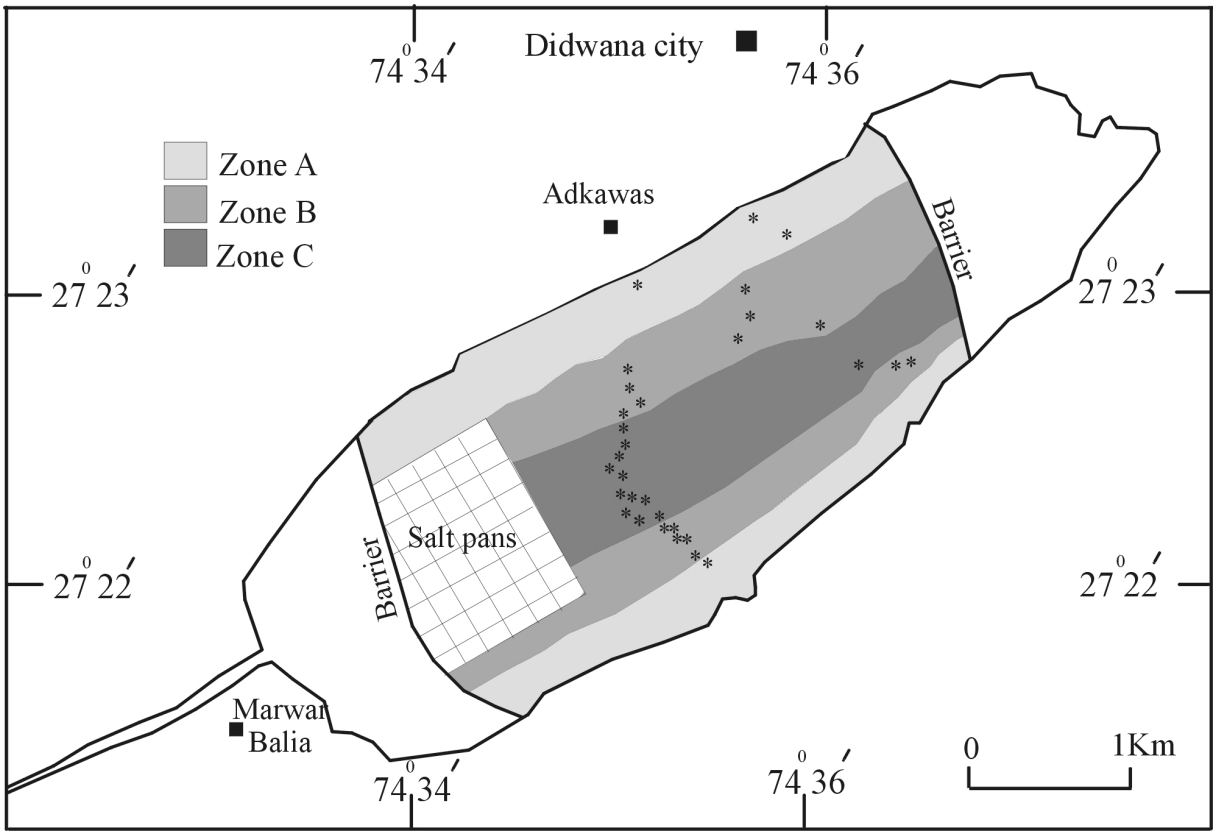

Figure 30 Map showing the geochemical zones due to the major and trace element concentrations in the Didwana playa

Table 16 Comparison between the geochemical zones of Sambhar and Didwana

	'A'		'B'		'C'	
Composition	Sambhar	Didwana	Sambhar	Didwana	Sambhar	Didwana
Na_2O	+	+	++	++	+++	+++
MgO	+	+	++	++	+++	+++
Al_2O_3	+	+	++	++	+++	+++
SiO_2	+++	+++	++	++	+	+
P_2O_5	+	+	++	++	+++	+++
CaO	+	+	++	++	+++	+++
K_2O	+	+	++	++	+++	+++
TiO_2	+++	+	+	++	++	+++
MnO	+	+	++	++	+++	+++
Fe_2O_3	+	+	++	++	+++	+++

(+ = lowest, ++ = intermediate, +++ = highest)

6.2.2 Depth profiles

Tables 17 to 22 present the distribution of major and trace elements for six playas (e.g. three from each region). Generally, the variation along the depth profiles is larger in the western

playas (Figure 31 to Figure 36). The remarkable enrichment of Sr, CaO, and MgO, in the horizon of 70 to 80 cm depth, is the most striking feature of the eastern playas. This enriched layer is very evident in the profiles of Phulera and Sambhar, less clear in Didwana. The western playas show a parallel enrichment of Sr with CaO (not with MgO) in two different horizons. The Pokhran playa shows two different Sr-enriched zones due to two different host minerals (e.g. at 40 cm due to gypsum and between 150 to 170 cm due to calcite). Similarly, Pachapadra playa exhibits a Sr enriched zone between 130 to 150 cm due to both calcite and gypsum.

Table 17 Major element (in mass %) and trace element (in ppm) distribution along the Phulera depth profile

Depth (cm)	Na_2O	MgO	Al_2O_3	SiO_2	P_2O_5	CaO	K_2O	TiO_2	Fe_2O_3	Cu	Zn	Br	Rb	Sr	Zr	Ba
	(mass %)									(ppm)						
0	3.62	2.51	8.70	67.94	0.15	5.87	1.62	0.40	2.55	16	35	10	69	449	197	523
20	2.11	6.83	10.37	53.69	0.22	7.98	2.19	0.47	4.37	20	64	6	87	954	145	347
30	2.03	7.63	9.78	51.16	0.22	8.69	1.98	0.45	4.16	27	63	8	77	1022	118	354
40	2.05	8.12	9.72	49.95	0.23	8.98	1.94	0.46	4.22	28	62	9	81	1199	134	324
50	2.00	8.72	9.42	48.07	0.22	9.46	1.84	0.44	4.07	24	57	9	76	1241	107	326
60	1.98	8.90	8.94	47.77	0.23	9.68	1.71	0.42	3.86	26	60	10	80	1405	133	332
70	1.82	11.91	7.13	37.30	0.17	12.57	1.28	0.35	3.24	22	52	11	64	2912	110	314
80	2.11	11.24	8.04	43.34	0.16	10.24	1.52	0.40	3.64	15	59	14	70	1704	115	319
90	2.18	10.98	8.03	44.30	0.15	10.53	1.54	0.40	3.72	20	52	12	62	1614	100	294
100	2.27	10.66	8.12	44.12	0.12	10.21	1.61	0.40	3.85	23	56	12	64	1680	101	282
110	2.28	10.11	9.17	47.15	0.12	8.77	1.94	0.44	4.37	24	58	10	73	1690	118	294

Table 18 Major element (in mass %) and trace element (in ppm) distribution along the Sambhar depth profile

Depth (cm)	Na_2O	MgO	Al_2O_3	SiO_2	P_2O_5	CaO	K_2O	TiO_2	Fe_2O_3	Cu	Zn	Br	Rb	Sr	Zr	Ba
	(mass %)									(ppm)						
0	2.55	3.16	12.99	50.84	0.15	5.53	2.62	0.55	5.27	23	55	110	75	257	171	262
25	2.17	5.45	13.34	47.05	0.17	7.83	2.69	0.59	5.97	38	65	52	99	921	149	437
50	2.32	6.92	12.96	44.84	0.14	8.24	2.4	0.55	5.76	34	67	71	89	1012	140	403
70	1.63	11.84	9.06	34.6	0.08	11.58	1.73	0.39	4.12	27	50	108	64	2211	81	354
100	1.71	10.82	8.63	41.2	0.13	11.65	1.7	0.39	3.84	35	57	130	63	1529	87	269
125	1.76	10.25	9.18	39.79	0.09	12.93	1.78	0.4	4.1	29	46	133	67	1312	89	328

Table 19 Major element (in mass %) and trace element (in ppm) distribution along the Didwana depth profile

Depth (cm)	Na_2O	MgO	Al_2O_3	SiO_2	P_2O_5	CaO	K_2O	TiO_2	Fe_2O_3	Cu	Zn	Br	Rb	Sr	Zr	Ba
	(mass %)									(ppm)						
0	2.75	1.81	10.31	77.70	0.14	5.15	1.92	0.50	2.52	15	29	48	60	367	228	313
15	2.61	4.80	13.99	54.70	0.21	5.63	2.90	0.62	5.49	29	79	35	108	563	150	375
30	2.60	4.51	13.81	56.44	0.19	5.27	2.86	0.59	5.28	30	76	40	107	560	154	369
45	2.54	5.14	13.99	53.11	0.22	6.09	2.97	0.61	5.49	33	68	39	107	653	130	363
60	2.52	5.05	14.13	52.23	0.19	6.16	2.86	0.60	5.77	33	76	37	113	704	133	388
75	2.55	5.72	13.27	53.97	0.19	5.55	2.79	0.56	5.29	33	66	39	101	682	134	350
90	2.56	6.00	12.88	52.29	0.20	6.67	2.75	0.56	5.07	27	78	37	99	804	109	351
105	2.71	6.33	13.43	50.34	0.19	7.11	2.82	0.58	5.53	28	71	48	99	786	109	363
120	2.55	6.33	12.70	50.87	0.16	7.83	2.68	0.58	5.12	26	64	60	93	838	118	344

Table 20 Major element (in mass %) and trace element (in ppm) distribution along the Bap-Malar depth profile

Depth (cm)	Na_2O	MgO	Al_2O_3	SiO_2	P_2O_5	CaO	K_2O	TiO_2	Fe_2O_3	Cu	Zn	Br	Rb	Sr	Zr	Ba
	(mass %)									(ppm)						
0	1.82	5.17	11.09	71.03	0.15	4.61	2.36	0.52	3.99	24	53	2	73	168	199	398
25	5.37	14.03	11.99	49.15	0.22	10.11	1.70	0.48	5.08	32	101	17	67	844	85	356
50	5.52	15.31	10.92	46.83	0.21	12.68	0.86	0.43	4.66	25	101	19	66	1105	90	339
70	5.51	15.22	10.76	47.05	0.20	13.27	0.87	0.43	4.47	32	107	17	67	1199	89	333

Table 21 Major element (in mass %) and trace element (in ppm) distribution along the Pokhran depth profile

Depth (cm)	Na_2O	MgO	Al_2O_3	SiO_2	P_2O_5	CaO	K_2O	TiO_2	Fe_2O_3	Cu	Zn	Br	Rb	Sr	Zr	Ba
	(mass %)									(ppm)						
10	2.71	3.41	16.11	62.78	0.19	5.00	3.47	0.66	6.45	26	74	5	109	173	163	387
20	2.15	3.72	16.92	61.46	0.20	5.17	3.65	0.71	6.91	29	73	4	120	177	174	391
30	2.11	3.85	17.17	60.24	0.22	5.52	3.71	0.72	7.03	31	83	3	119	183	166	384
40	1.32	1.61	7.33	29.22	0.11	25.47	1.66	0.32	3.19	12	33	5	47	302	75	167
50	2.98	3.60	14.64	58.00	0.20	8.84	3.31	0.68	6.11	25	68	6	110	241	165	374
60	3.15	4.48	15.88	59.91	0.22	6.32	3.61	0.73	6.60	26	71	8	127	239	185	410
70	3.63	4.30	15.63	59.55	0.21	7.09	3.38	0.73	6.42	26	67	11	117	245	191	383
80	3.56	4.29	14.17	62.34	0.20	7.07	2.93	0.71	5.70	26	62	9	108	245	219	387
90	3.53	3.60	12.16	66.28	0.18	8.05	1.99	0.76	4.84	18	47	9	78	244	319	377
100	3.15	2.87	10.60	68.14	0.16	7.98	1.64	0.81	4.88	17	44	8	63	227	400	377
110	2.13	1.47	7.63	76.82	0.10	7.73	1.85	0.40	2.99	15	36	4	48	178	241	467
120	2.62	1.39	9.86	73.51	0.07	8.63	1.68	0.35	2.92	12	29	5	57	176	126	372
130	3.24	1.70	10.97	71.40	0.08	7.55	1.59	0.52	3.74	16	44	6	62	470	222	344
140	2.31	1.37	8.31	71.68	0.10	11.98	1.75	0.49	3.61	14	39	4	47	159	292	425
150	2.07	1.27	7.34	71.53	0.11	12.93	1.68	0.49	3.75	11	33	5	42	485	285	615
160	2.05	1.16	7.01	72.20	0.10	13.50	1.59	0.42	3.21	10	34	5	40	1230	217	525
170	2.64	1.96	13.91	69.01	0.11	2.91	3.72	0.67	4.90	19	50	5	120	2561	237	950
180	2.36	2.78	20.53	58.44	0.17	0.80	5.51	0.81	8.35	43	79	5	172	112	194	366
190	2.20	2.79	20.48	58.49	0.15	1.24	5.69	0.77	8.15	19	74	4	182	105	182	406

Table 22 Major element (in mass %) and trace element (in ppm) distribution along the Pachapadra depth profile

Depth (cm)	Na_2O	MgO	Al_2O_3	SiO_2	P_2O_5	CaO	K_2O	TiO_2	Fe_2O_3	Cu	Zn	Br	Rb	Sr	Zr	Ba
	(mass %)									(ppm)						
0	8.77	3.28	12.30	56.58	0.14	8.41	1.27	0.58	4.77	27	56	45	91	252	138	305
10	4.07	3.87	15.31	58.27	0.18	8.62	2.23	0.74	6.62	33	76	27	119	228	142	367
20	4.52	4.75	16.42	53.42	0.18	9.02	2.26	0.76	7.79	58	84	32	124	226	114	332
30	4.51	5.16	17.23	51.10	0.18	9.07	2.48	0.77	8.48	42	93	31	136	230	102	328
40	4.59	4.69	17.28	51.88	0.19	8.28	2.59	0.79	8.38	47	95	37	140	226	105	359
50	4.11	5.34	15.86	53.51	0.19	8.32	2.58	0.73	7.42	39	79	28	120	246	118	360
60	4.34	5.24	16.83	54.67	0.20	7.22	2.67	0.76	7.94	38	89	32	128	218	118	372
70	4.46	5.15	17.48	52.16	0.19	7.67	2.70	0.78	8.46	44	95	31	138	226	105	344
80	4.79	5.06	18.05	50.21	0.20	7.54	2.74	0.77	9.01	46	100	35	132	233	95	353
90	4.36	5.43	17.00	53.59	0.19	7.03	2.72	0.74	8.09	37	87	30	132	233	108	372
100	4.66	5.38	17.90	51.77	0.20	7.05	2.81	0.77	8.95	48	97	35	145	208	99	361
110	4.74	4.93	16.84	53.89	0.20	7.62	2.50	0.69	7.92	47	92	35	124	238	102	371
120	4.80	4.71	16.97	53.61	0.19	7.14	2.54	0.73	7.97	45	88	34	127	218	100	355
130	3.98	3.41	12.02	67.44	0.14	5.40	2.10	0.46	4.10	25	49	23	84	209	104	360
140	4.60	4.29	10.55	40.28	0.11	19.96	1.75	0.49	5.22	31	60	31	70	4327	133	272
150	4.61	4.99	12.03	46.84	0.12	17.51	1.77	0.58	5.39	29	60	34	84	642	107	227

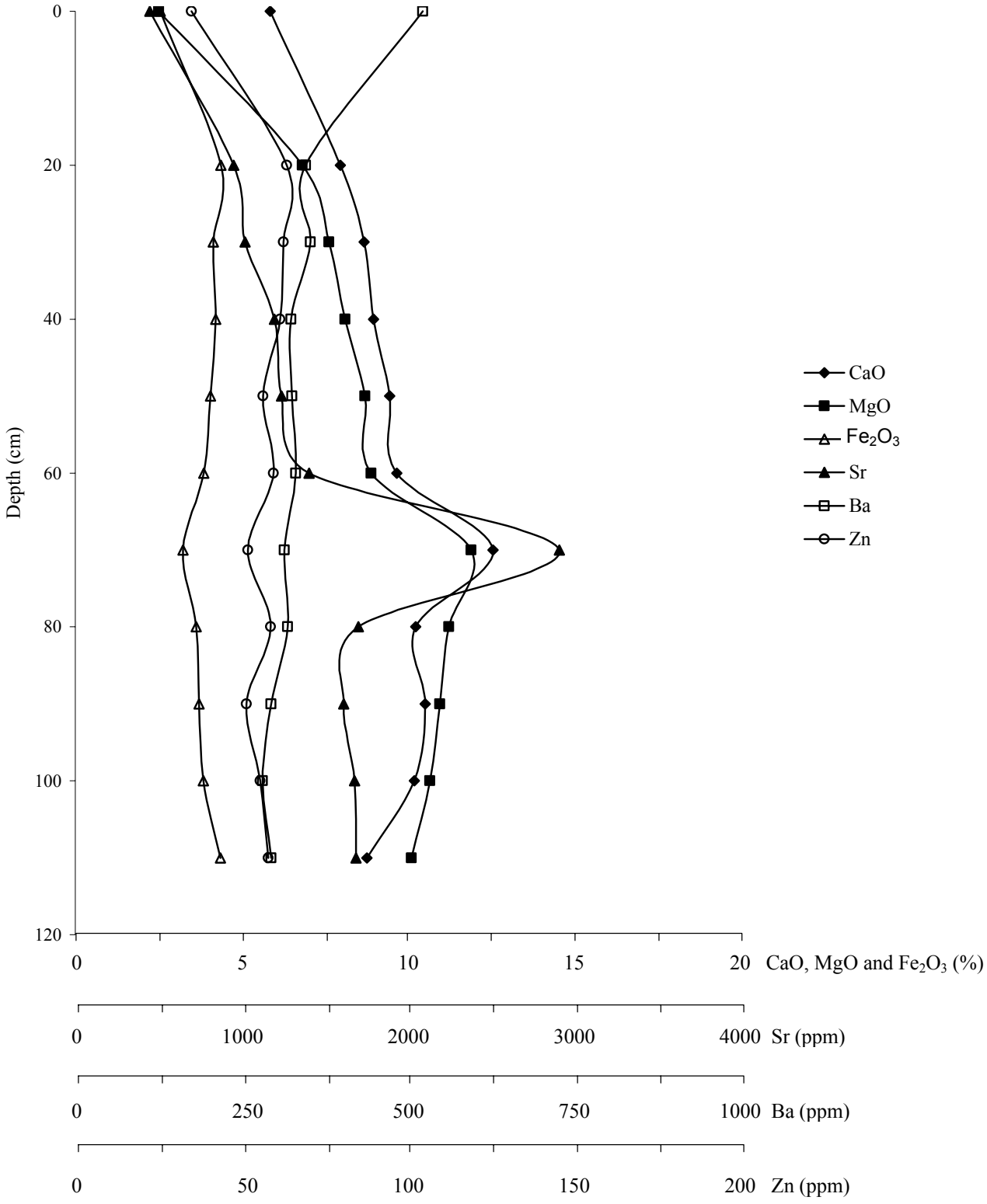

Figure 31. Distribution of some major and trace elements along the Phulera profile

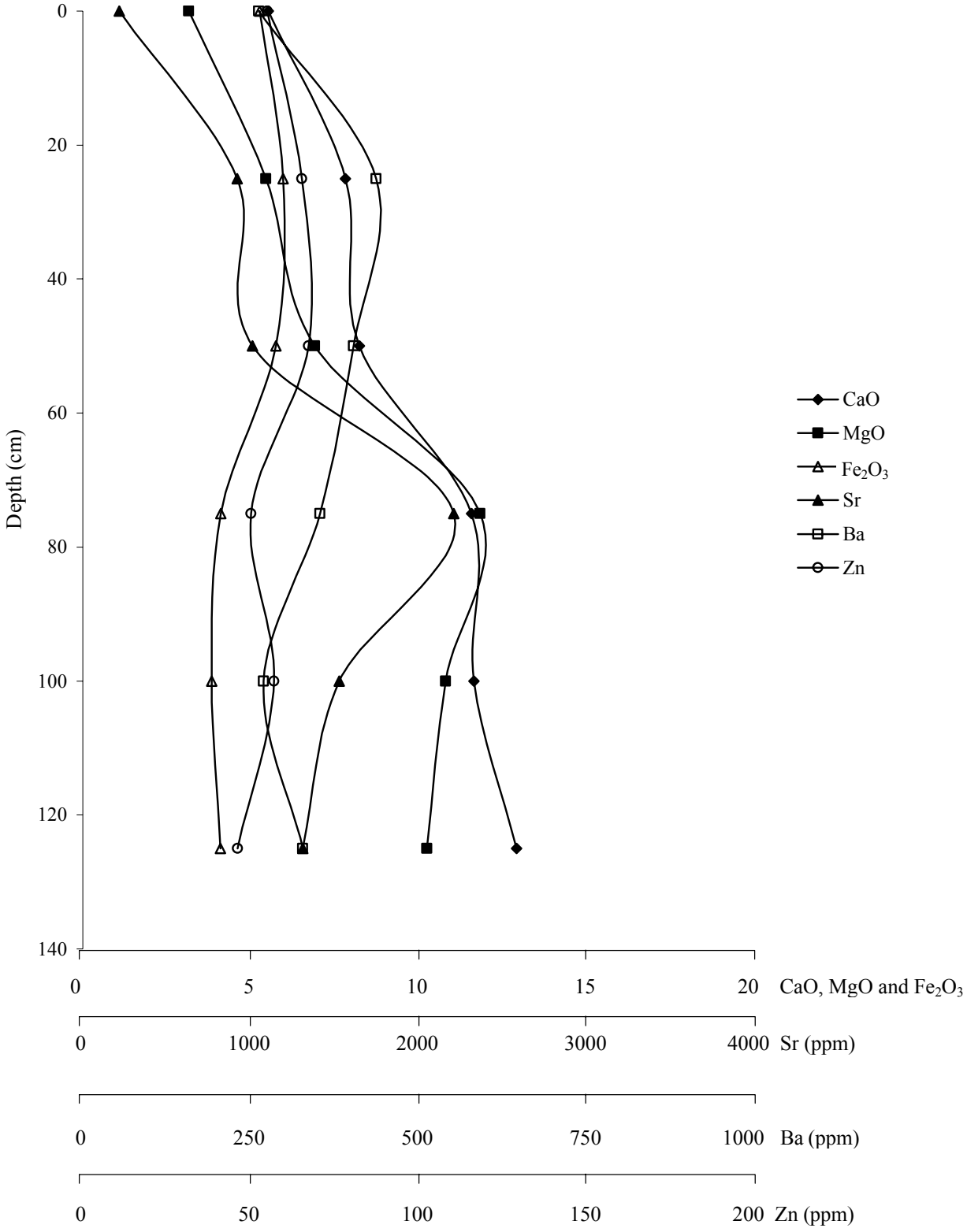

Figure 32 Distribution of some major and trace elements along the Sambhar profile

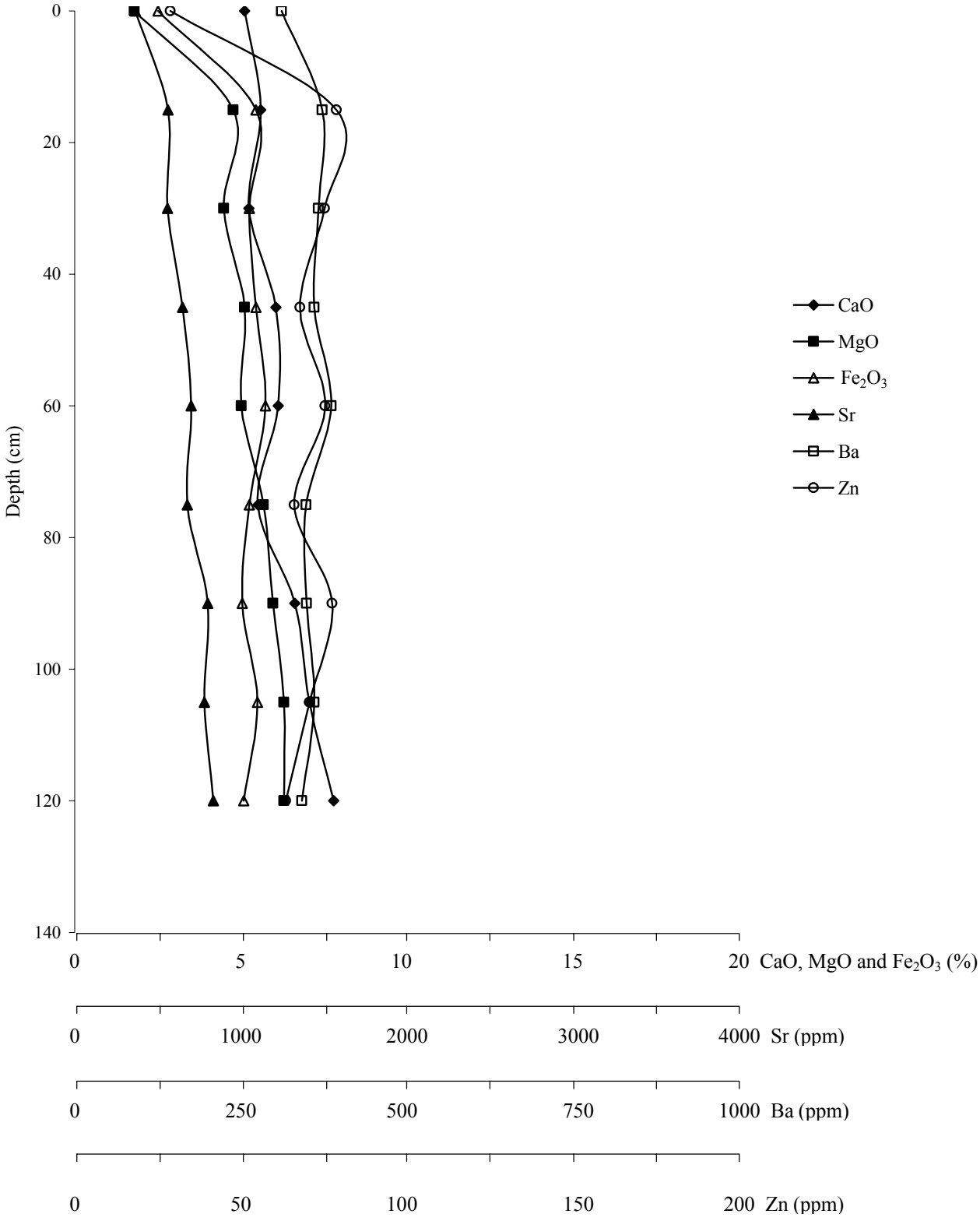

Figure 33 Distribution of some major and trace elements along the Didwana profile

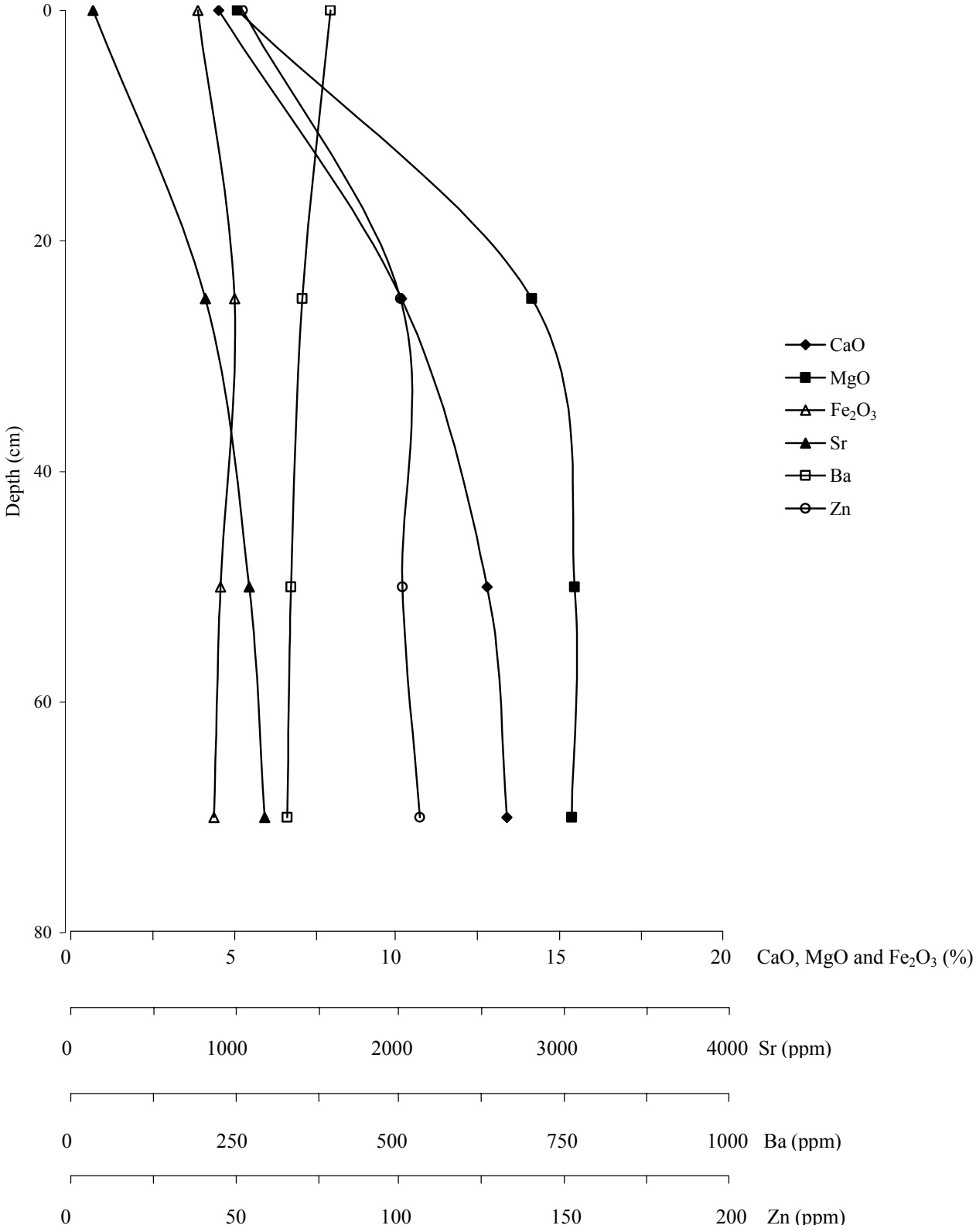

Figure 34 Distribution of some major and trace elements along the Bap-Malar profile

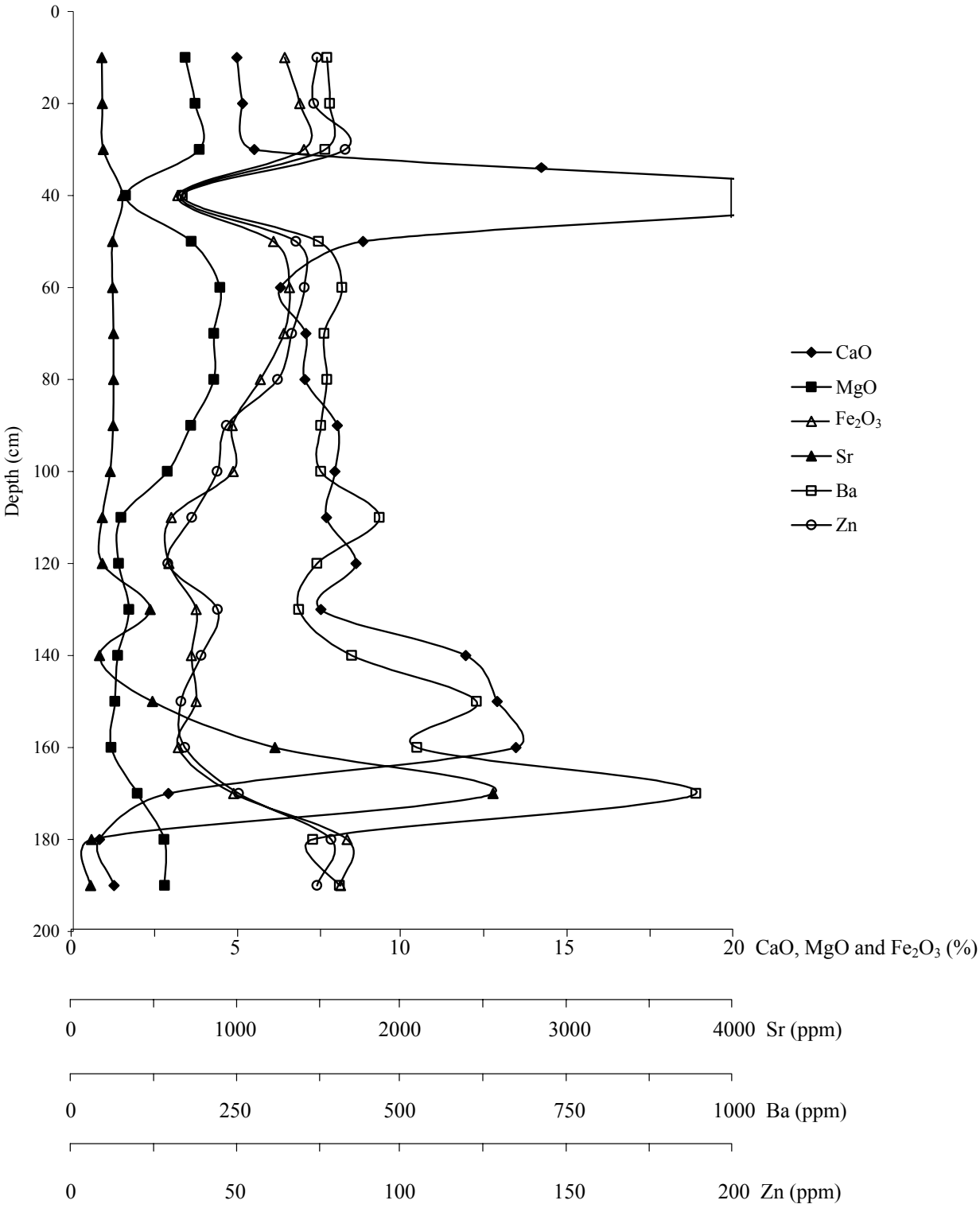

Figure 35 Distribution of some major and trace elements along the Pokhran profile

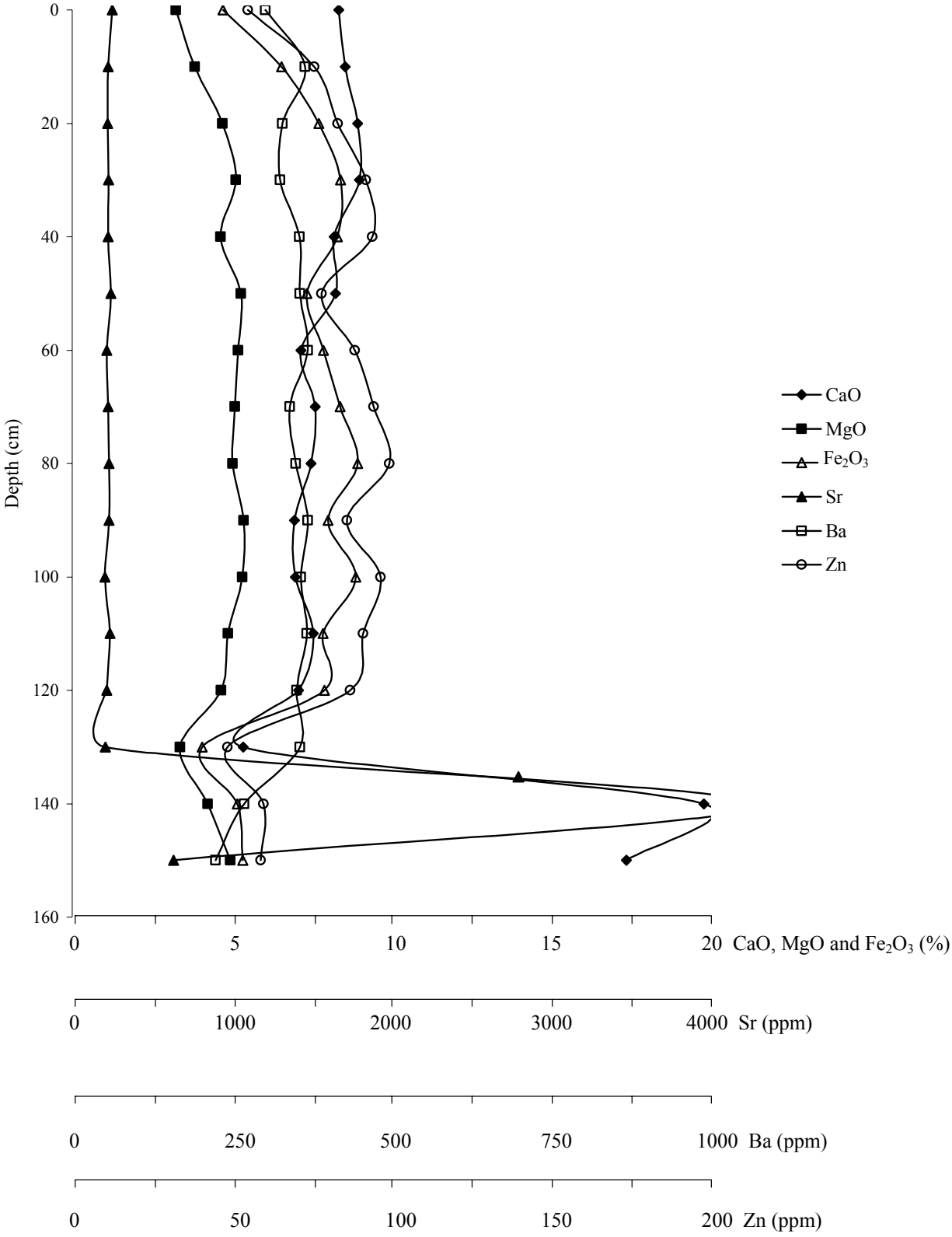

Figure 36 Distribution of some major and trace elements along the Pachapadra profile

Table 23 Average major and trace element concentration in different geochemical zones of Phulera playa

Zone	Depth (cm)	Na_2O	MgO	Al_2O_3	SiO_2	P_2O_5	CaO	K_2O	TiO_2	MnO	Fe_2O_3	Cu	Zn	Rb	Sr	Zr	Ba
		(mass %)										(ppm)					
I	0-20	2.64	3.49	9.68	65.64	0.16	5.66	2.00	0.47	0.06	3.47	19	39	70	496	185	357
II	20-60	2.03	8.04	9.65	50.13	0.22	8.96	1.93	0.45	0.08	4.14	25	61	80	1165	128	337
III	60-100	2.04	11.38	7.73	41.65	0.16	11.11	1.45	0.38	0.08	3.53	19	54	65	2077	108	309
IV	100-110	2.28	10.39	8.65	45.64	0.12	9.49	1.78	0.42	0.08	4.11	23	57	68	1685	110	288

Table 24 Average major and trace element concentration in different geochemical zones of Sambhar playa

Zone	Depth (cm)	Na_2O	MgO	Al_2O_3	SiO_2	P_2O_5	CaO	K_2O	TiO_2	MnO	Fe_2O_3	Cu	Zn	Rb	Sr	Zr	Ba
		(mass %)										(ppm)					
I	0-25	2.55	3.16	12.99	50.84	0.15	5.53	2.62	0.55	0.09	5.27	23	55	75	257	171	262
II	25-75	2.25	6.19	13.15	45.95	0.16	8.04	2.55	0.57	0.10	5.87	36	66	94	966	145	420
III	75-125	1.70	10.97	8.96	38.53	0.10	12.05	1.74	0.39	0.08	4.02	30	51	65	1684	86	317

Table 25 Average major and trace element concentration in different geochemical zones of Didwana playa

Zone	Depth (cm)	Na_2O	MgO	Al_2O_3	SiO_2	P_2O_5	CaO	K_2O	TiO_2	MnO	Fe_2O_3	Cu	Zn	Rb	Sr	Zr	Ba
		(mass %)										(ppm)					
I	0-15	2.75	1.81	10.31	77.70	0.14	5.15	1.92	0.50	0.08	2.52	15	29	60	367	228	313
II	15-90	2.56	5.04	13.84	54.09	0.20	5.74	2.88	0.60	0.10	5.47	31	73	107	632	140	369
III	90-120	2.61	6.22	13.00	51.17	0.18	7.20	2.75	0.57	0.10	5.24	27	71	97	809	112	352

Table 26 Average major and trace element concentration in different geochemical zones of Bap-Malar playa

Zone	Depth (cm)	Na_2O	MgO	Al_2O_3	SiO_2	P_2O_5	CaO	K_2O	TiO_2	MnO	Fe_2O_3	Cu	Zn	Rb	Sr	Zr	Ba
		(mass %)										(ppm)					
I	0-25	1.82	5.17	11.09	71.03	0.15	4.61	2.36	0.52	0.08	3.99	24	53	73	168	199	398
II	25-70	5.47	14.85	11.22	47.68	0.21	12.02	1.14	0.45	0.10	4.74	30	103	139	194	139	362

Table 27 Average major and trace element concentration in different geochemical zones of Pokhran playa

Zone	Depth (cm)	Na_2O	MgO	Al_2O_3	SiO_2	P_2O_5	CaO	K_2O	TiO_2	MnO	Fe_2O_3	Cu	Zn	Rb	Sr	Zr	Ba
		(mass %)										(ppm)					
I	0-10	3.15	2.08	11.35	63.38	0.12	4.39	2.12	0.53	0.06	4.15	23	53	87	187	200	368
II	10-30	2.32	3.66	16.74	61.49	0.20	5.23	3.61	0.70	0.09	6.80	29	77	116	178	168	387
III	30-50	1.32	1.61	7.33	29.22	0.11	25.47	1.66	0.32	0.04	3.19	12	33	47	302	75	167
IV	50-110	3.33	3.86	13.85	62.37	0.19	7.56	2.81	0.74	0.09	5.76	23	60	100	240	247	385
V	110-180	2.43	1.47	9.29	72.31	0.10	9.32	1.98	0.48	0.07	3.59	14	38	59	751	231	528
VI	180-190	2.28	2.79	20.50	58.46	0.16	1.02	5.60	0.79	0.05	8.25	31	77	177	109	188	386

Table 28 Average major and trace element concentration in different geochemical zones of Pachapadra playa

Zone	Depth (cm)	Na_2O	MgO	Al_2O_3	SiO_2	P_2O_5	CaO	K_2O	TiO_2	MnO	Fe_2O_3	Cu	Zn	Rb	Sr	Zr	Ba
		(mass %)										(ppm)					
I	0-10	8.77	3.28	12.30	56.58	0.14	8.41	1.27	0.58	0.09	4.77	27	56	91	252	138	305
II	10-120	4.50	4.98	16.93	53.17	0.19	7.88	2.57	0.75	0.13	8.09	44	90	130	227	109	356
III	130-150	4.40	4.23	11.53	51.52	0.12	14.29	1.87	0.51	0.10	4.91	28	56	79	1726	115	286

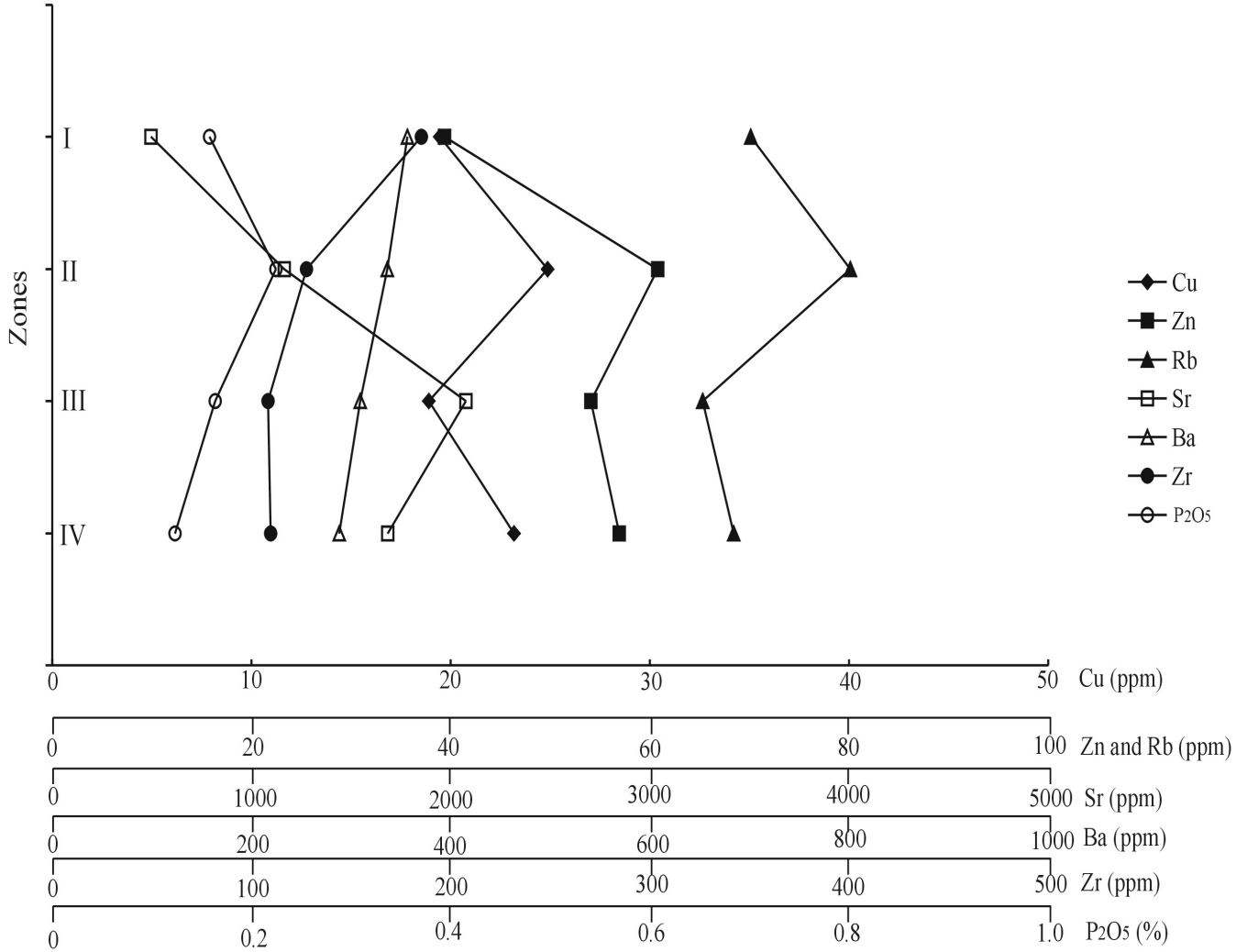

Figure 37 Average concentration of some trace elements in the four geochemical zones of Phulera playa

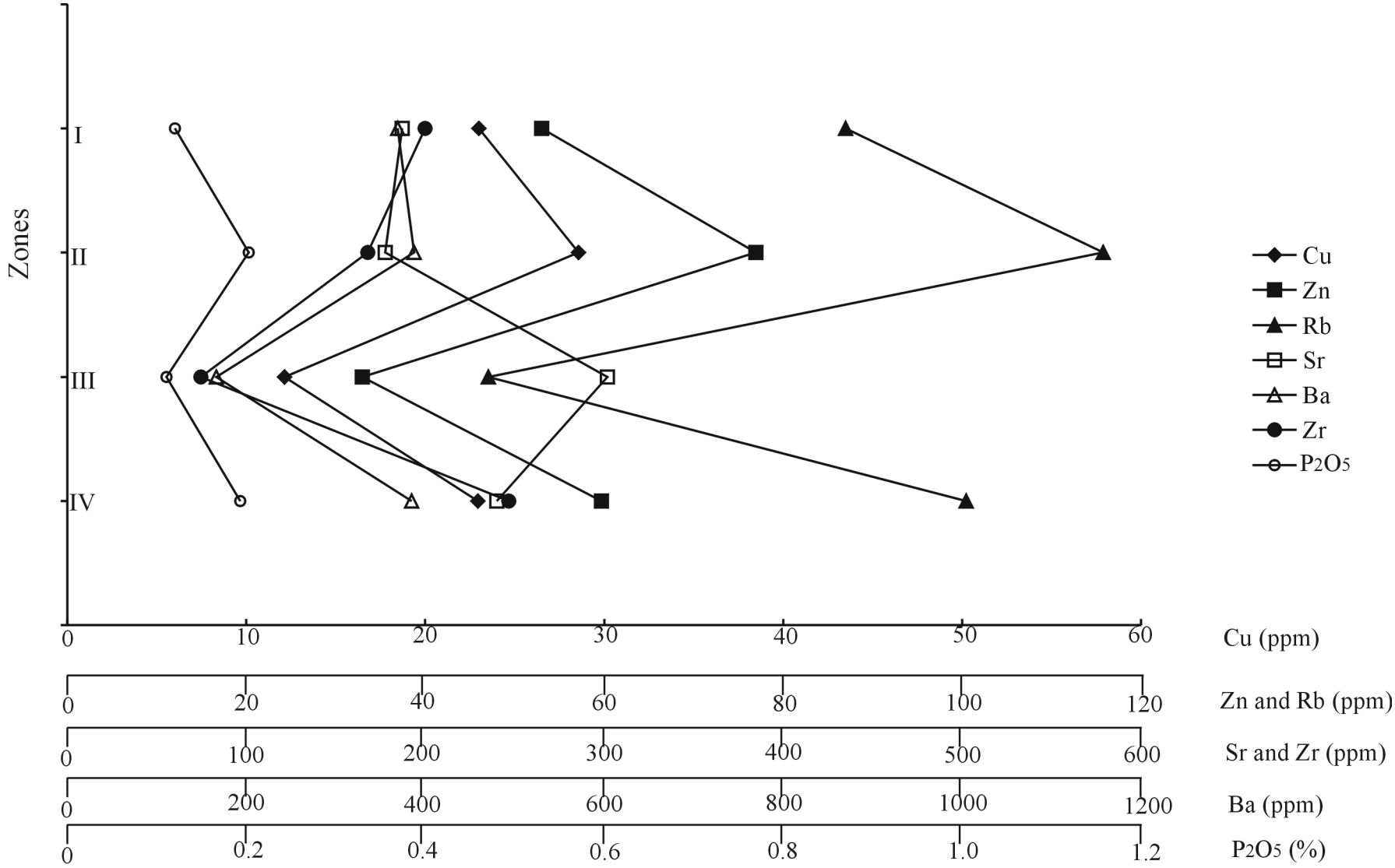

Figure 38 Average concentration of some trace elements in the geochemical zones of Pokhran playa

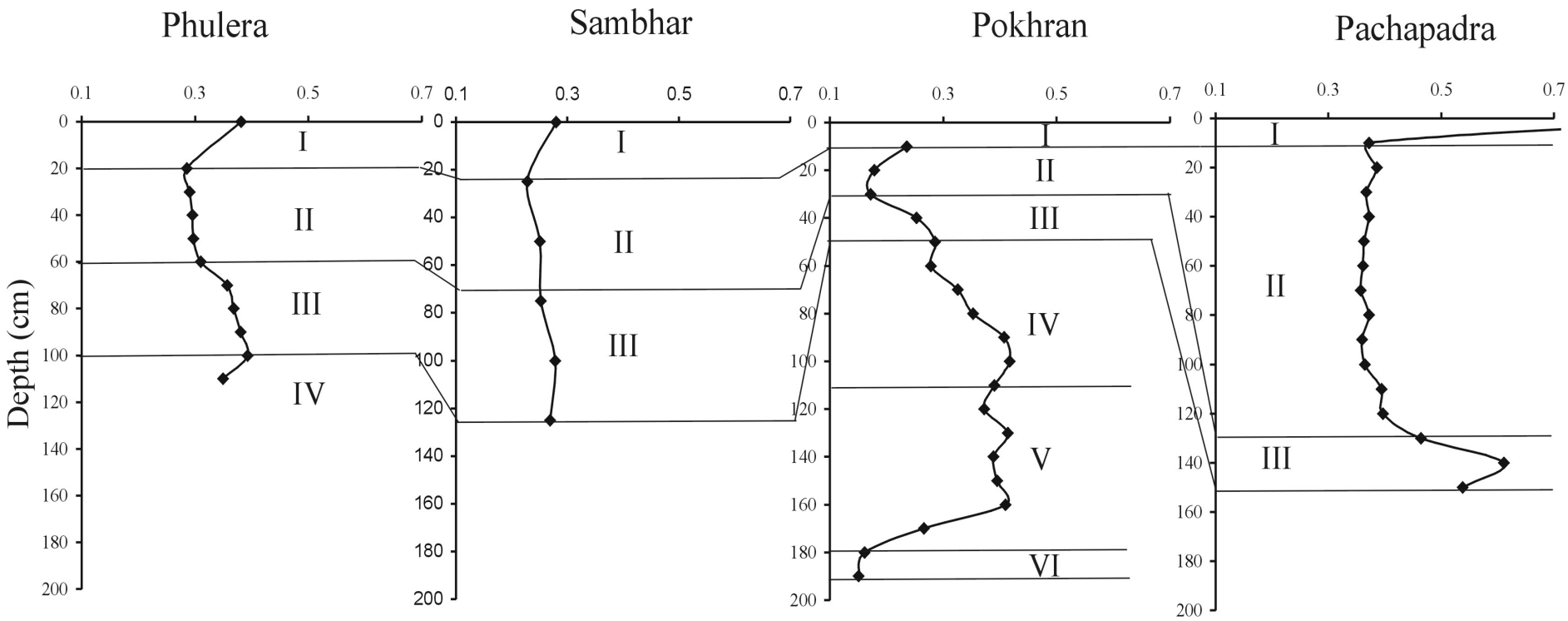

Figure 39 The variation of Na/Al along the depth profiles of Phulera, Sambhar, Pokhran and Pachapadra playas

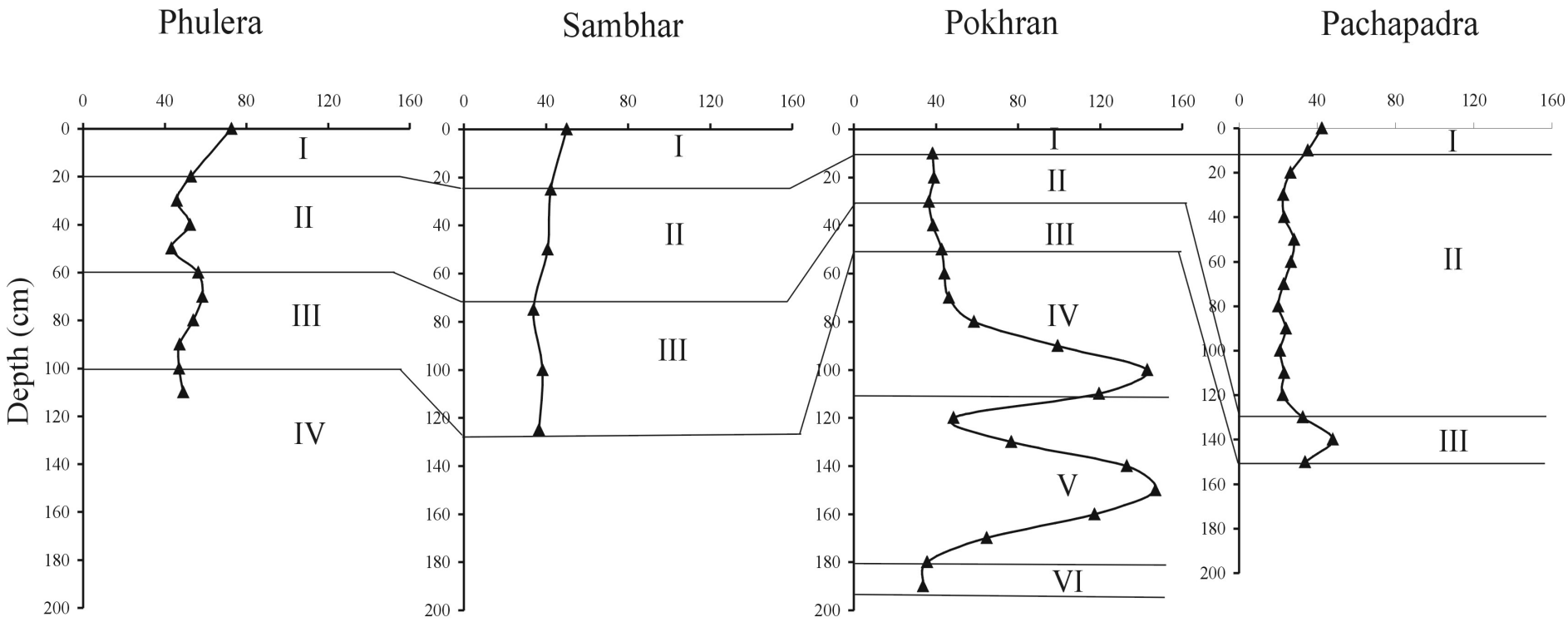

Figure 40 The variation of Zr/Al × 10^{-4} along the depth profiles of Phulera, Sambhar, Pokhran and Pachapadra playas

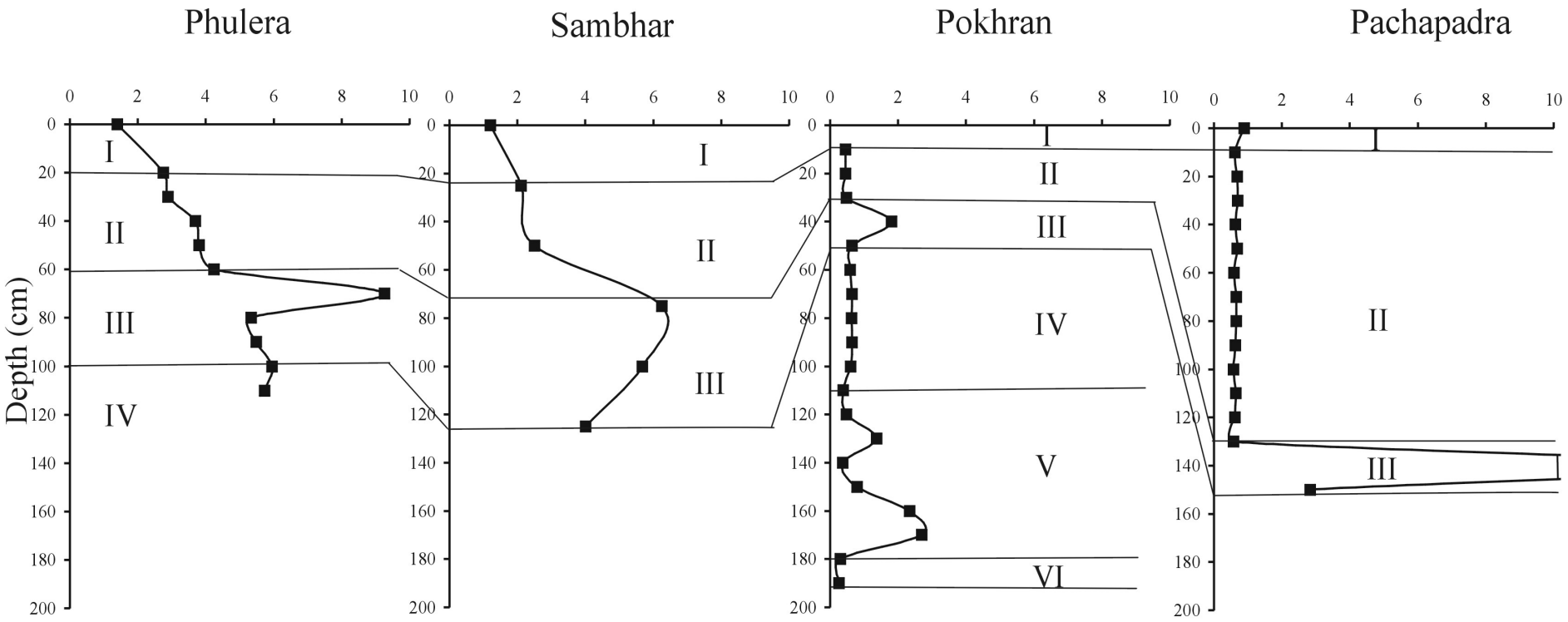

Figure 41 The variation of Sr/Ba along the depth profiles of Phulera, Sambhar, Pokhran and Pachapadra playas

The variations of major and trace elements divided the depth profiles into several geochemical zones. These zones are very prominent in the Phulera, Sambhar, Pokhran, Bap-Malar, and Pachapadra profiles and less clearly seen in the Didwana profile. Tables 23 to 28 present the average major and trace elemental concentrations in the geochemical zones of different playas. The depth profile of Bap-Malar shows two, the profiles of Sambhar, Didwana and Pachapadra playas show three, the Phulera playa shows four and the Pokhran playa six different geochemical zones. The zone I of all the playas is enriched in SiO_2 and Zr. The zone II of the eastern playas exhibits the concentration of Al_2O_3, P_2O_5, Fe_2O_3, Cu, Zn, Rb and Ba in higher amounts, whereas in the western playas this zone shows enrichment of all the above mentioned elements along with MgO. The zone III of the eastern playas shows the highest concentration of Sr, CaO and MgO, whereas in western playas it is enriched only in Sr and CaO. For both the regions, this zone exhibits lowest SiO_2, Al_2O_3, TiO_2, and Zr contents. The zone IV is similar to zone II and shows relatively higher Al_2O_3, SiO_2, TiO_2, Fe_2O_3, Cu, Zn, and Rb. The Pokhran playa shows two additional geochemical zones. The zone V has highest SiO_2, Ba, and Sr contents with relatively higher Zr. The zone VI has highest K_2O, TiO_2, Al_2O_3, Cu, Zn, and Rb contents. Figure 37 and Figure 38 compare the average concentration of some trace elements in the first four zones of Phulera (east) and Pokhran (west).

From this comparison, three features are evident: (a) the variation of the trace elements in different geochemical zones of the Pokhran playa is much larger, and (b) the abundance of elements is larger as well, (c) with the exception of Sr, all measured elements (e.g. Cu, Zn, Rb, Ba, Zr and P) behave similar. These elements are showing a maximum in zone II and IV and a minimum in zone III, where the Sr has its maximum. Figure 39 exhibits the Na/Al ratio and Figure 40 shows the Zr/Al ratio of two eastern (Phulera and Sambhar) and two western playas (Pokhran and Pachapadra). The elemental ratios of Na/Al and Zr/Al show more homogeneous trends for the eastern playas and random for the western region. The Sr/Ba ratio exhibits a maximum in the zone III of all the playas (Figure 41).

6.2.3 Rare earth element (REE) geochemistry

The rare earth elements (REE) form a coherent group of trace elements in the geochemical process, due to its predominance stable trivalent oxidation state and similar ionic radii. The slight differences in their ionic size and existence of some of the elements in oxidation state other than 3+ make them one of the most studied trace element group to decipher the petrological processes. The REE are insoluble (present in relatively low concentrations in

river and see waters) and are unaffected by diagenesis and metamorphism. Thus they are mainly transported as particulate matter and reflect the chemistry of their source. The REE distributions in the playa sediments of the Thar desert were studied to identify their provenance and to study their relationship with average upper continental crust (UCC). Clastic sediments are transported to the playa lakes, both by aeolian processes, during the summer months and by fluvial processes, during the monsoon months. So the sediments deposited in the playa lakes reflect the chemistry of their catchments. The samples were selected from four different playas from the eastern desert margin and five other playas from the western arid desert core with different proportions of detrital and evaporitic mineralogy.

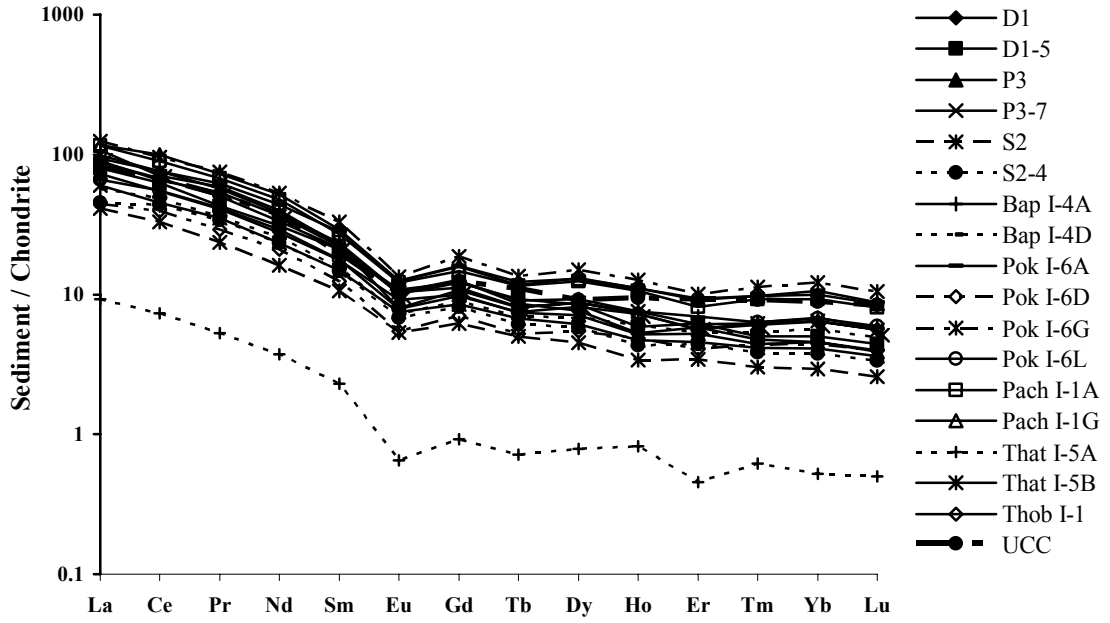

Figure 42 Chondrite-normalised REE diagrams for playa sediments and UCC. All the samples have very similar patterns characterized by LREE enrichment and negative Eu-anomalies

The chondrite normalised patterns of the playa sediments (Figure 42) are very similar to upper continental crust (UCC), with enriched LREE, depleted HREE, and similarly pronounced negative Eu anomaly, expressed by Eu/Eu*. But in abundance they differ among themselves and to that of UCC. Table 29 presents the chondrite normalised REE geochemistry of the playa sediments and UCC. They exhibit depletion in their HREE abundance compared to the UCC. The analysis of an unleached sample and its carbonate leached counter part do not show any significant difference in their pattern (Figure 43), but they show some characteristic differences in abundance.The untreated sample exhibits enriched HREE compared to the

carbonate leached sample. This confirms the higher stability of the HREE-carbonate complexes compared to the LREE.

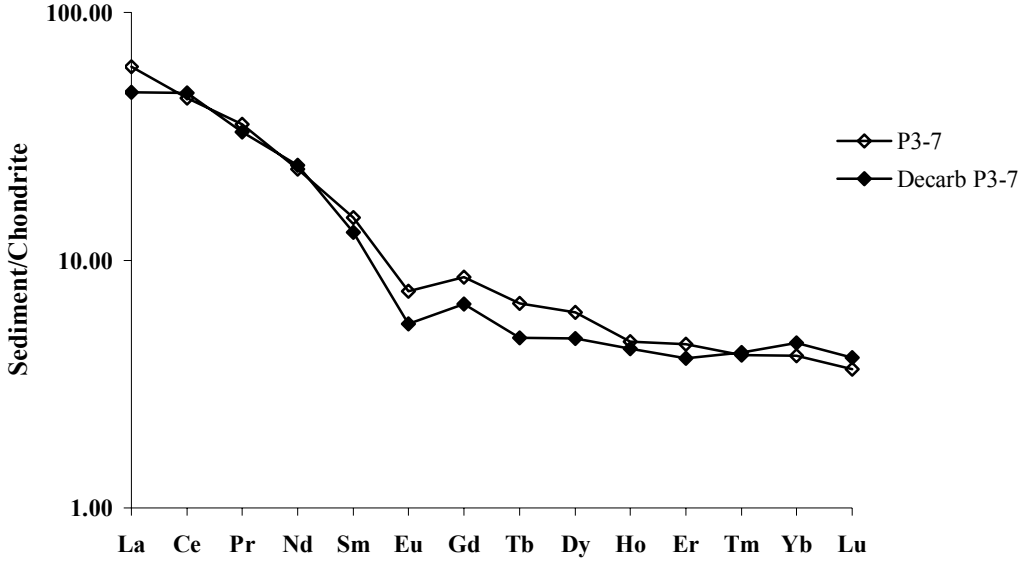

Figure 43 Chondrite normalised patterns of untreated (P3-7) and carbonate leached (Decarb P3-7) samples

According to the REE pattern and relative enrichment and deficiencies of different elements, the UCC normalised sediments are divided into two different groups. The sediments of the eastern desert margin playas (Phulera, Sambhar, Kuchaman and Didwana) are enriched in LREE (La/Sm = 0.74-0.98), and depleted in HREE (Gd/Yb =1.48-1.95), with a positive Eu anomaly (0.96-1.07). Table 30 presents the UCC normalised REE geochemistry of the playa sediments. Figure 44 shows the UCC normalised REE patterns of the eastern desert margin playa sediments. The sediments of the western desert core playas (Bap, That, Pokhran, Pachapdra, and Thob) show similarly fractionated LREE (La/Sm = 0.85-1.13) and HREE (Gd/Yb = 1.03-1.30) pattern and a negative Eu anomaly (0.89-0.99). Figure 45 shows the UCC normalised REE patterns of the western arid core playa sediments. In this section the group “east” always stands for the eastern desert margin playas and the group “west” always stands for the western arid core playas. The eastern sediments show a positive Er anomaly, where as western sediments show a negative Er anomaly.

Table 29 Chondrite normalised REE geochemistry of the playa sediments

Playa	Sample	La	Ce	Pr	Nd	Sm	Eu	Gd	Tb	Dy	Ho	Er	Tm	Yb	Lu	La/Sm	Gd/Yb	La/Yb	Eu/Eu*
Didwana	D1	88.36	67.87	50.33	33.53	21.46	10.29	12.49	8.60	7.69	5.27	5.80	4.75	4.58	3.98	4.12	2.73	19.28	0.63
	D1-5	79.71	62.67	43.19	31.11	21.08	10.84	12.14	9.28	8.51	5.89	6.17	4.99	5.02	4.44	3.78	2.42	15.89	0.68
Kuchaman	K3	70.32	54.31	37.98	25.41	17.42	8.70	9.63	7.50	6.72	4.81	4.80	4.14	4.11	3.63	4.04	2.34	17.11	0.67
Phulera	P3	72.45	54.95	40.97	27.51	17.58	9.17	9.92	7.38	7.07	5.16	5.25	4.42	4.55	3.89	4.12	2.18	15.91	0.69
	P3-7	60.35	45.06	35.35	23.39	14.82	7.48	8.52	6.71	6.14	4.69	4.58	4.14	4.11	3.63	4.07	2.07	14.69	0.67
	P3-7*	47.55	47.39	32.93	24.13	12.95	5.54	6.66	4.87	4.82	4.38	4.02	4.25	4.63	4.05	3.67	1.44	10.26	0.60
Sambhar	S2	41.11	32.95	23.67	16.09	10.61	5.34	6.22	5.03	4.50	3.40	3.42	3.03	2.94	2.58	3.87	2.11	13.99	0.66
	S2-4	45.09	43.92	34.04	23.27	14.62	6.82	8.12	6.16	5.80	4.34	4.44	3.86	3.79	3.37	3.08	2.15	11.91	0.63
Bap-Malar	BapI-4A	107.51	70.12	58.79	39.78	22.64	10.02	12.35	9.07	9.20	7.56	6.92	6.34	6.78	5.76	4.75	1.82	15.85	0.60
	BapI-4D	56.90	48.58	35.79	25.54	15.26	7.27	8.92	6.96	6.90	5.97	5.33	5.32	5.72	4.94	3.73	1.56	9.94	0.62
Pokhran	PokI-6A	93.17	76.02	62.22	43.70	28.25	12.35	15.80	11.65	13.07	11.11	9.36	9.69	10.61	8.74	3.30	1.49	8.78	0.58
	PokI-6D	44.25	39.37	29.08	20.97	12.47	5.44	7.06	5.24	5.44	4.85	4.07	4.38	4.42	3.98	3.55	1.60	10.00	0.58
	PokI-6G	124.89	95.95	74.81	53.06	33.20	13.33	18.70	13.48	14.93	12.69	10.07	11.27	12.20	10.47	3.76	1.53	10.24	0.53
	PokI-6L	66.27	55.42	41.76	29.19	17.74	7.92	9.73	7.52	8.14	7.25	5.66	6.35	6.74	5.94	3.73	1.44	9.83	0.60
Pachapadra	PachI-1A	115.30	89.47	67.41	47.88	27.13	12.11	14.74	11.52	12.40	10.54	8.15	9.28	9.24	8.09	4.25	1.60	12.48	0.61
	PachI-1G	116.44	99.98	72.94	51.85	29.02	12.56	15.91	12.25	12.97	11.05	9.13	9.73	9.97	8.57	4.01	1.60	11.68	0.58
Thob	ThobI-1	89.69	65.78	53.64	36.85	22.02	7.93	10.69	8.02	8.73	7.24	5.64	6.06	6.43	5.61	4.07	1.66	13.96	0.52
That	ThatI-5A	9.24	7.30	5.32	3.72	2.30	0.65	0.92	0.71	0.79	0.82	0.46	0.62	0.52	0.50	4.02	1.76	17.74	0.45
	ThatI-5B	98.54	75.80	57.00	38.46	23.40	10.39	11.18	8.13	8.71	7.55	6.16	6.18	6.47	5.56	4.21	1.73	15.23	0.64
	UCC	81.74	66.88	51.82	36.57	19.48	10.11	12.42	11.03	9.19	9.41	9.24	9.17	8.87	8.42	4.20	1.40	9.21	0.65

Data source: Chondrite and upper continental crust (UCC) (Taylor & McLennan, 1985)
(P3-7* is the sample from 70 cm depth of Phulera playa after treatment with 1 M HCl)

This table includes the REE contents of the upper continental crust (UCC).

Table 30 UCC normalised REE geochemistry of the playa sediments

Playa	Sample	La	Ce	Pr	Nd	Sm	Eu	Gd	Tb	Dy	Ho	Er	Tm	Yb	Lu	La/Sm	Gd/Yb	La/Yb	Eu/Eu*
Didwana	D1	1.08	1.01	0.97	0.92	1.10	1.02	1.01	0.78	0.84	0.56	0.63	0.52	0.52	0.47	0.98	1.95	2.09	0.97
	D1-5	0.98	0.94	0.83	0.85	1.08	1.07	0.98	0.84	0.93	0.63	0.67	0.54	0.57	0.53	0.90	1.73	1.72	1.04
Kuchaman	K1	0.86	0.81	0.73	0.69	0.89	0.86	0.78	0.68	0.73	0.51	0.52	0.45	0.46	0.43	0.96	1.67	1.86	1.03
Phulera	P3	0.89	0.82	0.79	0.75	0.90	0.91	0.80	0.67	0.77	0.55	0.57	0.48	0.51	0.46	0.98	1.56	1.73	1.07
	P3-7	0.74	0.67	0.68	0.64	0.76	0.74	0.69	0.61	0.67	0.50	0.50	0.45	0.46	0.43	0.87	1.48	1.59	1.02
Sambhar	S2	0.50	0.49	0.46	0.44	0.54	0.53	0.50	0.46	0.49	0.36	0.37	0.33	0.33	0.31	0.92	1.51	1.52	1.01
	S2-4	0.55	0.66	0.66	0.64	0.75	0.67	0.65	0.56	0.63	0.46	0.48	0.42	0.43	0.40	0.74	1.53	1.29	0.96
Bap-Malar	BapI-4A	1.32	1.05	1.13	1.09	1.16	0.99	0.99	0.82	1.00	0.80	0.75	0.69	0.76	0.68	1.13	1.30	1.72	0.92
	BapI-4D	0.70	0.73	0.69	0.70	0.78	0.72	0.72	0.63	0.75	0.63	0.58	0.58	0.65	0.59	0.89	1.11	1.08	0.96
Pokhran	PokI-6A	1.14	1.14	1.20	1.20	1.45	1.22	1.27	1.06	1.42	1.18	1.01	1.06	1.20	1.04	0.79	1.06	0.95	0.90
	PokI-6D	0.54	0.59	0.56	0.57	0.64	0.54	0.57	0.48	0.59	0.52	0.44	0.48	0.50	0.47	0.85	1.14	1.09	0.89
	PokI-6G	1.53	1.43	1.44	1.45	1.70	1.32	1.51	1.22	1.63	1.35	1.09	1.23	1.37	1.24	0.90	1.10	1.11	0.82
	PokI-6L	0.81	0.83	0.81	0.80	0.91	0.78	0.78	0.68	0.89	0.77	0.61	0.69	0.76	0.71	0.89	1.03	1.07	0.93
Pachapadra	PachI-1A	1.41	1.34	1.30	1.31	1.39	1.20	1.19	1.04	1.35	1.12	0.88	1.01	1.04	0.96	1.01	1.14	1.35	0.93
	PachI-1G	1.42	1.49	1.41	1.42	1.49	1.24	1.28	1.11	1.41	1.17	0.99	1.06	1.12	1.02	0.96	1.14	1.27	0.90
Thob	ThobI-1	1.10	0.98	1.04	1.01	1.13	0.78	0.86	0.73	0.95	0.77	0.61	0.66	0.72	0.67	0.97	1.19	1.51	0.80
That	ThatI-5A	0.11	0.11	0.10	0.10	0.12	0.06	0.07	0.06	0.09	0.09	0.05	0.07	0.06	0.06	0.96	1.26	1.93	0.69
	ThatI-5B	1.21	1.13	1.10	1.05	1.20	1.03	0.90	0.74	0.95	0.80	0.67	0.67	0.73	0.66	1.00	1.23	1.65	0.99

The samples are collected from following depths D1 : 0 cm, D1-5 : 60 cm, K1 : 0 cm, P3 : 0 cm, P3-7: 70 cm, S2: 0 cm, S2-4: 100 cm, BapI-4A: 0 cm, BapI-4D: 70 cm, PokI-6A: 10 cm, PokI-6D: 40 cm, PokI-6G: 70 cm, PokI-6L: 120 cm, PachI-1A: 10 cm, PachI-1G: 70 cm, ThobI-1: 0 cm, ThatI-5A: 0 cm, ThatI-5B: 10 cm.

All the samples have similar fractionated REE contents; for eastern playa sediments La/Yb ranges from 1.29 to 2.09 and for western playa sediments La/Yb varies from 1.03 to 1.93.

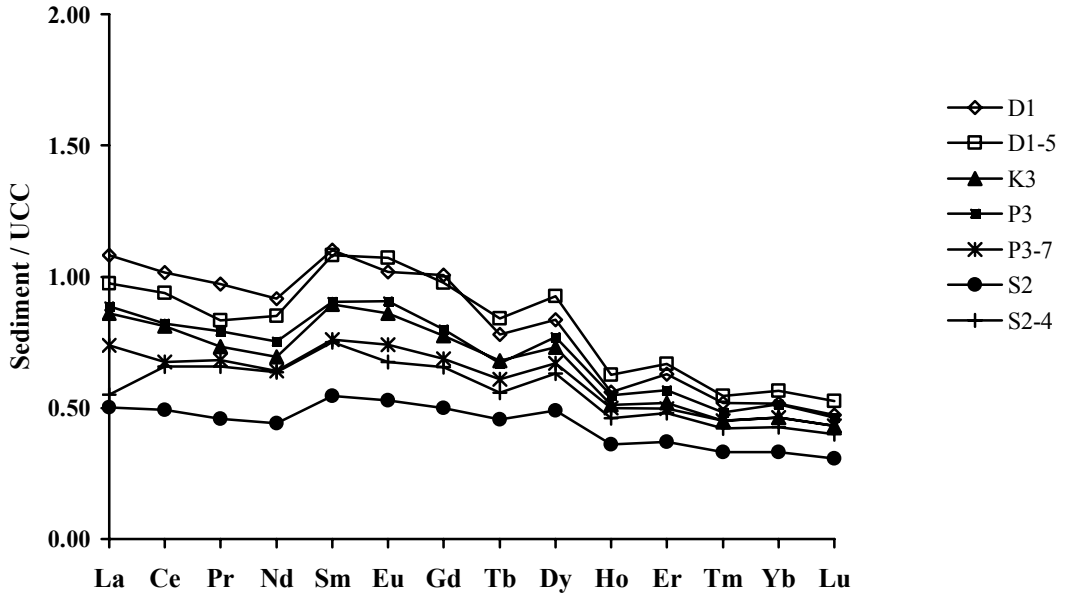

Figure 44 Upper continental crust normalised REE patterns of the eastern desert margin playa sediments

Another characteristic feature, which differentiates the sediments of eastern playas from those of western playas, is their REE contents (for absolute concentration see appendix). The REE contents in the western playa samples are showing a large variation and they are also relatively higher in abundance than that of eastern playa samples (sample ThatI-5A is an exception). According to the mineralogy, the playa samples are grouped into two different groups; (a) rich in detrital minerals (D1, D1-5, K3, P3-1, Bap I-4A, Pok I-6A, Pok I-6G, Pach I-1A, Pach I-1G, Thob I-1 and That I-5B) and (b) rich in evaporitic minerals (P3-7, S2, S2-4, BapI-4D, Pok I-6D and That I-5A). The REE contents are higher in the samples rich in detrital minerals than the samples rich in evaporites (carbonates, sulphates and chlorides). In the detrital rich group, the samples rich in quartz have relatively lower absolute abundance of REE. The reason for the lower absolute abundance is the dilution effect of quartz, which typically has very low REE content. The carbonate rich samples have an intermediate REE abundance. They are also characterised by the relatively low depletion of HREE. The HREE form stable complexes with carbonate ions in the alkaline solution leading to the enrichment of HREE in the sediments precipitated from the brine. The UCC normalised carbonate rich samples show a positive Ce anomaly. This anomaly apparently results from the stabilisation

of carbonate complexes of Ce (IV) in solution and leading to increasing its residence time in the brine. Finally, the enrichment of Ce is reflected in the (chemical) sediments which precipitate from the brine. The UCC normalised REE pattern of the gypsum rich sediment is similar to that of carbonate rich samples. Both the type of sediments shows a positive Ce anomaly (Bap I-4D; gypsum rich and S2-4, Pok I-6D, PokI-6L, PachI-1G; carbonate rich). The REE abundance is lowest in the sample (ThatI-5A) rich in halite (NaCl).

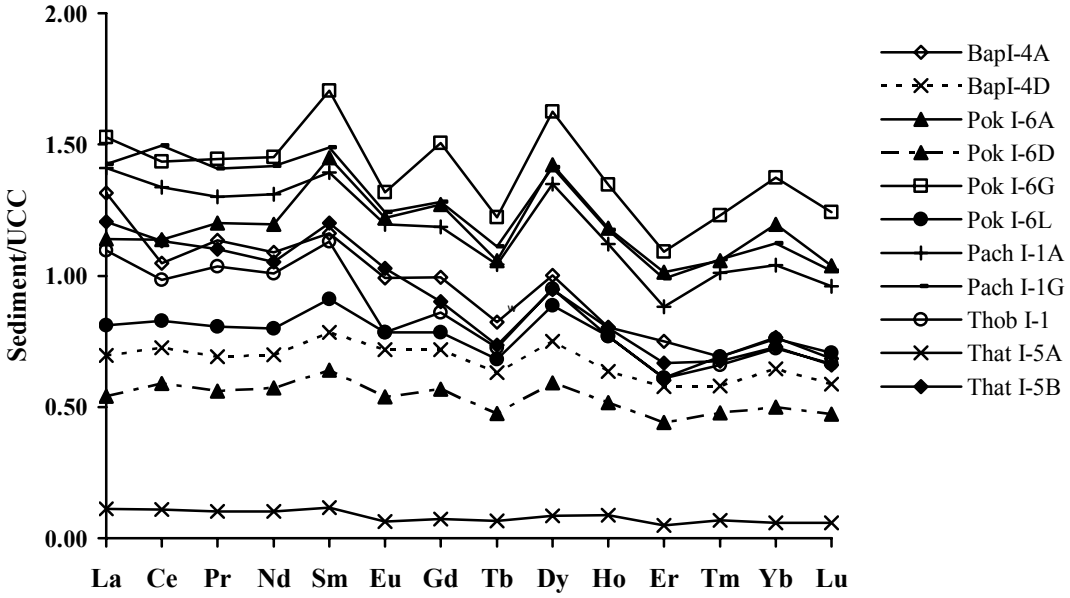

Figure 45 Upper continental crust normalised REE patterns of the western arid core playa sediments

Table 31 presents the coefficient of correlation between the REE and different major and trace elements. Among the compositional variables of the sediments, the Y, Th, and TiO_2 contents are showing a strong positive correlation with La, total REE and to a less extent Yb. Zr is however not showing any significant correlation with the REE contents and in fact it is showing low correlation with HREE. Other major and trace constituents like Pb, Rb and Ba are coupled strongly, where as Zn, Al_2O_3, K_2O and Fe_2O_3 are showing significant relationship with the REE. Constituents like CaO, MgO and Sr are showing a negative correlation with the REE (not shown in the table). The relationship between TiO_2, Rb, Pb, Ba, Zn, Al_2O_3, K_2O, and REE are significant enough to consider the influence of titaniferous minerals like biotite, sphene, ilmenite or rutile on the REE chemistry.

Table 31 Correlation coefficient among various REE, different trace and major components of the playa sediments

REE	Zr	Y	Zn	Rb	Ba	Pb	Th	Al_20_3	K_2O	TiO_2	Fe_20_3
La	0.60	0.89	0.54	0.77	0.78	0.84	0.94	0.61	0.44	0.75	0.48
Ce	0.50	0.90	0.61	0.81	0.79	0.88	0.95	0.66	0.48	0.77	0.55
Pr	0.52	0.89	0.55	0.77	0.77	0.86	0.97	0.62	0.46	0.73	0.51
Nd	0.48	0.90	0.56	0.79	0.77	0.87	0.97	0.64	0.49	0.74	0.54
Sm	0.57	0.94	0.57	0.80	0.79	0.83	0.93	0.66	0.57	0.75	0.53
Eu	0.58	0.96	0.73	0.89	0.87	0.83	0.82	0.72	0.65	0.81	0.59
Gd	0.56	0.96	0.65	0.86	0.77	0.79	0.88	0.72	0.68	0.78	0.61
Tb	0.50	0.96	0.67	0.88	0.79	0.84	0.89	0.74	0.66	0.80	0.64
Dy	0.46	0.94	0.56	0.82	0.78	0.85	0.93	0.69	0.61	0.74	0.59
Ho	0.37	0.89	0.46	0.74	0.75	0.85	0.93	0.64	0.54	0.68	0.56
Er	0.44	0.94	0.62	0.85	0.79	0.84	0.90	0.72	0.66	0.76	0.63
Tm	0.35	0.88	0.48	0.75	0.73	0.84	0.92	0.66	0.56	0.68	0.58
Yb	0.37	0.88	0.44	0.72	0.72	0.82	0.91	0.63	0.56	0.65	0.55
Lu	0.36	0.87	0.44	0.72	0.72	0.82	0.91	0.62	0.54	0.65	0.54
TREE	0.52	0.91	0.58	0.80	0.79	0.87	0.96	0.66	0.49	0.76	0.54

6.2.4 Isotope geochemistry

Some carbonate-enriched sediment samples from Phulera (east) and Pokhran (west) playas were analysed for $\delta\ ^{18}O$ and $\delta\ ^{13}C$. Table 32 presents the V-PDB normalised $\delta\ ^{18}O$ and $\delta\ ^{13}C$ values. Figure 46 shows the distribution of $\delta\ ^{18}O$ and $\delta\ ^{13}C$ in the playa samples. The Pokhran carbonates are showing a large variation for both $\delta\ ^{18}O$ and $\delta\ ^{13}C$ compared to the Phulera carbonates. They are also depleted in both the isotopes compared to the Pokhran (Figure 45). Figure 47 shows the variation of $\delta\ ^{13}C$ and $\delta\ ^{18}O$ along the depth profiles of Phulera and Pokhran playas.

In case of Phulera playa, the carbonates from 70 and 80 cm depth are enriched, and the carbonates of 20-60 cm and 100-110 cm depth zones are depleted in the heavier isotope of O. Similarly, the Pokhran carbonates are showing an enriched zone of δ^{18} O in the depth horizon of 120-160 cm and depleted zones both for 10-30 cm and 60-100 cm horizons. The $\delta^{18}O_{carbonate}$ values from both the playas show an increasing trend with increasing carbonate contents (CaO %) (Figure 48), whereas they behave differently with increasing MgO (%) contents (Figure 49).

Table 32 The V-PDB normalised δ ^{18}O and δ ^{13}C values of carbonates and CaO %, MgO % contents of the bulk sediments

Playa	Geochemical zone	Depth (cm)	δ^{18} O (V-PDB)	δ^{13} C (V-PDB)	CaO (mass %)	MgO (mass %)
Phulera	II	20	-0.56	-0.11	7.98	6.83
		40	-1.77	-1.08	8.98	8.12
		60	-0.64	-0.70	9.68	8.90
	III	70	1.31	-0.57	12.57	11.91
		80	0.73	-0.50	10.24	11.24
	IV	100	-0.40	-0.44	10.21	10.66
		110	-0.67	0.12	8.77	10.11
Pokhran	II	10	-4.06	-1.65	5.00	3.41
		30	-5.27	-2.35	5.52	3.85
	IV	60	-7.22	-6.14	6.32	4.48
		80	-4.33	-3.94	7.07	4.29
		100	-4.94	-2.09	7.98	2.87
	V	120	-1.91	0.50	8.63	1.39
		140	-1.70	0.30	11.98	1.37
		160	-1.15	-0.07	13.50	1.16

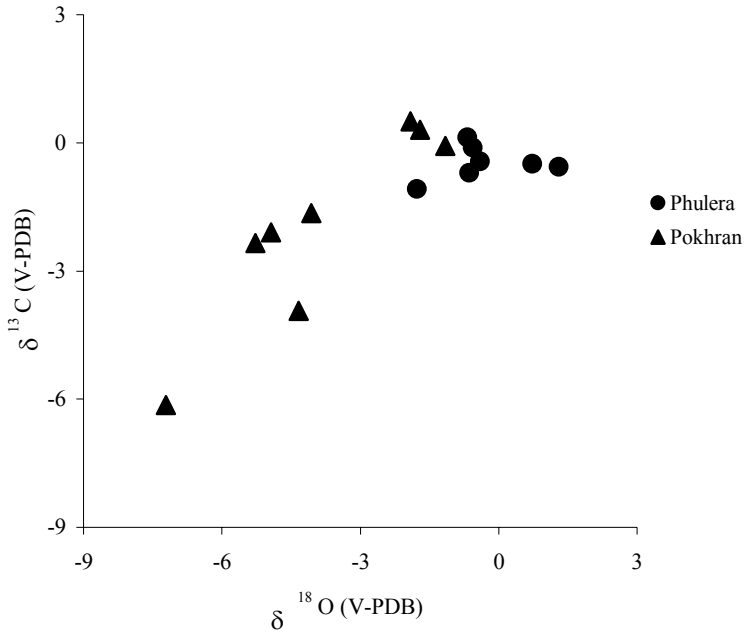

Figure 46 Distribution of δ ^{18}O (V-PDB) and δ ^{13}C (V-PDB) in playa carbonates

The high Mg-carbonates of Phulera exhibit an increasing trend, whereas the low Mg-carbonates show a decreasing trend. Again with increasing carbonate content (CaO %), the $\delta^{13}C_{carbonate}$ from the Pokhran playa is showing an increasing trend, but it does not show any significant variation for Phulera samples (Figure 50).

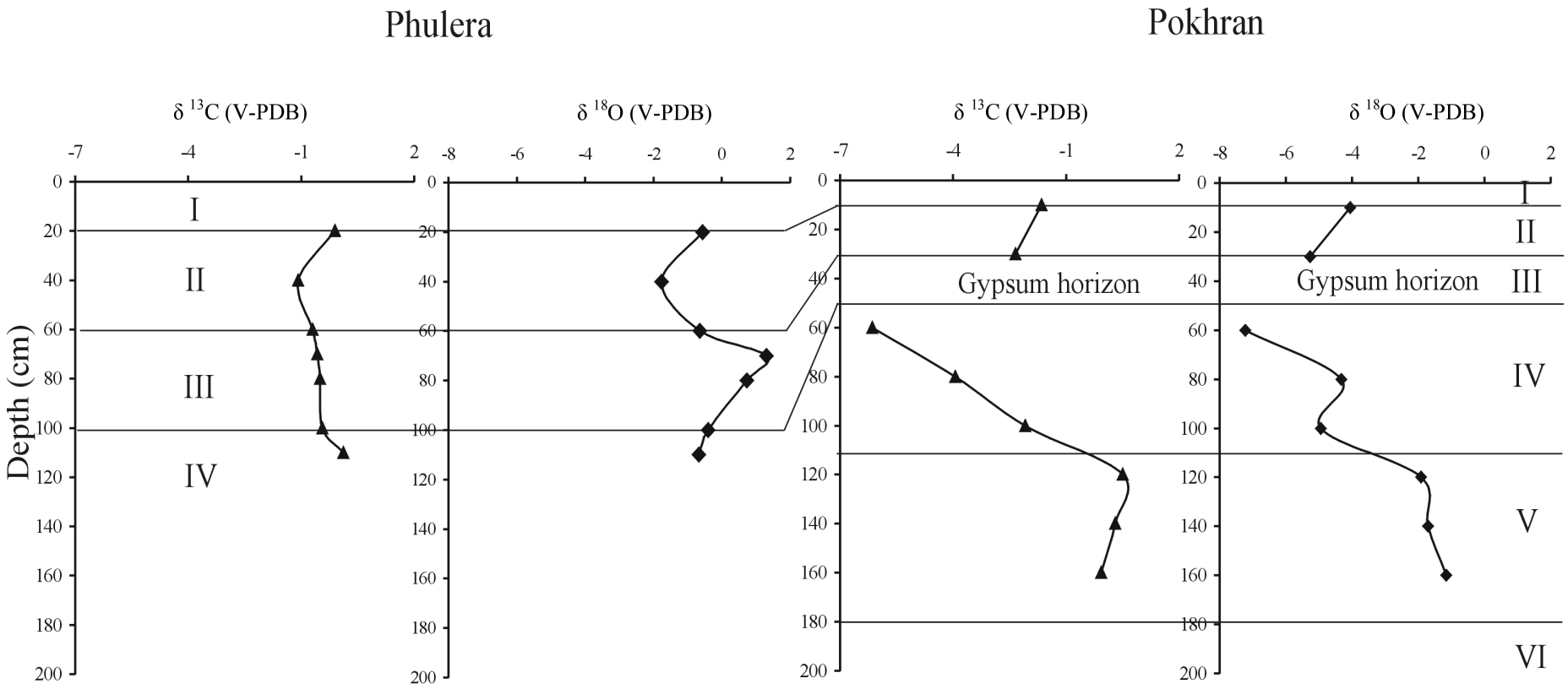

Figure 47 Variation of $\delta^{13}C$ and $\delta^{18}O$ in different geochemical zones of Phulera (east) and Pokhran (west) playas

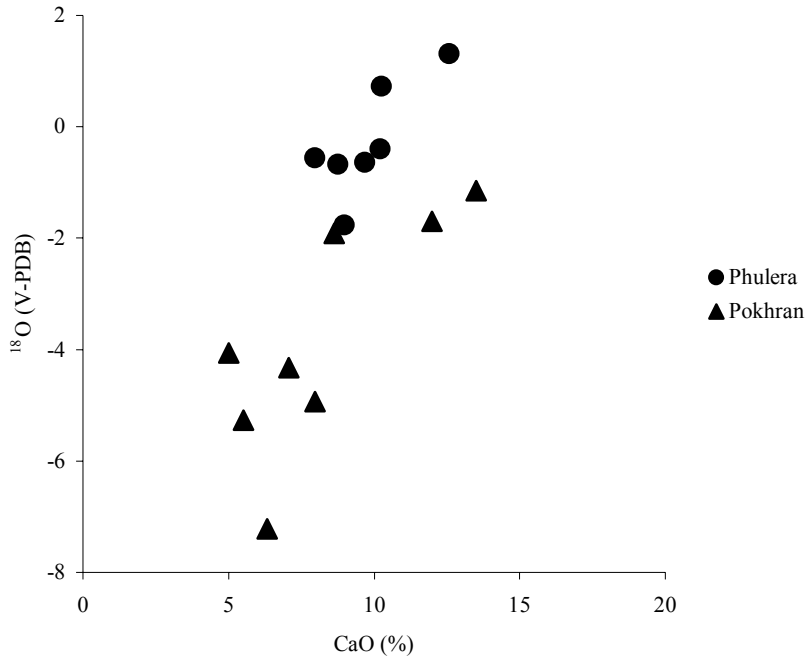

Figure 48 Variation of $\delta^{18}O_{carbonate}$ with increasing CaO (%) contents

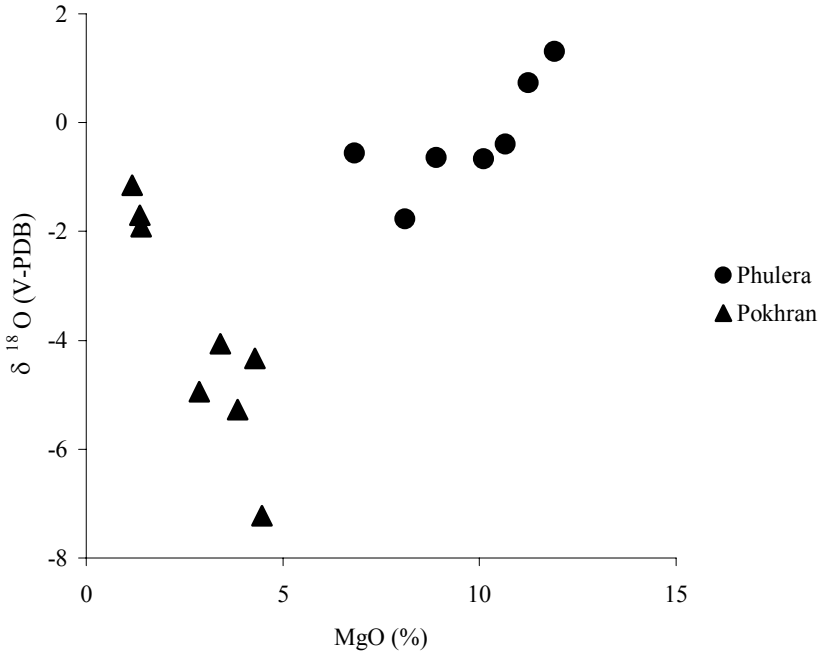

Figure 49 Variation of δ18 $O_{carbonate}$ with increasing MgO (%) contents

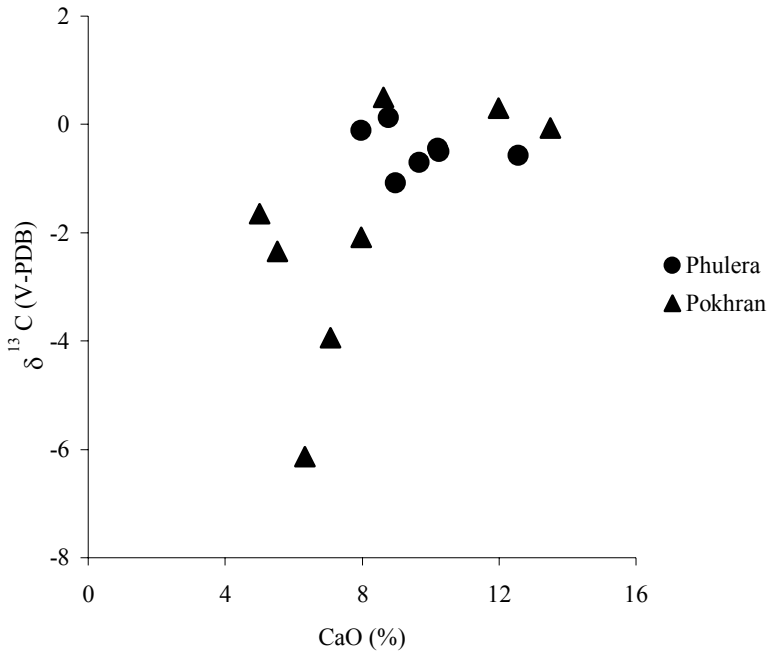

Figure 50 Variation of $\delta^{13}C_{carbonate}$ with increasing CaO (%) contents

6.2.5 Hydrogeochemistry

The analysis of the alkaline (pH 8 to 9) shallow ground water and lake brine samples from eastern and western Thar desert indicates: Cl^- is the dominant anion and Na^+ is the dominant cation (Table 33). According to the nomenclature of Eugster and Hardie (1978), the brine and ground waters are classified to be of Na-Cl-(SO_4) type. Though the number of samples analysed are few, the brine and ground waters are showing characteristic differences in their compositions. The sample of eastern desert margin playa (Sambhar) is showing an enrichment of Na^+ compared to the arid core playas (Pokhran and Pachapadra) of the western region, but it is depleted in Cl^-, K^+, Ca^{2+}, and Mg^{2+}. The samples of the western playas are also showing some compositional differences between them. The ground water of Pokhran is enriched in Ca^{2+} and depleted in Cl^-, SO_4^{2-} and Mg^{2+}, compared to the Pachapadra ground water. Both the playas exhibit similar concentrations of Na^+ and K^+ in their ground water. The surface brine of the Pachapadra playa is highly enriched in Na^+ and depleted in SO_4^{2-}, Ca^{2+} and Cl^- compared to the ground water (150 cm). Though insignificant, K^+ and Mg^{2+} concentrations are also relatively higher in the surface brine. The compositional variation between Pachapadra ground water and surface brine is governed by the crystallisation of calcite and

gypsum, and the recycling of the solutes through fractional dissolution of halite (NaCl) present in the efflorescent crust, which selectively enriches Na^+ in the surface brine.

Table 34 presents the ratios between various cations and anions of the brine and ground waters. The different assemblages of evaporites occurring in the playa sediments can be explained by the compositional difference between the brines. The presence of thenardite (Na_2SO_4) in the sediments of eastern playas and their absence in western playas can be explained by the higher values of Na/Cl, and lower values of Ca/SO_4 ratios in the eastern playa brine. Even after the precipitation of trace amounts of gypsum ($CaSO_4 \cdot 2H_2O$) and halite (NaCl), Na and SO_4 are still available in the brine which later forms the sulphate complex and precipitate. The higher value of Na/Ca in the brine of the eastern playa explains the abundance of Na-bearing chloride and sulphate and presence in trace amount of Ca-bearing sulphates (gypsum and anhydrite) in the sediments.

Table 33 Composition of ground and surface water from the playas

Playa	Depth (cm)	Cl^-	SO_4^{2-}	Na^+	K^+	Ca^{2+}	Mg^{2+}
		(g/l)					
Sambhar	200	18.51	3.79	61.55	0.19	0.64	0.24
Pokhran	210	47.63	3.65	32.45	0.29	3.33	0.85
Pachapadra	150	177.97	23.85	36.46	0.31	1.98	2.33
Pachapadra	0	114.21	4.20	126.07	0.58	1.04	2.57

Table 34 Calculated ratios of major solutes present in the playa brine and ground waters

Divisions	Playa name	Depth (cm)	Na/K	Ca/Mg	Na/Ca	K/Mg	Na/Cl	Ca/SO_4	SO_4/Cl
East	Sambhar	200	320.20	2.62	96.68	0.79	3.33	0.17	0.21
West	Pokhran	210	111.47	3.91	9.76	0.34	0.68	0.91	0.08
	Pachapadra	150	116.51	0.85	18.41	0.13	0.20	0.08	0.13
	Pachapadra	0	218.45	0.40	121.63	0.22	1.10	0.25	0.04

6.2.6 Organic, inorganic carbon and sulphate geochemistry

In terms of C_{org} (organic carbon), CO_3 (carbonate) and SO_4 (sulphate) contents the samples of playa lakes are divided into two distinct groups. The group 1 comprises of three eastern desert margin playas, Phulera, Sambhar, and Didwana, located in front of the Aravalli mountains.

The group 2 consists of three desert core playas, e.g. Bap-Malar, Pokhran, and Pachapadra, located in the western part of the Thar desert.

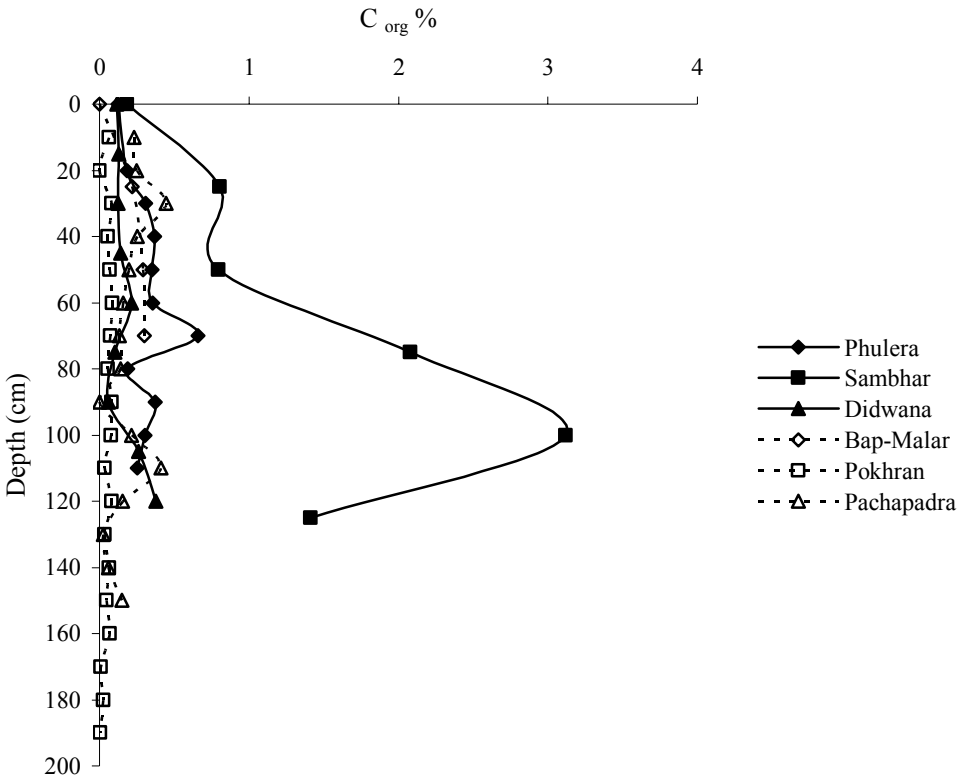

Figure 51 Organic carbon contents (%) in the sediments of the Thar playas

Figure 51 shows the organic carbon contents in the sediments of the Thar playas along their depth profiles. The sediments of the shallow profiles of group 1 playas have higher contents of organic carbon compared to the group 2 playa sediments. In case of group 1 (eastern playas), the organic carbon content is ranging from less than 0.1 % to 3 % (Figure 51). The sediments of Didwana playa are showing the lowest concentrations, the sediments of Phulera playa are showing the intermediate and the sediments of Sambhar playa the highest concentration of organic carbon. There is no similarity between the distributions of C_{org} along the depth profiles of the three above mentioned eastern playas. In case of the Sambhar playa, the organic carbon content is increasing gradually up to 100 cm depth and then it is decreasing. Similarly the Phulera playa sediments are exhibiting a gradual increase up to 70 cm depth, and then it is decreasing gradually. In case of Didwana playa, the organic carbon content is not showing any significant variation in the top 90 cm sediments. But the zone from

75 to 90 cm depth has relative low organic carbon and the zone from 105 to 120 cm has relatively enriched organic carbon content. The shallow core sediments of group 2 playas, located in the arid core of the desert, contain very low organic carbon. It is varying from 0 % to 0.44 % in all the three investigated western playas. The sediments of Pokhran have lowest concentration of organic carbon; it is intermediate in the sediments of Bap-Malar and highest in the sediments of Pachapadra playa. In case of Bap-Malar, the organic carbon is absent in the surface sediments, and then it is showing gradual increase with depth. The sediments of Pokhran playa have almost negligible C_{org} (organic carbon) contents. Except the depth zone of 170 to 190 cm (where there is almost no organic carbon present), C_{org} content in the rest of the depth profile is varying from 0.03 % to 0.08 %. The sediments of Pachapadra playa are showing a highly fluctuating organic carbon content along its depth profile. It is showing two maxima, one at 30 cm depth and other at 110 cm depth and two minima, one at 90 cm depth and other at 130 cm depth.

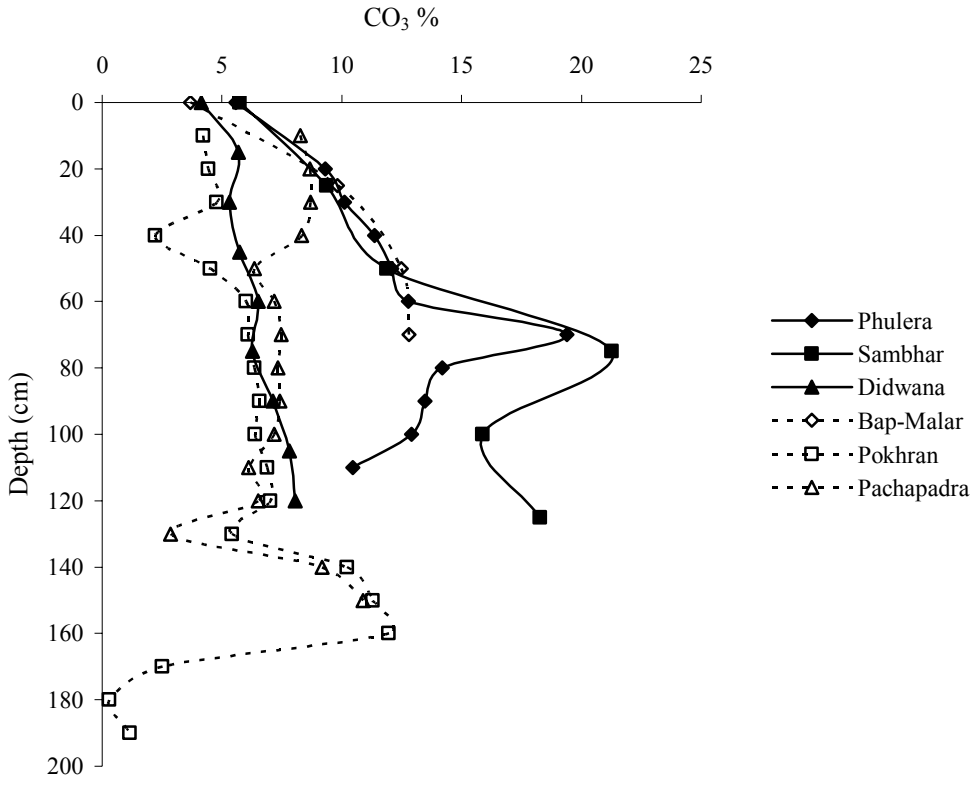

Figure 52 Carbonate contents (%) in the sediments of the Thar playas

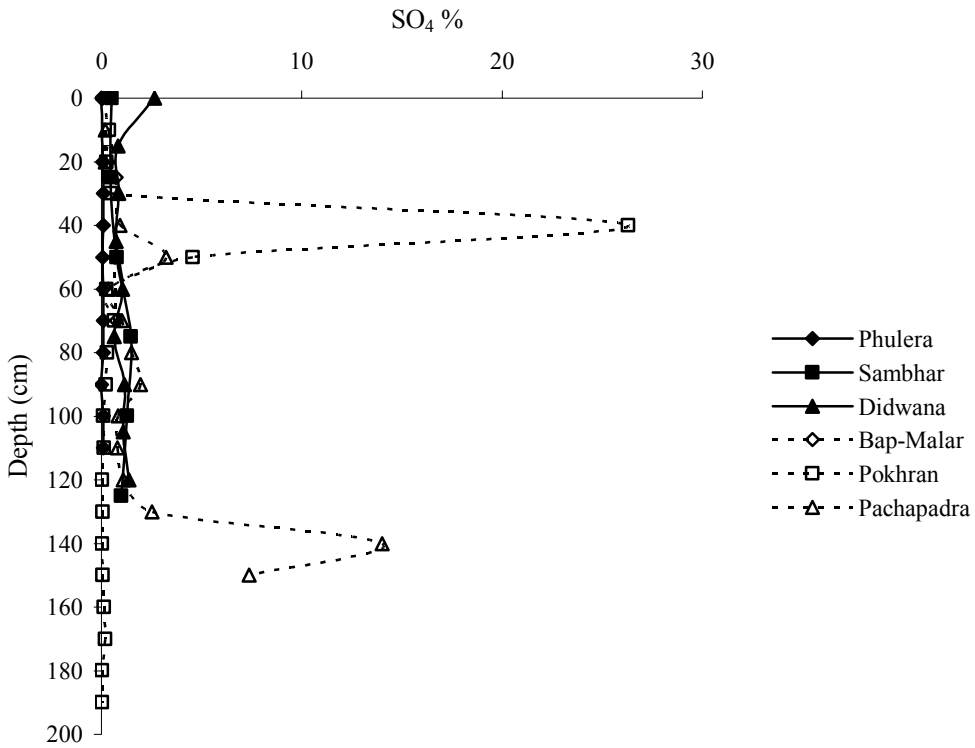

Figure 53 Sulphate contents (%) in the sediments of the Thar playas

Similarly, the shallow core sediments of group 1 playas are having relatively higher carbonate (CO_3) contents, compared to the sediments of group 2 playas. Figure 52 shows the variation of carbonate content along the depth profiles of the studied playas. In the group 1, the sediments of Sambhar are showing the highest, Phulera sediments the intermediate and Didwana sediments the lowest amount of carbonate. The carbonate contents of Sambhar and Phulera profiles are very similar in abundance; both are showing a maximum with in the depth horizon of 70 to 75 cm. The Didwana samples are showing a gradual increase up to 120 cm depth, with some minor fluctuations. In the group 2, the sediments of Bap-Malar are showing highest concentration of carbonate. The concentration of CO_3 is relatively more in the sediments of Pachapadra than Pokhran. Along the depth profile, Bap-Malar sediments are showing an increasing trend. The variation of carbonate for both Pokhran and Pachapadra profiles is very similar. Both of them are showing a minimum in the depth zone of 40 to 50 cm and again at 130 cm depth. The highest contents are in the horizon of 140 to 160 cm depth.

The sediments of group 2 playas show much higher contents of sulphate (SO_4) compared to the group 1 playa sediments. Figure 53 shows the concentration of sulphate along the depth

profile of the investigated playas. The sediments of Phulera have very low concentration of sulphate and it shows no significant change along the depth profile. The SO_4 pattern of Sambhar along the depth profile is very similar to its CO_3 pattern. It shows a maximum content of SO_4 at the same depth (75 cm), where it has highest CO_3 content. The Didwana sediments show maximum content of SO_4 on the playa surface and along the depth profile; it shows an increasing trend with some minor fluctuations. Among the group 2 playas, Bap-Malar sediments show an increasing trend up to 70 cm depth. Pokhran sediments show a maximum (26 %) at a depth of 40 cm, and Pachapadra sediments show two maximums; one at a depth of 50 cm (3 %) and the other at a depth of 140 cm (14 %).

7. Discussion

The results of this investigation permits the discussion in four different aspects, (a) the possible differentiation of the two climatically different regions, (b) the source of the detrital, dissolved and finally precipitated material, (c) the correlation of the depth horizons of different playas, and (d) the palaeoclimatic development of the Thar.

7.1 Differentiation between western and eastern Thar playas

The most evident result in this aspect is the chemical and mineralogical variation between both the areas: the western playas (Bap-Malar, Pokhran and Pachapadra) exhibit large variations in their geochemistry (clearly seen in the ratios of several oxides, Table 35). Especially, the ratios of Na_2O/Al_2O_3, Na_2O/TiO_2, Na_2O/K_2O and SiO_2/Al_2O_3 (Figure 54 and Figure 55) show the different behaviour in the profiles of both the regions.

Table 35 Calculated ratios of several oxides and trace elements in the different geochemical zones along the playa profiles

Playas	Geo-chemical zones	CaO/Sr	CaO/MgO	Na_2O/Al_2O_3	Na_2O/TiO_2	Na_2O/K_2O	Zr/Al_2O_3	SiO_2/Al_2O_3	Sr/Ba
Phulera	I	113.98	1.62	0.27	5.57	1.32	0.0019	6.78	1.39
	II	76.92	1.11	0.21	4.53	1.05	0.0013	5.20	3.46
	III	53.51	0.98	0.26	5.30	1.41	0.0014	5.38	6.71
	IV	56.30	0.91	0.26	5.43	1.28	0.0013	5.28	5.85
Sambhar	I	215.18	1.75	0.20	4.64	0.97	0.0013	3.91	0.98
	II	83.14	1.30	0.17	3.94	0.88	0.0011	3.49	2.30
	III	71.58	1.10	0.19	4.32	0.98	0.0010	4.30	5.32
Didwana	I	140.33	2.84	0.27	5.50	1.43	0.0022	7.54	1.17
	II	90.73	1.14	0.19	4.31	0.89	0.0010	3.91	1.71
	III	88.99	1.16	0.20	4.55	0.95	0.0009	3.94	2.30
Bap-Malar	I	274.40	0.89	0.16	3.50	0.77	0.0018	6.40	0.42
	II	619.59	0.81	0.49	12.16	4.80	0.0012	4.25	0.54
Pokhran	I	235.44	2.11	0.28	5.94	1.50	0.0017	5.58	0.51
	II	294.32	1.43	0.14	3.34	0.64	0.0010	3.67	0.46
	III	843.84	15.85	0.18	4.14	0.80	0.0010	3.99	1.81
	IV	314.81	1.96	0.24	4.53	1.19	0.0018	4.50	0.62
	V	124.01	6.32	0.26	5.10	1.23	0.0025	7.78	1.42
	VI	93.97	0.37	0.11	2.89	0.41	0.0009	2.85	0.28
Pachapadra	I	333.39	2.57	0.71	15.01	6.91	0.0011	4.60	0.83
	II	346.64	1.58	0.27	5.97	1.75	0.0006	3.14	0.64
	III	82.80	3.38	0.38	8.65	2.35	0.0010	4.47	6.03

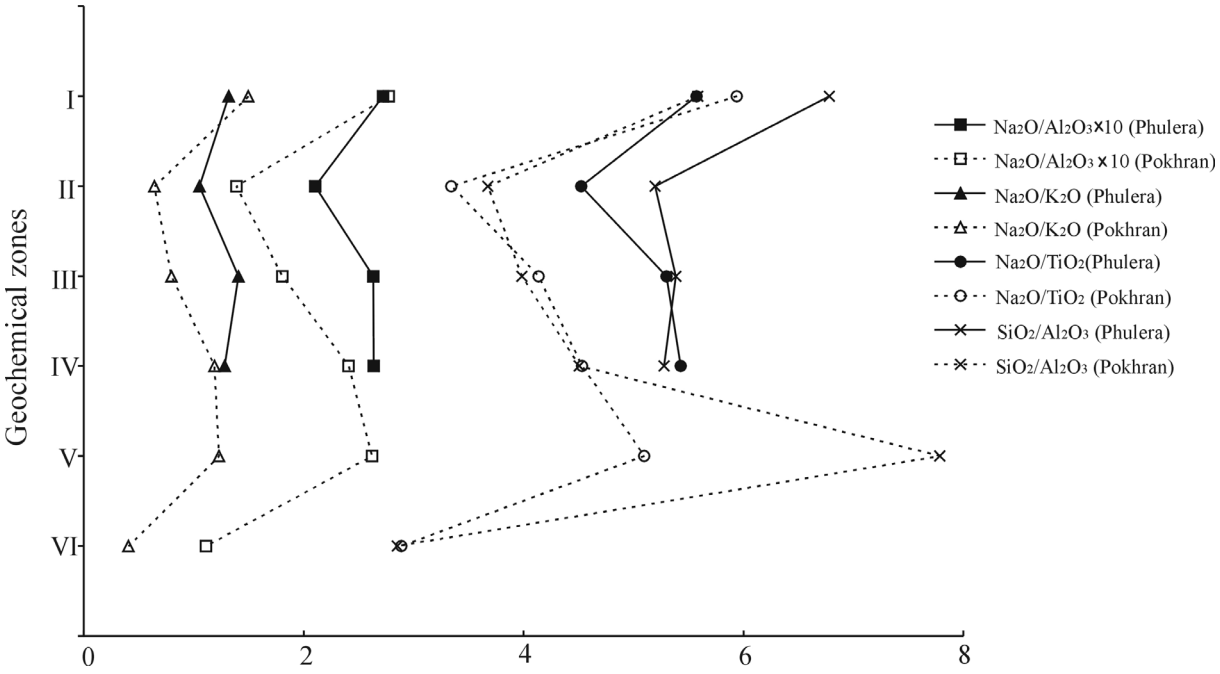

Figure 54 Variation of major oxide ratios along the depth profiles of Phulera and Pokhran playas

This is also mirrored by the abundance of minerals and their degree of weathering. The relatively low abundance of the primary minerals (pyroxene, amphibole, garnet etc.) indicates a relatively higher degree of weathering in the eastern playas, while they are quite abundant in the arid western ones. The primary minerals have disappeared in the eastern playas due to the low resistance against the chemical dissolution processes. This feature is reflected by the abundance of major and trace minerals and rock fragments as well (Table 36).

Evidently, these differences are caused by the higher degree of chemical weathering. In the more humid eastern region, the higher water availability and activity for long periods led to the breakdown of the pyroxenes and the other trace minerals. The zeolite type mineral, analcime ($NaAlSi_2O_6 \cdot H_2O$) is only occurring in the sediments of Didwana playa. Analcime has been reported from both fossil and modern saline lacustrine sediments (Hay, 1966; Surdam & Eugster, 1976; English, 2001). Generally, it is formed by the reaction between saline solutions and volcanic glass. But the absence of any volcanic rocks in the surroundings of the Didwana playa ruled out such an origin of this mineral. But comparable to the Lake Lewis (Australia), the Didwana playa sediments are sourced from the Precambrian crystalline (schists, gneiss, quartzite and granite) catchment rocks (Biswas et al, 1982; Misra, 1982).

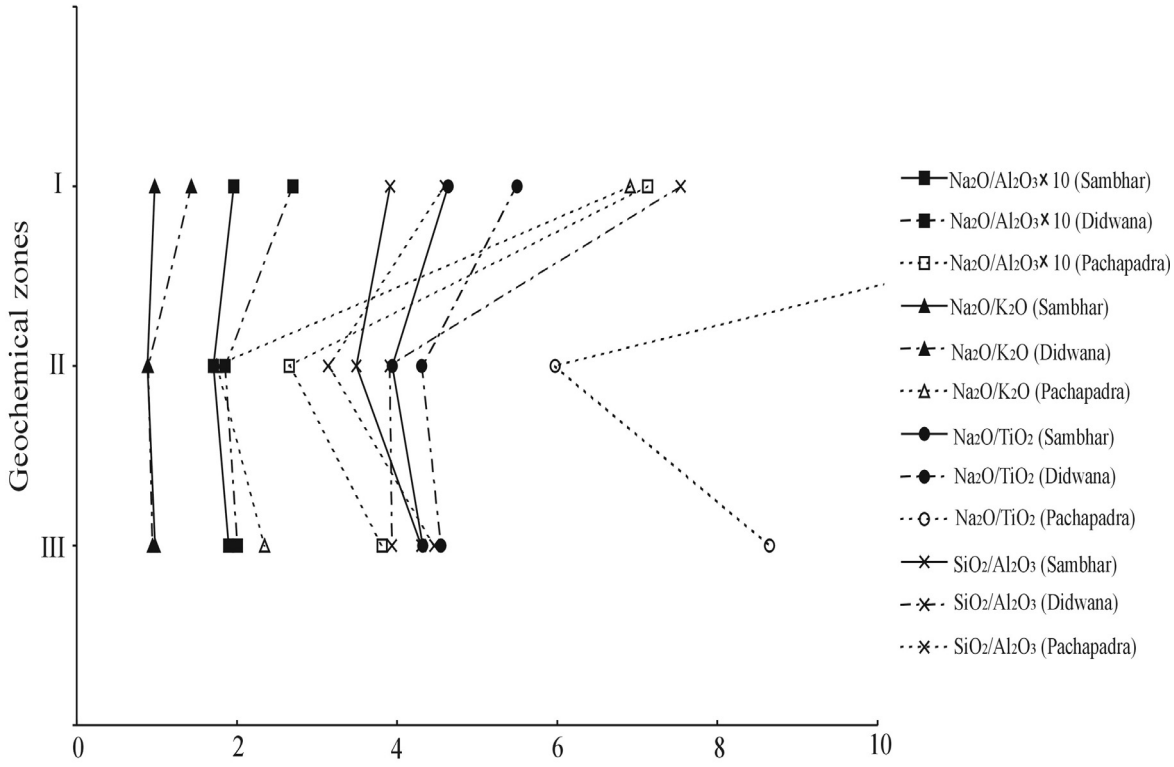

Figure 55 Variation of major oxide ratios along the depth profiles of Sambhar, Didwana and Pachapadra playas

The chemical reaction of the detrital feldspars with highly saline pore fluids for a longer period may have led to the formation of analcime. This interpretation is supported by the presence of traces of analcime on the playa surface and the relatively higher amounts in the deeper horizons.

Concerning the evaporites the picture seems to be reverse: the eastern playas exhibit a large number of evaporitic minerals (Table 5, chapter-results). This can be explained by the different water availability of both the regions. The water-bearing chloride e.g. carnallite ($KMgCl_3 \cdot 6H_2O$), sulphates e.g. mirabilite ($Na_2SO_4 \cdot 10H_2O$), polyhalite ($K_2MgCa_2(SO_4)_4 \cdot 2H_2O$), and carbonate e.g. trona ($Na_3H(CO_3)_2 \cdot 2H_2O$), are occurring only in the more humid eastern region. Among the Ca and Na-sulphates, only the water free types (e.g. anhydrite, $CaSO_4$ and thenardite, Na_2SO_4) are dominant. This is as a consequence of the high temperature of the region, which is higher than 30 °C (even during the winter months). The precipitations of the water free-sulphates indicate they are more stable at elevated temperatures (after Braitsch, 1971; Cooke, 1981; Usdowski & Dietzel, 1998). In the western

playas, both in the surface as well as in depth profiles the amount of gypsum is much higher. Additionally, the eastern playa Sambhar shows traces of sylvite (KCl) in the same horizon with carnallite ($KMgCl_3 \cdot 6H_2O$), which is quite unusual. After Braitsch (1971) and Kössl (1988), only one K-bearing chloride should occur in the same horizon. The association of both the minerals imply a state of disequilibrium in the region of relatively higher water activity.

Table 36 Characteristic playa minerals of both regions

Minerals	Western playas	Eastern playas
quartz	+++	++
feldspars	++	++
amphiboles	+	+
garnet	+	+
zircon	+	+
biotite	+	+
ilmenite	+	
magnetite	+	
titano-magnetite	+	
hematite	+	
epidote	+	
rutile	+	
monazite	+	
xenotime	+	
lawsonite	+	
pyroxenes	+	
allanite		+
analcime		+
rock fragments	+	

+++ = dominant, ++ = abundant. + = traces

The behaviour of the iron minerals is very obvious. In the eastern playas, characterised by high water activity and higher contents of organic carbon (Table 37), the Fe^{2+} is stable (due to negative Eh) and is available for incorporation in authigenic neo-formations (dolomites). In the more arid western environment, where the reducing materials (organic carbon) are more or less absent, the iron gets oxidised and consequently the Fe^{3+}-oxide hematite is occurring. The different water availability (even if only periodically) is the reason for the occurrence of Mg-bearing evaporites only in the eastern playas. The soluble cation Mg^{2+} ($+Ca^{2+}$) (after the precipitation of gypsum) forms the Mg-carbonates, dolomite ($CaMg(CO_3)_2$, and huntite ($CaMg_3(CO_3)_4$). The remaining Na^+ (after the evaporitic formation of halite) forms (rarely) glauberite ($Na_2Ca(SO_4)_2$) or mirabilite ($Na_2SO_4 \cdot 10H_2O$) and then thenardite (Na_2SO_4) respectively. After the precipitation of thenardite the brine gets enriched with K and Mg,

which then evaporates to form polyhalite ($K_2MgCa_2(SO_4)_4 \cdot 2H_2O$), carnallite ($KMgCl_3 \cdot 6H_2O$) and finally sylvite (KCl). In the deeper horizons (around 3m) of Didwana playa, Wasson et al., (1984) reported an additional Mg-Na carbonate-chloride, e.g. $Na_3Mg(CO_3)_2Cl$, northupite. Striking is the absence of any Mg-bearing evaporite in the western playa sediments. Another convincing support to the above interpretation of monsoonal influence is shown by the quite homogeneous chemical composition, e.g. variation of oxide ratios in the eastern profiles is much smaller compared to the western profiles, but significant enough to delineate the phases of palaeoclimatic changes (for details see section 7.4).

Table 37 Comparison of C_{org}, carbonate and sulphate abundance between western and eastern playas

		Western playas	Eastern playas
Surface	C_{org}	0	0.1-0.2 %
	Carbonate	~5 %	~5%
	Sulphate	2-3 %	3-5 %
Depth profile	C_{org}	-	++
	Carbonate	+	+++
	Sulphate	+++	+

(+=<3 %, ++= 3-10 %, +++= 10-20 %)

The dominance of carbonates in the eastern depth profiles and of sulphates in the western depth profiles mirrors the different development of the evaporation cycles in both the regions (east and west). The higher water active eastern areas evaporate only to the extent of ~80 %, thus enabling the precipitation of mainly carbonates (and minor amount of sulphates), whereas the low water active western playas exhibit the larger evaporation cycle, up to the formation of sulphates (Figure 56). The occurrence of highly soluble K-Mg-evaporites (polyhalite, carnallite and sylvite) in the eastern playas can be explained by the mechanism of dissolution of the soluble chlorides and sulphates during the monsoon period and later their re-precipitation during the non-monsoonal summer months. That would mean that the low amounts of polyhalite, carnallite, sylvite, glauberite and trona are quite recent formations. This interpretation is supported by the fact that these mentioned highly soluble evaporites are found only in the surface samples, but never in deeper horizons. In the deeper horizons of the eastern profiles carbonates occur more abundantly.

Dolomite is occurring in the carbonate-rich eastern profiles. It is always a type of Fe-rich proto-dolomite, showing a disordered structure (seen both in DTA and XRD diagrams) and

non-stoichiometry (e.g. Ca > Mg+Fe). The relatively enriched values of $\delta^{18}O_{carbonate}$ is attributed to the higher Mg contents in carbonates (Table 32) and $\delta^{13}C_{carbonate}$ to the early precipitated calcites which are later dolomitised (after Dutkiewicz et al., 2000). Similar dolomites are also reported by Sinha & Smykatz-Kloss (2003) from the deeper horizons (4 to13 m depth) of the Sambhar playa. In the western profiles (Pokhran and Pachapadra), dolomite is almost absent. The depleted values of $\delta^{18}O$ and $\delta^{13}C$ in the western playa carbonates suggest them to be of low Mg-calcite.

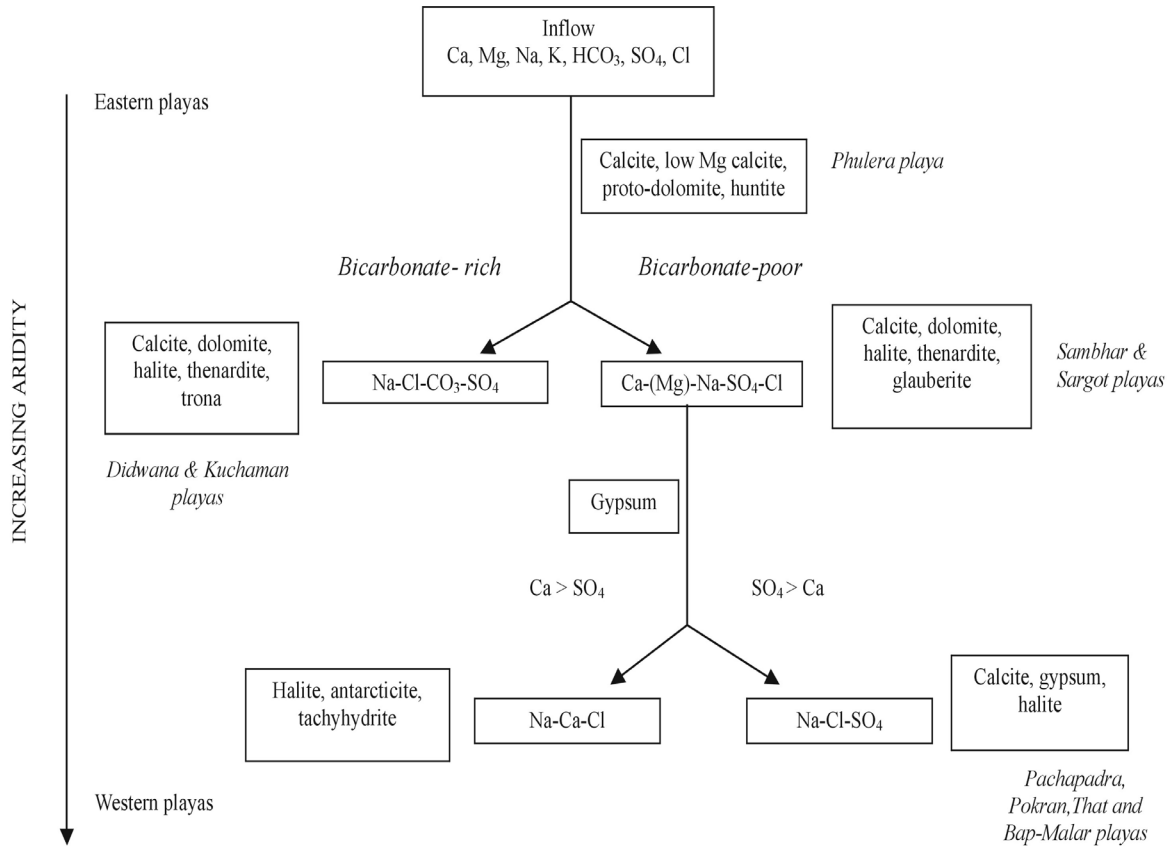

Figure 56 Theoretical diagram of the evaporative concentration of saline solutions of different playa lakes in the Thar desert in accordance with the model of Eugster and Hardie (1978).

7.2 Provenance

The detrital and dissolved materials of the eastern and western playas are sourced from the Aravalli mountains situated in the eastern desert margin. Additionally, some of the detrital fractions of the western playas are also derived from the outcrops in their surroundings, e.g. some rock fragments (mainly basalts), angular in their degree of roundness and of 0.2 to 0.5 mm in diameter (Figure 21) and a lot of aeolian sand and silt. This is mirrored in large variation of the silica contents in the western playas (Pokhran and Pachapadra).

Rock fragments occur only in the western playa sediments, e.g. in an environment with lower degree of chemical weathering. Besides the mentioned basaltic fragments (showing a very low degree of roundness) and minerals like labradorite, pyroxenes, and (Ti-) magnetite, there is also a second type of rock fragments occurring in the western playa sediments. This type is different from the first type in its degree of roundness and in its petrographic character: it is well rounded and metamorphic (mica schist, epidote-bearing schist, and quartzite) in origin (Figure 18, Figure 19, Figure 20). These type rocks have their source in the eastern desert margins (Sen & Ramalingam, 1976; Biswas et al., 1982; Misra, 1982; Rai & Sinha, 1990; Rai & Absar, 1996). The perfect degree of roundness mirrors an intensive mechanical influence on the grains due to the relatively long transportation. The distance from the Aravallis to the western playas is around 200 km with a regional slope from east to west (e.g. Sambhar is situated at an elevation of ~500 m and Pokhran at ~200 m) (Figure 2). This favours the transportation of the rock fragments from east to west. Another observation from this investigation is that the thickness of the lacustrine sediments is showing a gradual decrease from east to west, with the exception of the Pachapadra playa. This playa is having a relatively thick profile as it is located on a palaeo river bed (after Ghose, 1964; Ghose et al., 1977). The different degree of weathering due to the difference in water availability is also observed in the abundance of the detrital minerals. While a number of primary minerals have disappeared in the eastern playas due to intensive interaction with rain, pore and ground waters, these minerals are abundant in the relatively arid western environment (Table 36). These far transported species (amphibole, biotite, hematite, epidote, rutile and pyroxenes and others) do not show any remarkable influence of chemical breakdown but they show a distinct degree of mechanical influence.

Geochemically, the two regions (east and west) are quite different, too. The difference in the behaviour of the elements (ions) in the two above mentioned regions is mainly controlled by their solubility. The easily soluble cations (Na^+, Mg^{2+}, and Cu^+) are transported and deposited in the surface sediments of western playas by evaporation. But the hydrolysates and similar elements are showing enrichment in the eastern playas. The western playas show an average Na_2O content of 7.93 %, whereas the eastern playas show an average content of 2.61 %. For MgO, the concentrations are 3.14 % and 2.66 % and for Cu, it is 41 ppm and 21 ppm respectively (see Table 12 and Table 13). The hydrolysates, e.g. Fe_2O_3, Al_2O_3, TiO_2, Zr, are all enriched in the eastern playas (tables 12, 13). This character is also shown by the large cations (K, Rb), which are partly adsorbed by the fine fragments (clay minerals and organic

carbon) shortly after the chemical dissolution and are not transported further. Sr and Ba may be partly adsorbed on the hydrolysates and partly incorporated in the carbonates and sulphates. This differential behaviour of the transported ions is also observed in the same playa, showing a typical zonal pattern (Figure 29 and Figure 30) with hydrolysates at the margin and the soluble compounds (e.g evaporites) in the centre. This effect of zonal evaporation and precipitation is only occurring in the closed basins of the eastern region (e.g. Sambhar and Didwana), but not in the western playas due to the lack of chemical weathering.

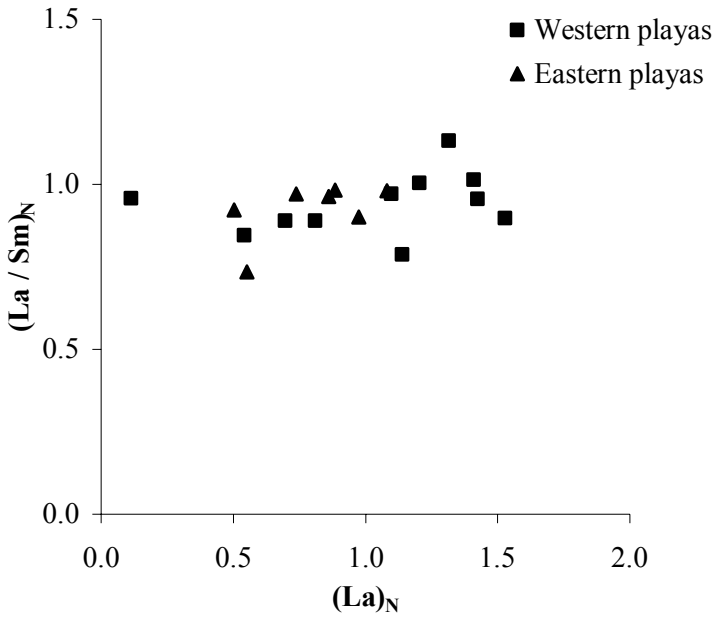

Figure 57 LREE fractionation of playa sediments with changing REE content

These observations of mineralogical and geochemical differentiations of the two regions are also supported by the REE geochemistry. The UCC normalised REE patterns of the playas of both the region (east and west) also show characteristic differences. The eastern sediments are showing more homogeneous REE patterns, whereas the western sediments are showing a large variation. Additionally, the western sediments are relatively enriched both in total REE and HREE (Figure 44 and Figure 45). The playa sediments are a mixture of clastics, derived from the weathering of the catchments and evaporites, precipitated depending upon the composition of the inflows. So the REE concentrations in these sediments result from the competing influences of provenance, weathering, sediment sorting, and aqueous geochemistry of the inflow precipitating the chemical sediments. The study of Singh & Rajamani (2001)

suggests that the REE abundance in the sediments is mainly controlled by its mineralogical composition. So the provenance should be the single most important factor contributing to the REE contents of the clastic sediments. Again, the chemically precipitated sediments (evaporites) have very low contents of REE, and the increasing amount of evaporite in the sediments has a diluting effect on the absolute concentration of REE. But their REE patterns show a positive Ce anomaly and increasing REE concentrations with increasing atomic number, which is a typical feature of alkaline, carbonate rich, low temperature water (Möller & Bau, 1993; Volkova, 1998).

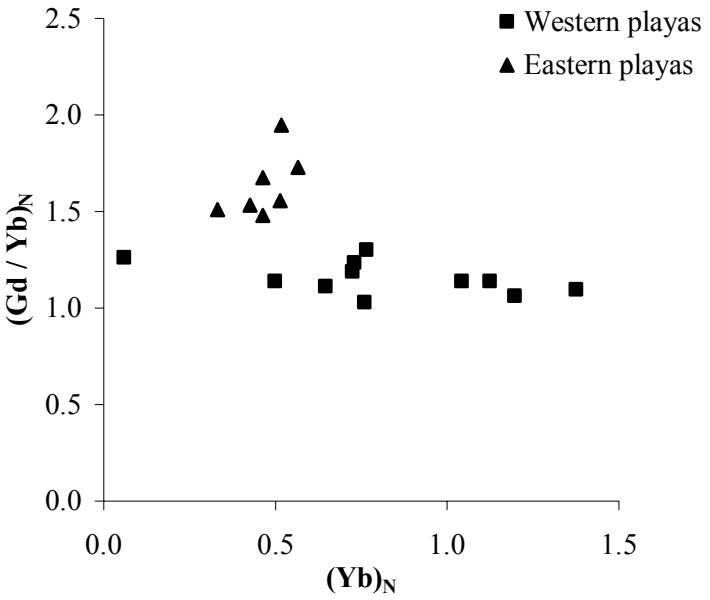

Figure 58 HREE fractionation of playa sediments with changing REE content

The UCC normalised eastern desert playa sediments (east) and western arid core playa sediments (west) do not show any LREE fractionation, expressed as $(La/Sm)_N$ (Figure 57), whereas they show varying degree of HREE fractionation expressed as $(Gd/Yb)_N$ (Figure 58), with changing REE contents. The western playa sediments are enriched in HREE compared to eastern sediments. This feature is also similar for total REE fractionation (Figure 59). So the difference in the REE patterns between western and eastern group of playa sediments is mainly due to the variation in the $(Gd/Yb)_N$ ratios. The distribution of $(La/Sm)_N$ and $(Gd/Yb)_N$ in the playa sediments of both the region indicate two distinct clusters (Figure 60). The dissimilarity in the degree of fractionation of HREE for both west and east playa sediments

indicate differential distribution of minerals, depending upon the resistance to weathering. The enrichment of both total REE and HREE in the western sediments is due to the presence of higher amount of heavy minerals, e.g. garnet, zircon, epidote, monazite, xenotime and sphene (after Taylor & McLennan, 1985; McLennan, 1989). The source of REE is undoubtedly the rocks present in the catchments of the playa basins. But it is believed that the relatively higher abundance of heavy minerals due to the lower degree of weathering and the presence of higher amount of evaporites controls enriched abundance and the large variation of the REE distribution in the western playa sediments.

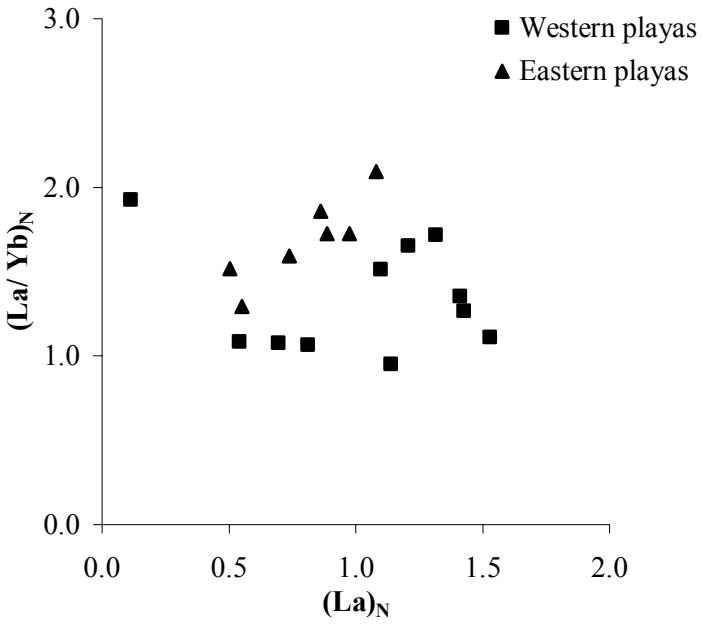

Figure 59 Total REE fractionation of playa sediments with changing REE content

So from the (REE) geochemistry, mineralogy and geology of the area it can be concluded that the source rocks of playas of both the regions are mainly metamorphic rocks of Aravallis, variable in type and metamorphic grade. The relicts of these rocks are observed in their well rounded fragments and a number of minerals typical for metamorphic rocks (epidote, zoisite, amphiboles, garnets, and well ordered mica and Fe-chlorite). Presence of trace minerals like monazite and xenotime in the playa sediments indicate a part of the source to be igneous rocks, especially pegmatites. But the relatively higher water activity in the east and the lower degree of chemical weathering in the arid western playas play a major role in the different mineral distribution, which is also mirrored by the REE geochemistry of the sediments. Additional to this the western lakes e.g. Bap, Pokhran, That and Pachapadra, also receive sediments from the Proterozoic and Mesozoic formations comprising of Malani igneous suit

(basalt and rhyolite), limestone, sandstone, shale and boulder beds located in their surroundings (Rai, 1990; Deotare et al., 2003). This interpretation is supported by the presence of rock fragments of basalt, rhyolite and limestone in the sediments of the western playas.

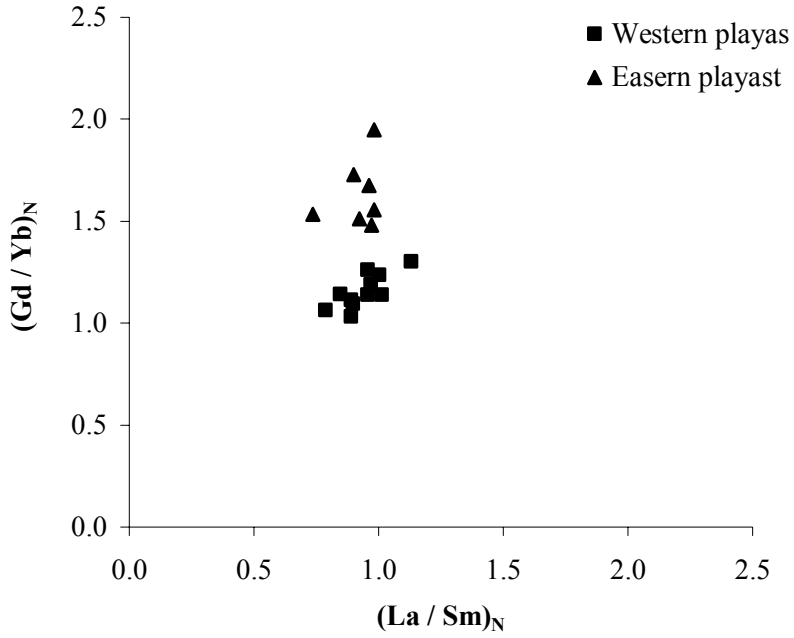

Figure 60 Distribution of $(La/Sm)_N$ and $(Gd/Yb)_N$ in the playa sediments

7.3 Correlation of the depth profiles

The comparison of the studied depth profiles leads to the correlation between different playas. The eastern playas show a horizon of enrichment of CaO, MgO and Sr in the depth of 70 to 80 cm. This horizon is characterised by the occurrence of calcite and mainly dolomite (Figure 31, Figure 32 and Figure 33). This carbonate enriched layer is very clearly visible in the profiles of Sambhar and Phulera and less distinct in Didwana. The Didwana profile is more or less homogeneous in the distribution of all the major and trace elements. Among the western playas, dolomite occurs only in the profile of the Bap-Malar playa, and the horizon of 40 to 50 cm shows the enrichment of CaO, MgO and Sr. But this layer is not as distinct as Phulera and Sambhar. This feature is very similar for the profile of the western Pokhran playa as well. An enriched horizon of CaO and Sr (not MgO) is observed at the depth of 40 to 50 cm, and this horizon is characterised by the presence of a thick gypsum layer. This evidence mirrors the decrease in sediment thickness from east to west. The same enriched horizon, e.g. higher Sr-CaO bound to the gypsum layer, is occurring in the Pachapadra playa at a depth of 140-

150 cm. This exceptional thick profile located in the arid western region can be explained by the special geomorphic characteristic of the profile location: the profile is located on a palaeo-river bed (after Ghose, 1964; Ghose et al., 1977), where the rate of sedimentation must have been higher than in the normal western playas. This interpretation is supported by other geochemical criteria, e.g. Na_2O/Al_2O_3 and Sr/Ba, which show peaks in the 140-150 cm depth at Pachapadra and 40-50 cm depth at the Pokhran playa respectively (Figure 39 and Figure 41). Other than this the playa profiles are divided into six (I to VI) different geochemical zones and are correlated in terms of the absolute concentrations and calculated ratios of major and trace elements.

This comparison of all the mineralogical and geochemical data leads to a regional picture of similarity and variation, which is expressed in the different vertical geochemical zones (see section 7.4).

7.4 Palaeoclimatological considerations

The geochemical zones I to VI mirror the different environment of deposition in the region. The useful criteria which lead to the milieu of deposition are the determined ratios of soluble cations to the hydrolysates, e.g. Na_2O/Al_2O_3, Na_2O/TiO_2, SiO_2/Al_2O_3 and in carbonate free environments CaO/Al_2O_3, MgO/Al_2O_3. Due to the different solution and adsorption behaviour of the alkalis (e.g. K is largely adsorbed on fine grained materials), the Na_2O/K_2O also enables the palaeoclimatic interpretations and considerations. Mineralogically, the ratio of carbonates to sulphate mirrors the development of chemical sedimentation. In a relatively humid to sub-humid environment (comparable to the present day eastern playas), mainly carbonates and periodically sulphates and chlorides precipitate. In a more arid (semi-arid) environment (comparable to the present day western playas) the dominant chemical sediments are sulphates and chlorides. The (sub-) recent climate of the region is mirrored by both the evaporite mineralogy and surface geochemistry. The highest values of SiO_2/Al_2O_3, Na_2O/Al_2O_3, Na_2O/TiO_2 and Na_2O/K_2O are observed in the recent evaporitic zone I (see Table 35), except partly Bap-Malar playa. This playa must have been in some special environmental conditions.

The following Table 38 presents the average values of the above mentioned ratios for the six vertical geochemical zones. The thickness of these zones is different in different playas (e.g. thicker in the eastern regions and thinner in the western region, except the special condition of sediment accumulation in the Pachapadra palaeo-river bed). But the ratios are always

comparable and "horizon-specific". So the environment of formation must have been similar (comparable) during the formations of these geochemical zones in all the studied profiles. This means, zones I and V should have been arid phases with low (or nearly no) sign of chemical weathering and zones II and VI, humid phases of sediment formation.

Table 38 Average values of different geochemical proxies in the geochemical zones

Zones	Na_2O/Al_2O_3		Na_2O/TiO_2		Na_2O/K_2O		SiO_2/Al_2O_3		Zr/Al_2O_3	
	East	West	East	West	East	West	East	West	East	West
I	0.25	0.59	5.31	12.87	1.38	4.95	6.77	4.91	0.0021	0.0013
II	0.19	0.25	4.34	5.66	0.96	1.56	4.38	3.40	0.0012	0.0007
III	0.22	0.33	4.72	7.17	1.11	2.01	4.54	3.90	0.0011	0.0011
IV	0.26	0.25	5.44	4.55	1.29	1.29	5.29	4.64	0.0013	0.0019
V		0.27		5.25		1.33		8.24		0.0027
VI		0.11		2.89		0.41		2.85		0.0009

Figure 61 shows the climatic development of the playa profiles. The oldest studied zone VI (available only from Pokhran playa) is showing the highest concentration of Al_2O_3, K_2O, TiO_2, Fe_2O_3, Cu, Zn and Rb. Again, this zone is showing the higher concentration of abiotic P_2O_5, mainly derived from the weathering of the pegmatites. So this zone with highest degree of chemical weathering (Table 38) and highest concentration of trace and major elements (Table 27) indicate the most humid phase of playa sedimentation. The zone V, characterised by the highest values of SiO_2/Al_2O_3 and Zr/Al_2O_3, lower concentration of major and trace elements and a lower degree of chemical weathering represent a phase of aridity. The enriched $\delta\ ^{18}O_{carbonate}$ values in this zone indicate a relatively higher temperature, too. The zone IV of Pokhran playa includes the occurrence of the Mg-silicate palygorskite (Table 10). Recently, this mineral has been reported from the aridic soils of northern Namibia (Eitel, 1993). The zone III in the eastern playas shows a dolomite enriched layer, whereas the same zone in the western playas shows a gypsum enriched layer. In both the regions this zone is characterised by lower concentration of major and trace elements and lower degree of chemical weathering. So all these evidences indicate that from zone V to II the milieu of formation gradually changes to more and more humid conditions, showing the zone II as a comparably humid phase (after VI). The $\delta\ ^{18}O_{carbonate}$ values, which are showing a gradual decrease from zone V to II support this interpretation (Figure 47). But its relatively enriched concentration along with presence of a dolomite (east) or gypsum (west) layer in the zone III

indicates it to be a relatively more arid phase than the phase IV. The remarkably humid zone II is showing highly rounded rock fragments. Evidently, this horizon represents a time of higher transport energy. The higher concentration of metal oxides, trace elements and abiotic phosphorus in the sediments during this phase supports higher weathering in the catchments. The (sub-) recent zone I is highly arid again. Like zone V, zone I is also showing higher SiO_2/Al_2O_3 and Zr/Al_2O_3, which seem to have accumulated due to the larger input of aeolian sand and silt. Tripathi & Rajamani (1999) interpreted an enrichment of SiO_2 and Zr in the eastern margin of Thar as aeolian input. Similar observations have also been reported by Juyal et al. (2003). These evidences support an arid environment with higher aeolian input in zones I and V.

Comparing the eastern and western profiles, it is evident that the geochemical changes between the zones (e.g. the development of horizons from bottom to top) are more intensive in the western region. The ratios of the major elements along the vertical zones indicate a higher humidity for the eastern region of the Thar during the history of sedimentation. Evidently, the absence of not very resistant silicates of the amphibole group in the deeper horizons of Sambhar is a further index for the higher humidity of the region. The present day higher humidity of the eastern region is also supported by the occurrence of H_2O-rich evaporites (e.g. trona, polyhalite, and carnallite) in the surface sediments. But in general the palaeoclimatic development of both the regions has been parallel. The greater geochemical variability, e.g. the larger palaeoclimatological changes, has occurred in the western region, where the sulphate gypsum has been the dominant evaporite (with a maximum in the zone III). The zone III in the eastern region is dominated by the carbonates, calcite and dolomite. The eastern region is enriched in organic carbon; especially the DTA curves enable the identification and differentiation of several C_{org}-Fe-rich horizons with partly reducing condition of mineral formations. Thus, the dolomites are disordered proto-dolomites and have incorporated distinct amounts of two valent Fe. This has also been reported by Sinha & Smykatz-Kloss (2003) from a Sambhar bore hole, which showed only one exceptional layer in 4 m depth, with very well ordered and stoichiometric dolomite.

As the present investigation is chronologically constrained, the published works of Wasson et al. (1984), Enzel et al. (1999) on playas of Thar, Sirocko et al. (1993), Sirocko (1995) and Lückge et al. (2001) on sediment core from Arabian Sea are taken into consideration for comparison. All the above mentioned workers constructed the palaeo-monsoon of the region using ^{14}C dating, mineralogy and geochemistry. But the contradictory present day climate of

Arabian Sea and Indian Thar desert rules out a comparison between our findings with the findings from the Arabian Sea sediment core. The (sub-) recent climate of northern Arabian Sea off Pakistan is dominated by the north-west winter monsoon (after Lückge et al., 2001), whereas the south-west summer monsoon controls the climate of the Thar (source: Indian Meteorological Division, Delhi and India Institute of Tropical Meteorology, Pune). So this investigation and characterisations are parallelised with the publications of Wasson et al. (1984) and Enzel et al. (1999).

These comparisons lead to very systematic palaeoclimatic changes of the region (Figure 62). From ~ 10,000 yr BP to ~8,300 yr BP (zone V and IV) the climate of the region was arid; the lakes were shallow with large input of aeolian sand and silt. The aeolian activity was lower towards the later parts as the aeolian input (measured by Si/Al, Zr/Al) decreased relatively. The relatively higher precipitation would have stabilised the sand dunes in the surroundings. From ~8,300 yr BP to ~6,300 yr BP (zone III) the climate of the region again shifted to a relative arid side, marked by more of gypsum (western region) and dolomite (eastern region) precipitation. The higher weathering index, depleted $\delta^{18}O$ (lower temperature) and higher concentration of metal oxides indicate a humid phase from ~6,300 yr BP to ~4,800 yr BP (zone II). The increased amount of evaporites and aeolian input indicates a more or less arid climate of the region during the last 4,800 yrs (zone I).

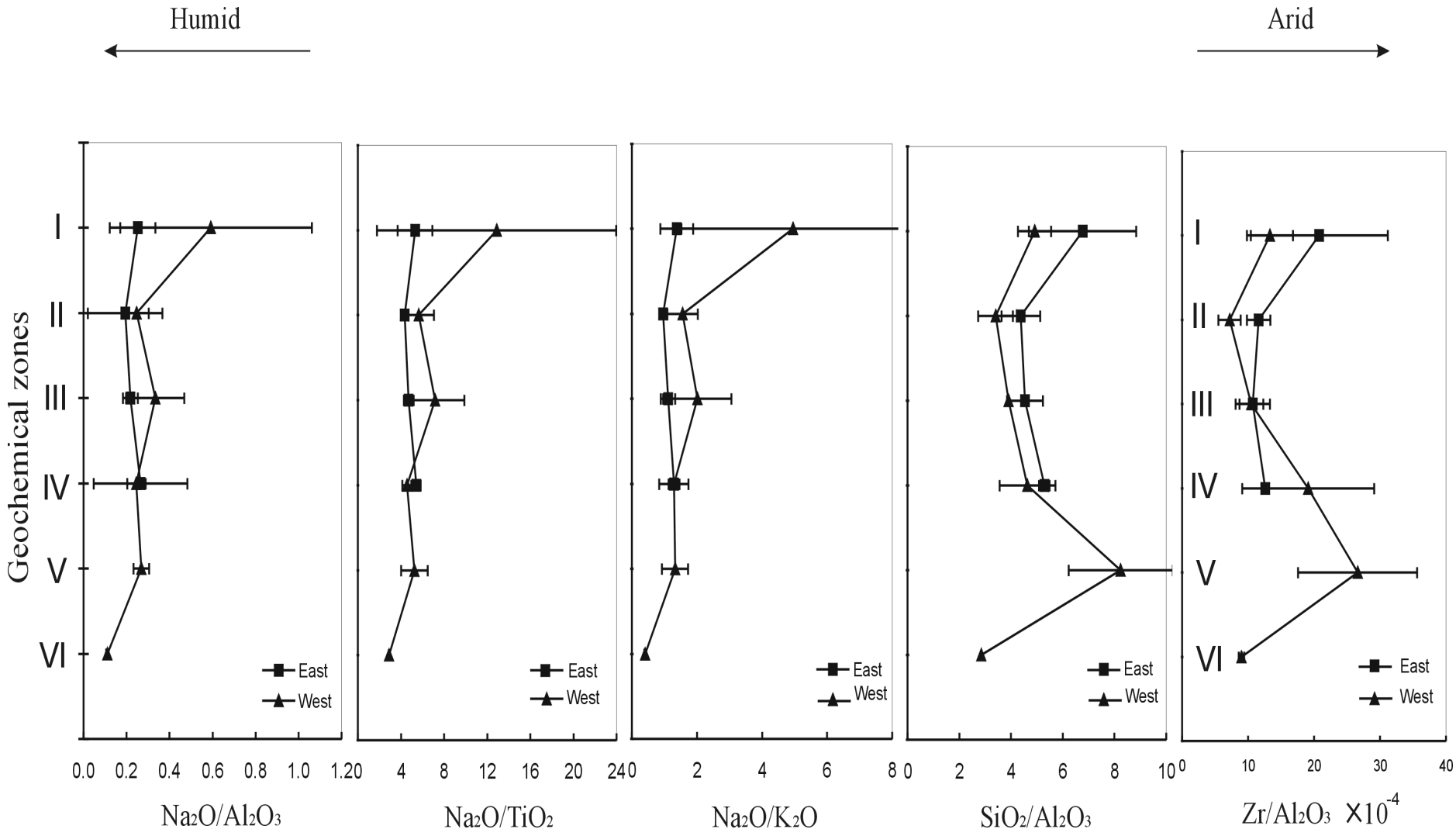

Figure 61 Variation of different geochemical proxies in the vertical geochemical zones

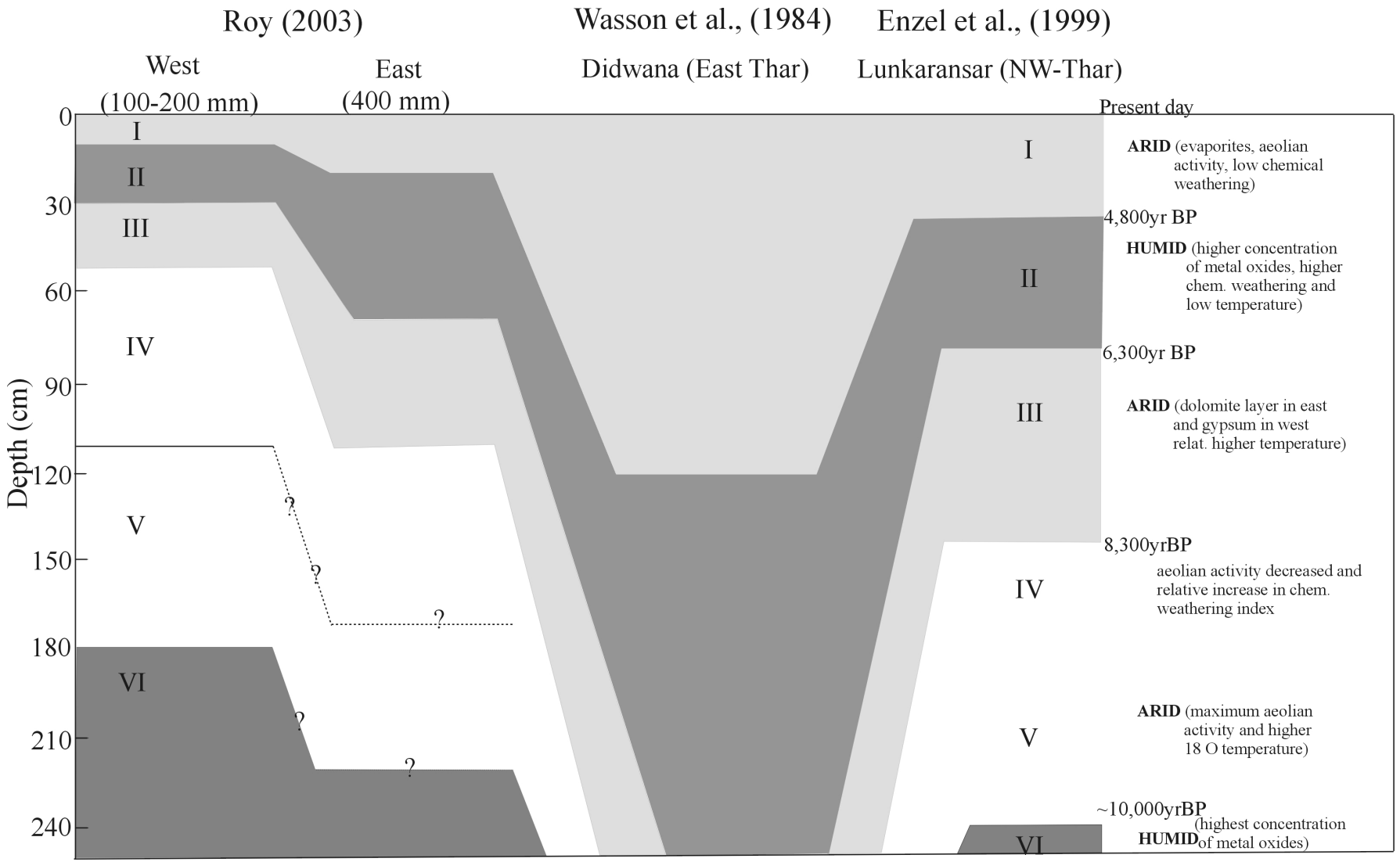

Figure 62 Reconstruction of palaeoclimatology of Thar desert by evaluating the mineralogical and geochemical investigations. The ^{14}C dates are from Wasson et al., 1984 and Enzel et al., 1999

8. Summary

The Thar desert of Rajasthan (India) stretches from the Aravalli mountains in the east to the border of Pakistan in the west. The climate is semi-humid to semi-arid (annual precipitation of ~300 to ~400 mm) in the eastern part, whereas it is semi-arid to arid (annual precipitation of ~100 to ~200 mm) in the western part. The sediments of ten different playas (five from each region) have been investigated by mineralogical (e.g. XRD, optical, and thermal analysis) and geochemical (e.g. XRF, ion chromatography, CWA/CSA, electron microprobe, gas ion mass spectrometry, and ICP-MS) methods. The results are outlined and discussed with respect to the following goals: (1) differentiation of the sediments of both regions, (2) source of the detrital and evaporitic material, (3) correlation between the profiles of the eastern and western playas, (4) palaeoclimatologic development of the region.

(1) Due to the lower water availability, the sediments of the western playas (e.g. Bap-Malar, Pachapadra, Pokhran, That, and Thob) show much less features of chemical weathering than those of the eastern playas (e.g. Didwana, Kuchaman, Sargot, Sambhar, and Phulera). This is manifested in the higher abundance of the primary (detrital) minerals and rock fragments in the western region, as well as in the large variation of bulk chemical composition in depth profiles of the western playas. Especially, the evaporitic phases show large differences: due to the difference in the development stage of the evaporation cycle, the main “western” evaporite is gypsum, while the eastern region only shows dominant carbonates (calcite, dolomite). Again, the larger water activity of the eastern region leads to the abundance of several H2O-bearing evaporites (e.g. carnallite, polyhalite, mirabilite, trona) and to several stages of disequilibrium (e.g. presence of carnallite and sylvite in the same horizon).

(2) Besides few angular fragments of basalt and rhyolite (sourced from the surroundings of the western playas), well-rounded small size metamorphic rock fragments in the sediments of the western playas mirror the transportation over several hundred of kms. This is reflected by the thickness of the playa sediments, which decreases from east to west, too (except the Pachapadra playa, which is located on a palaeo-river bed). Geochemically, the eastern region shows enrichment of the hydrolysates, while the western part is enriched by the evaporation of the highly soluble cations and anions (e.g. Na-chloride, Mg-Ca-Na-sulphates). For example, the Na_2O content is three times higher in the western than in the eastern sediments

(e.g. ~8 to 2.6 mass %, respectively). All these results show the source of the transported material (in solid and dissolved form) to be the eastern-most part of the Thar, e.g. the metamorphic and (to a smaller extent) igneous rocks of the Aravalli mountains.

(3) The mineralogical and geochemical composition of different horizons leads to the correlation between several of the playa profiles. This correlation is clearly seen in the parallel development of geochemical zones of different depth profiles.

(4) From the vertical zonation and characteristic ratios of the oxides of soluble cations (e.g. Na_2O, K_2O) to hydrolysates (e.g. Al_2O_3, TiO_2, Zr), very systematic palaeoclimatic development of the region has been made. A comparison with the results of earlier investigations on sediment cores of the Arabian Sea (Sirocko et al., 1993; Sirocko, 1995; Lückge et al., 2001) and mainly with the playa sediments of the Thar desert (Wasson et al., 1984; Enzel et al., 1999) enables a rough time scale for the different climatic zones. A change from an older humid to a distinct arid phase occurred around 10,000 yr BP (zone VI to V). Aridity decreased continuously from zone V to zone II, with a phase (zone V) of remarkable aeolian input. A decrease in aeolian activity occurred after 8,300 yr BP (zone IV to III). Around 6,300 yr BP the climate of the region changed from arid to humid and the period between 6,300 to 4,800 yr BP (zone II) was the most humid zone in the whole Thar. Finally, around 4,800 yr BP a change from this humid phase (zone II) to the (sub-) recent arid phase (zone I) occurred.

9. References

Abbott, M. B., Wolfe, B. B., Wolfe, A. P., Seltzer, G. O., Aravena, R., Mark, B. G., Polissar, P. J., Rodbell, D. T., Roxe, H. D. & Vuille, M. (2003): Holocene paleohydrology and glacial history of the central Andes using multiproxy lake sediment studies. Palaeogeography, Palaeoclimatology, Palaeoecology, 194, 123-138.

Abu-Hamatteh, Z. S. H. (2002): Geochemistry and tectonic framework of Proterozoic mafic Metavolcanics of Aravalli-Delhi orogen, NW India. Chem. Erde, 62, 123-144.

Agarwal, S. C. (1957): Pachapadra and Didwana Salt Source. Gov. Ind. Press, Delhi, 206.

Anderson, D. M., Overpeck, J. T. & Gupta, A. K. (2002): Increase in the Asian southwest monsoon during the past four centuries. Science, 297, 596-599.

Bakker, R. J. & Mamtani, M. A. (2000): Fluid inclusions as metamorphic process indicators in the southern Aravalli Mountain Belt (India). Contrib. Mineral. Petrol. 139, 163-179.

Bakliwal, P. C. & Grover, A. K. (1999): Signatures and migration of Saraswati river in Thar desert, western India. Memoir Geol. Soc. India, 42, 113-119.

Bhattacharya, B. N., Gupta, S. K., Rishi, B. P., Mitra, A. K. & Kashyap, V. K. (1982): Seasonal variation in the composition of Sambhar lake brine and possible origin of its salinity. Rec. Geol. Sur. Ind. Misc. Pub. 49.

Biswas, R. K., Chattopadhyay, G. S. & Sinha, S. (1982): Some observations on the salinity problems of the inland lakes of Rajasthan. Rec. Geol. Sur. Ind. Misc. Pub. 49.

Braitsch, O. (1971): Salt Deposits. Their origin and composition. Springer-Verlag, Heidelberg NewYork.

Brindley, G. W. & Brown, G. (1980): Crystal Structures of Clay Minerals and Their X-Ray Identification. Mineralogical Society, Monograph No. 5, London.

Brown, G. (1961): The X-Ray Identification and Crystal Structures of Clay Minerals. Mineralogical Society, London.

Camur, M. Z. & Mutlu, H. (1996): Major-ion geochemistry and mineralogy of the salt lake (Tuz Gölü) basin, Turkey. Chemical Geology, 127, 313-329.

Cooke, R. U. (1981): Salt weathering on deserts. Proce. Geol. Assoc. London, 92, 1-16.

Dassarma, D. C. (1988): Post orogenic deformation of the Pre-Cambrian crust in north eastern Rajasthan.- In: Precambrian of the Aravalli Mountains, Rajasthan. Memoir Geol. Soc. India, 7, 109- 120.

Deotare, B. C., Kajale, M. D., Kshirsagar, A. A. & Rajaguru, S. N. (1998): Geoarcheological and palaeoenvironmental studies around Bap-Malar playa, district Jodhpur, Rajasthan. Current Science, 3, 316-320.

Deotare, B. C., Kajale, M. D. & Rajaguru, S. N. (2003): Palaeoenvironmental history of Bap-Malar and Kanod playas of western Rajasthan, Thar Desert. Paper for the inclusion in special issue of the proceedings of Indian Academy of Sciences, Bangalore (unpublished).

Dhir, R. P., Kar, A., Wadhawan, S. K., Rajaguru, S. N., Misra, V. N., Singhvi, A. K. & Sharma, S. B. (1992): Thar Desert in Rajasthan: Land, man and environment. A. K. Singhvi & Amal Kar (Ed.), Geol. Soc. India, Bangalore, 191.

Dickson, R. R. (1984): Eurasian snow cover versus Indian monsoon rainfall- an extension of the Hahn-Shukla results. J. Clim. Appl. Meteorology, 23, 171-173.

Dutkiewicz, A., Herczeg, A. L. & Dighton, J. C. (2000): Past changes to isotopic and solute balances in a continental playa: clues from stable isotope of lacustrine carbonates. Chemical Geology, 165, 309-329.

Eitel, B. (1993): Kalkkrustgenerationen in Namibia: Carbonatherkunft und genetische Beziehungen. Die Erde, 124, 85-104.

Eitel, B., Blümel, W. D. & Hüser, K. (2003): Palaeoenvironmental Transitions Between 22 ka and 8 ka in Monsoonally influenced Namibia. In: Palaeoecology of Quaternary Drylands, W. Smykatz-Kloss & P. Felix-Henningsen (Eds); Lecture Notes in Earth Sciences, Vol. 102, 169-196, Springer-Verlag.

Emmerich, K. & Smykatz-Kloss, W. (2002): Exothermic effects in soils during thermal analysis. Clay Minerals, 37, 575-582.

English, P. M. (2001): Formation of analcime and moganite at Lake Lewis, central Australia: significance of groundwater evolution in diagenesis. Sedimentary Geology, 143, 219-244.

Enzel, Y., Ely, L. L., Mishra, S., Ramesh, R., Amit, R., Lazar, B., Rajguru, S.N., Baker, V.R. & Sandler, A. (1999): High resolution Holocene environmental changes in the Thar desert, northwestern India. Science, 284, 125-128.

Eugster, H. P. (1970): Chemistry and origin of the brines of Lake Magadi, Kenya. Mineral. Soc. Amer. Spec. Pap., 3, 213-235.

Eugster, H. P. & Hardie, L. A. (1978): Saline lakes. In: Lakes: Chemistry, Geology, Physics. A. Lerman (Ed.), Springer-Verlag, 237-293.

Eugster, H. P. & Jones, B. F.(1979): Behavior of major solutes during closed-basin brine evolution. American Journal of Science, 279, 609-631.

Felix-Henningsen, P. (2003): Genesis and Paleo-ecological interpretation of Swamp Ore Deposits at Sahara Paleo-lakes of East Niger. In: Palaeoecology of Quaternary Drylands, W. Smykatz-Kloss & P. Felix-Henningsen (Eds); Lecture Notes in Earth Sciences, Vol.102, 49-74, Springer-Verlag.

Fritz, J. S., Gjerde, D. T. & Pohlandt, C. (1982): Ion chromatography. Springer-Verlag, Heidelberg.

Ghosh, B. (1964): Geomorphological aspects of the formation of salt basins in western Rajasthan. Proc. Symp. Problems of Indian Arid Zone, Minist. Educ. Gov. India and UNESCO, CAZRI, Jodhpur, 79-83.

Ghosh, B. (1965): J. Indian Soc. Soil Sci., 13, 123-126.

Ghosh, B., Singh, S. & Kar, A. (1977): Desertification around the Thar-a geomorphological interpretation. Ann. Arid Zone, 16, 290-301.

Giralt, S., Burjachs, F., Roca, J. R. & Julia, R. (1999): Late glacial to early Holocene environmental adjustment in the Mediterranean semi-arid zone of saline playa-lake (Alicante, Spain). Jour. Paleolimnology, 21, 449-460.

Godbole, N. N. (1952): The salinity of Sambhar lake. Bull. Nat. Inst. Sci. Ind. No. 1.

Godbole, N. N. (1972): Theories on origin of salt lakes in Rajasthan, India. Proc. 24th Int. Geol. Cong., Canada.

Govindaraju, K. (1994): Special issue Geostandard newsletters. Vol. XVIII, July 1994.

Grim, R. E. (1953): Clay Mineralogy, Mc Graw-Hill Book Company, New York.

Grosjean, M., Cartajena, I., Geyh, M. A. & Nunez, L. (2003): From proxy data to palaeoclimate interpretation : the mid-Holocene paradox of the Atacama desert, northern Chile. Palaeogeography, Palaeoclimatology, Palaeoecology, 194, 247-258.

Gupta, A. K., Anderson, D. M. & Overpeck, J. (2003): Abrupt changes in the Asian southwest monsoon during the Holocene and their links to the North Atlantic Ocean. Nature, 421, 354-357.

Gupta, S. N., Arora, Y. K., Mathur, R. K., Iqbaluddin Prasad, B., Sahai, T. N. & Sharma, S. B. (1980): Lithostratigraphic map of the Aravalli region. Geol. Surv. India, Calcutta.

Hardie, L. A. & Eugster, H. (1970): The evolution of closed basin brines. Mineral. Soc. Amer. Spec. Pap., 3, 273-290.

Hay, R. L. (1966): Zeolites and zeolitic reactions in sedimentary rocks. Geol. Soc. Amer. Special Paper, 85, 130.

Heine, K. (2003): Little Ice Age climatic fluctuations in the Namib Desert, Namibia and adjacent areas: Evidence of exceptionally large floods from slack water deposits and desert soil sequences. In: Palaeoecology of Quaternary Drylands, W. Smykatz-Kloss & P. Felix-Henningsen (Eds); Lecture Notes in Earth Scinces, Vol.102, 139-167, Springer-Verlag, Heidelberg.

Heron, A. M. (1935): Synopsis of the pre-Vindhyan geology of Rajputana. Trans. Nat. Inst. Sci. India, 1, 17-33.

Heron, A. M. (1953): The geology of central Rajputana. Mem. Geol. Surv. India, 79, 389.

Holland, T. G. & Christie, W. A. K.(1909): The origin of the salt deposits in Rajputana. Rec. Geol. Sur. Ind. 38, pt 2.

Humes (1967-68): Report of Land Customs Department.

Ingebritsen, S. E. & Sanford, W. E. (1998): Chapter 9- Evaporites. In: Groundwater in Geologic Processes, Cambridge Uni. Press, 246-254.

Inglés, M., Salvany, J. M., Munoz, A. & Pérez, A. (1998): Relationship of mineralogy to depositional environments in the non-marine Tertiary mudstones of the southwestern Ebro Basin (Spain). Sedimentary Geology, 116, 159-176.

Juyal, N., Kar, A., Rajaguru, S. N. & Singhvi, A. K. (2003): Luminescence chronology of aeolian deposition during the Late Quaternary on the southern margin of the Thar Desert, India. Quaternary International, 104, 87-98.

Kajale, M. D. & Deotare, B. C. (1997): Late Quaternary environmental studies on salt lakes in western Rajasthan, India: a summarised view. Quaternary Science 12(5), 405-412.

Kar, A. (1989): Geog. Rev. India, 51, 48-99.

Kar, A. (1990): A stream trap hypothesis for the evolution of some saline lakes in the Indian desert. In: Saline lakes in Indian deserts. Sen, A. K. and Kar, A.(Eds), Scientific Publishers, Jodhpur, 395-418.

Kar, A. (1993): Present day geomorphic processes as key to the reconstruction of Quaternary landform history in the Thar desert. Jour. Geol. Soc. India, 41, 513-517.

Khadkikar, A. S., Mathew, G., Malik, J. N., Gundu Rao, T. K., Chowgaonkar, M. P. & Merh, S. S. (1999): The influence of the south-west Indian monsoon on the continental deposition over the past 130 kyr, Gujarat, western India. Terra Nova, 11, 273-277.

Khandelwal, N. N. (1975): On the occurrence of halite in Didwana salt lake area, Rajasthan. Current Science, 44, No 1.

Kössl, H. (1988): Mineralogische und hydrogeochemische Untersuchungen im Gipskarstgebiet von Foum Tatahouine (SE-Tunesien) und im südwestdeutschen Gipskeuper (Obersontheim, Raum Schwäbisch Hall). Dissertation Universität Karlsruhe (TH), Karlsruhe.

Last, W. M. (1983): Sedimentology of playa lakes of the northern Great plains. Can. J. Earth Sci., 27, 107-125.

Lerman, A. (1970): Chemical equilibria and evolution of chloride brines. Mineral. Soc. Amer. Spec. Pap., 3, 291-306.

Leuschner, D. C., Sirocko, F., Schettler, G. & Garbe-Schönberg, D. (2003): Geochemical implications for changing dust supply by the Indian Monsoon system to the Arabian Sea during the last glacial cycle. In: Palaeoecology of Quaternary Drylands, W. Smykatz-Kloss & P. Felix-Henningsen (Eds); Lecture Notes in Earth Sciences, Vol.102, 121-137, Springer-Verlag, Heidelberg.

Lillesand, T. M. & Kiefer, R. W. (1994): Remotesensing and Image Interpretation. 3rd Ed., John Wiley & Sons.

Liu, W. G., Xiao, Y. K., Wang, Q. Z., Qi, H. P., Wang, Y. H., Zhou, Y. M. & Shirodkar, P.V. (1997): Chlorine isotopic geochemistry of salt lakes in the Qaidam basin, China. Chemical Geology, 136, 271-279.

Longmore, M. E., Torgersen, T., O'Leary, B. M. & Luly, J. G. (1986): Cesium-137 redistribution in the sediments of the playa, lake Tyrrell, north-western Victoria. Palaeogeography, Palaeoclimatology, Palaeoecology, 54, 181-195.

Lückge, A., Doose-Rolinski, H., Khan, A. A., Schulz, H. & von Rad, U. (2001): Monsoonal variability in the northeastern Arabian sea during the past 5000 years: geochemical evidence from laminated sediments. Palaeogeography, Palaeoclimatology, Palaeoecology, 167, 273-286.

Magee, J. W. & Miller, G. H. (1998): Lake Eyre palaeohydrology from 60 ka to the present: beach ridges and glacial maximum aridity. Palaeogeography, Palaeoclimatology, Palaeoecology, 144, 307-329.

Mayayo, M. J., Bauluz, B., López-Galindo, A. & González-López, J. M. (1996): Mineralogy and geochemistry of the carbonates in the Calatayud basin (Zaragoza, Spain). Chemical Geology, 130, 123-136.

McLennan, S. M. (1989): Rare earth elements in sedimentary rocks: Influence of provenance and sedimentary processes. In: Geochemistry and mineralogy of rare earth elements, B. R. Lipin & G. A. McKay (Ed.), Reviews in Mineralogy, 21, 169-200.

Meehl, G. A. (1994): Coupled land-ocean-atmosphere processes and south Asian monsoon variability. Science, 266, 263-266.

Mensching, H. (1979): Tunesien, eine geographische Landskunde. Darmstadt (Wiss. Buchges.).

Misra, S. P. (1982): Geochemical evolution of Sambhar salt lake, Jaipur and Nagaur district, Rajasthan, Proc. Workshop on the problem of deserts in India, Geol. Soc. India, 92-99.

Moore, D. M. & Reynolds, R. C. (1997): X-ray diffraction and the identification and analysis of clay minerals. Oxford University Press, New York.

Möller, P. & Bau, M. (1993): Rare-earth patterns with positive cerium anomaly in alkaline waters from lake Van, Turkey. Earth Plan. Sci. Letters, 117, 671-676.

Ordónez, S., Calvo, J. P., García Del Cura, M. A., Alonso-Zarza, A. M. & Hoyos, M. (1991): Sedimentology of sodium sulphate deposits and special clay from the Tertiary Madrid Basin (Spain). Spec. Publ. Int. Ass. Sedimentology, 13, 39-55.

Ordónez, S. & García Del Cura, M. A. (1994): Deposition and diagenesis of sodium-calcium sulfate salts in the Tertiary saline lakes of the Madrid Basin, Spain. In: Sedimentology and Geochemistry of Modern and Ancient Saline lakes, SEPM Special Publication, 50, 229-238.

Pant, R. K. (1993): Spread of loess and march of desert in western India. Current Science, 64, 841-847.

Raghav, K. S. (1992): Quaternary history of a part of the North Eastern fringe of the Thar Desert, India. Annals of Arid Zone, 31(1), 1-7.

Rai, V. (1990): Facies analysis and depositional environment of Pokaran saline rann, district Jaisalmer, Rajasthan, India, Jour. Geol. Soc. India, 36, 317-322.

Rai, V. & Sinha, A. K. (1990): Geological evolution of Kuchaman lake, district Nagaur, Rajasthan. J. Palaeontological Soc. Ind., 35, 137-142.

Rai, V. & Absar, A. (1996): Sub-lacustrine hydrothermal activity in Kuchaman and Sargot saline lakes, District Nagaur, Rajasthan. Geothermal Energy in India. GSI. Spl. Pub., 45, 361-366.

Ramesh, R., Jani, R. A. & Bhushan, R. (1993): Stable isotopic evidence for the origin of water in salt lakes of Rajasthan ad Gujarat. J. Arid Environment, 25 , 117-123.

Reinhardt, L. & Ricken, W. (2000): The stratigraphy and geochemical record of Playa Cycles: monitoring a Pangean monsoon-like system (Triassic, Middle Keuper, S. Germany), Palaeogeography, Palaeoclimatology, Palaeoecology, 161, 205-227.

Rettig, S. L., Jones, B. F. & Risacher, F. (1980): Geochemical evolution of brines in the salar of Uyuni, Bolivia, Chemical Geology, 30, 57-79.

Risacher, F.& Fritz, B. (1991): Quaternary geochemical evolution of the salars of Uyuni and Coipasa, Central Altiplano, Bolivia, Chemical Geology, 90, 211-231.

Rossignol-Strick, M., Paterne, M., Bassinot, F. C., Emeis, K. C. & De Langes, G. J. (1998): An annual mid-Pleistocene monsoon period over Africa and Asia, Nature, 392, 269-272.

Rouchy, J. M., Taberner, C. & Peryt. T. M. (2001): Sedimentary and diagenetic transitions between carbonates and evaporites (Editorial). - Sedimentary Geology, 140, 1-8.

Roy, A. B. (1988): Stratigraphic and tectonic framework of the Aravalli mountain range. Geol. Soc. India, Mem. 7, 3-31.

Roy, A. B. (1999): Evolution of saline lakes in Rajasthan. Current Science,.76, 290-295.

Roy, P. D. (2001): Sedimentology and geochemistry of the Sambhar playa, Thar desert, Rajasthan, India. M.Tech dissertation (Indian Institute of Technology, Kanpur).

Roy, P. D., Sinha, R. & Smykatz-Kloss, W. (2001): Mineralogy and geochemistry of the evaporitic crust from the hypersaline Sambhar lake playa, Thar desert, India. Chem. der Erde (Geochemistry), 61, 241-253.

Rögner, K., Knabe, K., Roscher, B., Smykatz-Kloss, W. & Zöller, L. (2003): Alluvial loess in the central Sinai: Occurrence, origin, and palaeoclimatological consideration. In: Palaeoecology of Quaternary Drylands, W. Smykatz-Kloss & P. Felix-Henningsen (Eds); Lecture Notes in Earth Sciences, Vol.102, 81-101, Springer-Verlag, Heidelberg.

Saxena, G. M. & Seshadri, T. R. (1966): The origin of salt in Rajasthan (as quoted in Biswas et al. 1982).

Schreiber, B. C. (1998): Sedimentary and diagenetic transitions between carbonates and evaporites.- 15th International Sedimentological Congress, Alicante, 1998, abstract vol.704-705.

Schütt, B. (1998): Reconstruction of palaeoenvironmental conditions by investigation of Holocene playa sediments in the Ebro Basin, Spain: preliminary results. Geomorphology, 23, 273-283.

Schütt, B. (2000): Holocene palaeohydrology of playa lakes in northern and central Spain: a reconstruction based on the mineral composition of lacustrine sediments. Quaternary International, 73/74, 7-27.

Sen, A. K. & Ramalingam, G. (1976): A report on the system at geological mapping of area between Latitude 27° to 27° 30′ to 75° in parts of Nagaur and Sikar districts, Rajasthan. Unpublished Report of Geol. Surv. India, 1975-76.

Sen, D. & Sen, S. (1983): Post neogen tectonics along Aravalli range, Rajasthan, India. Tectono Physics, 93, 75-98.

Shi, Y., Yu, G., Liu, X., Li, B. & Yao, T. (2001): Reconstruction of the 30-40 ka B.P. enhanced Indian monsoon climate based on geological records from Tibetan Plateau. Palaeogeography, Palaeoclimatology, Palaeoecology, 169, 69-83.

Singh, G., Joshi, R. D. & Singh, A. B. (1972): Stratigraphic and radiocarbon evidence for the age and development of three salt lake deposits in Rajasthan, India. Quat. Res. 2 (4) , 496-505.

Singh, G., Joshi, R. D., Chopra, S. K. & Singh, A. B. (1974): Late Quaternary history of vegetation and climate of the Rajasthan desert, India. Phil. Trans. Royal soc. London, 267B, 467-501.

Singh, G., Wasson, R. J. & Agarwal, D. P. (1990): Vegetational and seasonal climatic changes since the last full glacial in the Thar Desert, northwestern India. Review of Palaeobotany and Palynology, 64, 351-358.

Singh, P. & Rajamani, V. (2001): REE geochemistry of recent clastic sediments from the Kaveri floodplain, southern India: Implication to source area weathering and sedimentary processes, Geochimica et Cosmochimica Acta, 65, 3093-3108.

Singh, S. (1988): Geomorphology and management of sand dunes in the great Indian desert. In: Geomorphology and Environment, S. Singh & R. C. Tewari (Eds), The Allahabad Geographical Society, Allahabad, India, 617-629.

Singhvi, A. K. & Kar, A. (1992): Thar Desert in Rajasthan - Land, Man and Environment. Geol. Soc. Ind., 186.

Sinha, R. & Raymahashay, B. C. (2000): Salinity model inferred from two shallow cores at Sambhar lake, Rajasthan. Jour. Geol. Soc. India,.56(2).

Sinha, R. & Smykatz-Kloss, W. (2003): Thermal characterization of lacustrine dolomites from the Sambhar Lake playa, Thar desert, India. Jour. Therm. Anal. Calorimetry, 71, 739-750.

Sinha-Roy, S. (1986): Proceedings of the International Symposium on Neotectonics in south Asia, Dehradun, India, 18-21.

Sinha-Roy, S. (1988): Proterozoic Wilson Cycles in Rajasthan. Geol. Soc. India, Mem. 7, 95-108.

Sirocko, F. (1995): Abrupt change in monsoonal climate: evidence from the geochemical composition of Arabian Sea sediments. Habilitation Thesis, Christian Albrecht Universität, Kiel.

Sirocko, F., Sarnthein, M., Erlenkeuser, H., Lange, H., Arnold, M. & Duplessy, J. C. (1993): Century-scale events in monsoonal climate over the past 24,000 years. Nature, 364, 322-324.

Smykatz-Kloss, W. (1974): Differential Thermal Analysis- Application and Results in Mineralogy. Springer-Verlag, Heidelberg.

Smykatz-Kloss, W., Smykatz-Kloss, B., Naguib, N. & Zöller, L. (2003): The reconstruction of palaeoclimatological changes from mineralogical and geochemical composition of loess and alluvial loess profiles. In: Palaeoecology of Quaternary Drylands, W. Smykatz-Kloss & P. Felix-Henningsen (Eds); Lecture Notes in Earth Sciences, Vol.102, 103-120, Springer-Verlag, Heidelber.

Sundaram, R. M. & Pareek, S. (1995): Quaternary facies and paleoenvironment in north and east of Sambhar lake, Rajasthan. J. Geol. Soc. India, 46, 385-392.

Surdam, R. C. & Eugster, H. P. (1976): Mineral reactions in the sedimentary deposits of the Lake Magadi region, Kenya. Geol. Soc. Amer. Bull. , 87, 1739-1752.

Taylor, S. R. & McLennan, S. M. (1985): The continental crust: its Composition and Evolution, Blackwell, London, 9-50.

Tertian, R. & Claisse, F. (1982): Principle of Quantitative X-Ray Fluorescence Analysis, Heyden & Sons , London.

Thomas, S. G. (1997): Reconstructing ancient arid environments.- In: Arid Zone Geomorphology, S. G. Thomas (Ed), John Willeys & sons, England, 577-607.

Thompson, L. G., Yao, T., Mosley-Thompson, E., Davis, M. E., Henderson, K. A. & Lin, P. N. (2000): A high-resolution millennial record of the south asian monsoon from Himalayan ice cores, Science, 289, 1916-1919.

Tripathi, J. K. & Rajamani, V. (1999): Geochemistry of the loessic sediments on Delhi ridge, eastern Thar desert, Rajasthan: implication for exogenic processes, Chemical Geology, 155, 265-278.

Usdowski, E. & Dietzel, M. (1998): Atlas and Data of Solid –Solution Equilibria of Marine Evaporites. Springer-Verlag, Heidelberg.

Volkova, N. I. (1998): Geochemistry of rare elements in waters and sediments of alkaline lakes in the Sasykkul depression, East Pamirs. Chemical Geology, 147, 265-277.

Wang, Y. J., Cheng, H., Edwards, R. L., An, Z. S., Wu, J. Y., Shen, C. C. & Dorale, J. A. (2001): A high-resolution absolute-dated late Pleistocene Monsoon record from Hulu cave, China. Science, 294, 2345-2348.

Wasson, R. J., Smith, G. I. & Aggarwal, D. P. (1984): Late Quaternary sediments, minerals and inferred geochemical history of Didwana lake. Paleogeo., Paleoclim., Paleoecol., 46 (4), 345-372.

Williams, K. L. (1987): An Introduction to X-Ray Spectrometry, Allen & Unwin, London.

Yadav, D. N. (1997): Oxygen isotope study of evaporating brines in Sambhar Lake, Rajasthan (India). Chemical Geology, 138, 109-118.

10. Appendix

Table1 Distribution of detrital and evaporitic mineralogy on Sambhar playa surface

S.N	Q	Pl	KF	M	Ch	ML	P	Am	Calcite	Dol.	Anhyd.	Thenardite	Halite	Sylvite
1	++++	++	+	+	+				++	+	+	++	++++	
2	+++	+	+	++	++	++	+		++	++	+	+	+++	++
3	++++	++		++	++	+	+	+	++	+	+	+	++++	
4	++++	+	+	+	+		+		++	+	+	++	++++	
5	++++	++		++	+		+		+++			+	++++	
6	++++	++	+	++	++	+	+	+	++	+	+	+	++++	
7	++++	++	+	++	++	+	+	+	++	+	++	+	++++	+
8	++++	+++	+	++	++				++	+	+	+	++++	++
9	++++	+++	+	++	+		+		++	+	+	++	++++	+
10	+++	++	+	++	+	+	+	+	++	+	+	+	++++	
11	++++	++	+	++	+		+	+	+++	+	+	+	++++	
12	++++	+	+	++	+				++	+	+	+	++++	++
13	++++	+	++	+	+	+	+		++	+	+	+	++++	+
14	++++	++	+	+	++		+	+	++		+	++	++++	+
15	++++	++	+	++	+				++	++	++	++	++++	
16	++++	++	++	+	+				++	+	+	++	++++	+
17	+++	++	+	++	++	+	+		++	+	+	+	++++	
18	++++	+++	+	+	+		+	+	++	+	+		++++	++
19	++++	++	+	+	+		+		++	+	++	+	+++	+
20	++++	++	++	++	+				++	+		++	++++	+
21	++++	+++	++	++	+		+	+	++	+	+	+	++++	+
22	++++	++++	+	++	++		+	+	++	+	+	+	++++	
23	++++	++	++	++	+				++	+	+	+	++++	+
24	++++	++	+	++	+	+	+		++	+	+	+	++++	
25	+++	++	+	++	++	++	+		+++	+	++	+	++++	

(Q= quartz, PL= plagioclase, KF= K-feldspar, M= mica, Ch= chlorite, ML= mixed layer, P= palygorskite, Am= amphibole, Dol. = dolomite, Anhyd. = anhydrite) (++++++ = >40%, +++++= 30-40%, ++++= 20-30%, +++= 10-20%, ++= 5-10%, += <5%)

(Traces of carnallite, polyhalite, mirabilite has also been detected from the surface samples of Sambhar playa.)

Table 2 Distribution of detrital and evaporitic mineralogy on Phulera playa surface

Sample	Quartz	Pl	KF	M	Ch	Am	Calcite	Dolomite	Anhydrite	Thenardite	Halite
1	++++++	++++	++++	++	++	+	+++	+	+		+
2	++++++	++++	++++	+	+	+	+++	+	+	+	++
3	++++++	+++	++	+	+	+	++	+	+		+
4	++++++	++++	++	+	+		++			+	+

(KF= K-feldspar, Pl= plagioclase, M= mica, Ch= chlorite, Am= amphibole)
(++++++ = >40%, +++++= 30-40%, ++++= 20-30%, +++= 10-20%, ++= 5-10%, += <5%)

Table 3 Distribution of detrital and evaporitic mineralogy on Kuchaman playa surface

Sample	Quartz	Pl	KF	M	Ch	Am	Calcite	Dolomite	Anhydrite	Gypsum	Thenardite	Halite	Trona
2	++++	+++	++	++	+	+	++	+	+		+	+	
3	++++	++++	++++	+	+	+	++	+	+		++	++++	+
4	+++	++	+	++	+	+	+++	+	+		+		

(KF= K-feldspar, Pl= plagioclase, M= mica, Ch= chlorite, Am= amphibole)
(++++++ = >40%, +++++= 30-40%, ++++= 20-30%, +++= 10-20%, ++= 5-10%, += <5%)

Table 4 Distribution of detrital and evaporitic mineralogy on Sargot playa surface

Sample	Quartz	Pl	KF	M	Ch	Am	Calcite	Dolomite	Anhydrite	Gypsum	Glauberite	Halite	Trona
1a	++++	++++	++	++	+	+	+	+	+		+	++++	
1b	++++	++++	++	++	+	+	++		+		+	++++	

(KF= K-feldspar, Pl= plagioclase, M= mica, Ch= chlorite, Am= amphibole)
(++++++ = >40%, +++++= 30-40%, ++++= 20-30%, +++= 10-20%, ++= 5-10%, += <5%)

Table 5 Distribution of detrital and evaporitic mineralogy on Didwana playa surface

Sample	Quartz	Pl	KF	M	Ch	Am	An	Calcite	Dolomite	Anhydrite	Thanardite	Halite	Trona
1	+++++	+++	++	+	+	+	+	+	+		+	+++++	+
2	++++++	++++	++	+	+	+	+	+		+		+	
3	+++++	+++	+	+	+	+	+	+	+	+	+	++++	+
4	+++++	+++	++	+	+	+	+	+	+	+	++	++++	+
5	++++++	+++	++	+	+	+		+	+	+	+	+++	+
6	++++++	++++	++	+	+	+	+	+	+	+	+	+++	+
7	++++++	+++	++	+	+	+	+	++	+	+	+	++	+
8	++++++	+++	+++	+	+	+	+	+	+	+	+	++	+
9	+++++	++++	+++	+	+	+		+	+	+	+	+++	+
10	++++++	+++	+++	+	+	+		+	+	+	+	++	+
11	++++++	++++	+	+	+	+		+	+	+	+	+++	+
12	++++++	++++	+	+	+	+	+	++		+	+	+++	+
13	++++++	+++	++	+	+	+		+		+	+	+++	+
14	++++++	+++	+	+	+	+		+	+	+		+++	+
15	+++++	+++	+	+	+	+	+	++			+	++++	+
16	+++++	+++	+	+	+	+	+	++	+		++	+++	+
17	+++++	++	+	+	+	+	+	+	+	+	++	+++++	
18	++++++	+++	+	+	+	+	+	+	+	+	+	+++	+
19	++++++	+++	+	+	+	+	+	+	+	+	+	+++	+
20	++++++	++	++	+		+	+	+	+	+	++	++++	+
21	+++++	+++	+	+	+	+	+	+		+	+	+++	+
22	++++++	+++	+	+	+	+	+	+	+	+	+	++	+
23	+++++	+++	++	+	+	+	+	+		+	+	++++	+
24	++++++	+++	+	+	+	+	+	+		+	+	+++	+
25	+++++	+++	++	+	+	+	+	+			+	+++	+
26	+++++	++++	++	+	+	+		+	+	+	+	+++	
27	++++++	++	+++	+	+	+	+	+	+	+	+	+++	+
28	++++++	+++	++	+	+	+	+	+	+		+	+++	
29	++++++	+++	++	+	+	+	+	+			+	+++	+
30	++++++	+++	+++	+	+	+	+	+	+	+	+	+++	
31	++++++	+++	+++	+	+	+	+	+	+		+	+++	

(KF= K-feldspar, Pl= plagioclase, M=mica, Ch= chlorite, Am= amphibole, An= analcime)
(++++++ = >40%, +++++= 30-40%, ++++= 20-30%, +++= 10-20%, ++= 5-10%, += <5%)

Table 6 Distribution of detrital and evaporitic mineralogy on Bap-Malar playa surface

Sample	Quartz	Pl	KF	M	Ch	Am	Calcite $CaCO_3$	Dolomite $CaMg(CO_3)_2$	Anhydrite $CaSO_4$	Gypsum $CaSO_4.2H_2O$	Halite NaCl
1a	++++++	++	++	+	+	+	++	+	+		
1b	++++++	+++	++	+	+	+	++	+	+		
1c	+++	+	+	+	+	+	+	+	+	+	++++++
1d	++++++	+++	+++	+	+	+	++	+	+		

(KF= K-feldspar, Pl= plagioclase, M= mica, Ch= chlorite, Am= amphibole, An= analcime)
(++++++ = >40%, +++++= 30-40%, ++++= 20-30%, +++= 10-20%, ++= 5-10%, += <5%)

Table 7 Distribution of detrital and evaporitic mineralogy on That playa surface

Sample	Depth (cm)	Quartz	Pl	KF	M	Ch	Am	Hematite	Calcite	Dolomite	Anhydrite	Gypsum	Halite
2	0	+++	++	++					+				++++++
3	0	+											++++++
4	0	++++	++	++			+		+				++++++
5	0	+											++++++
6	0	++++	+	+					+			+	++++++
2	10	++++++	+++	++		+	+	+	+	+	+		++
3	10	++++++	+++	+	+	+	+		+	+	+	+	++
4	10	++++++	+++	+	+	+	+	+	+		+	+	++
5	10	++++++	+++	+	+	+	+	+	+		+	+	++
6	10	++++++	+++	+	+	+	+		++		+	++	++

(KF= K-feldspar, Pl= plagioclase, M= mica, Ch= chlorite, Am= amphibole)
(++++++ = >40%, +++++= 30-40%, ++++= 20-30%, +++= 10-20%, ++= 5-10%, += <5%)

Table 8 Distribution of detrital and evaporitic mineralogy on Thob playa surface

Sample	Quartz	KF	Pl	M	Ch	Am	Hematite	Calcite $CaCO_3$	Anhydrite $CaSO_4$	Gypsum $CaSO_4.2H_2O$	Halite NaCl
1	++++++	+	+					+	+	+	+++++
2	++++++	+	+++	+	+	+		++	+	+	++++

(KF= K-feldspar, Pl= plagioclase, M= mica, Ch= chlorite, Am= amphibole)
(++++++ = >40%, +++++= 30-40%, ++++= 20-30%, +++= 10-20%, ++= 5-10%, += <5%)

Table 9 Distribution of detrital and evaporitic mineralogy on Pokhran playa surface

Sample	Quartz	Pl	KF	M	Ch	Am	Hematite	Calcite $CaCO_3$	Dolomite $CaMg(CO_3)_2$	Anhydrite $CaSO_4$	Gypsum $CaSO_4.2H_2O$	Halite NaCl
1	++++++	++	+	+	+		+	++				+++
2	+++	+	+	+	+		+	+		+		++++++
3	++++++	++++		+	+	+		++				+++
4	++++++	+++	+	+	+		+	++	+	+		+++
5	++++++	++	++	+	+	+	+	++			+	++

(KF= K-feldspar, Pl= plagioclase, M= mica, Ch= chlorite, Am= amphibole)
(++++++ = >40%, +++++= 30-40%, ++++= 20-30%, +++= 10-20%, ++= 5-10%, += <5%)

Table 10 Distribution of detrital and evaporitic mineralogy on Pachapadra playa surface

Sample	Quartz	Pl	KF	P	M	Ch	Am	Calcite	Dolomite	Anhydrite	Gypsum	Halite
2	+++++	+++	+		+	+	+	++	+	+		++++
3	++++++	+++	+		+	+	+	+++	+	+		++++
4	+++++	+++	++		+	+	+	++	+	+		++++
5	+++++	++	+		+	+	+	+++	+	+		+++++
6	+++++	+++	+		+	+	+	+++	+	+		++++
7	+++++	++	+		+	+	+	+++	+	+	+	+++++
8	++++	+	+		+	+		++			++	++++++
9	+++++	++	+	+	+	+	+	+++			+	+++++
10	+++++	+	+		+	+	+	+++		+	+	+++++
11	+++++	+	+		+	+	+	+++		+	+	+++++

(KF= K-feldspar, Pl= plagioclase, M= mica, Ch= chlorite, Am= amphibole, P= palygorskite)
(++++++ = >40%, +++++= 30-40%, ++++= 20-30%, +++= 10-20%, ++= 5-10%, += <5%)

Table 11 Chemical composition of plagioclases of Pokhran and Didwana playas

	Pokhran						Didwana		
Composition	Albite	Oligoclase	Oligoclase-andesine	Andesine-labradorite	Labradorite		Albite-oligoclase	Andesine	
SiO_2	67.9	60.9	60.2	57.8	52.6	51.7	62.8	58.2	58.1
TiO_2	0.00	0.0	0.0	0.0	0.1	0.1	0.0	0.0	0.0
Al_2O_3	18.6	23.2	24.2	26.2	27.4	27.7	22.1	24.1	25.3
FeO	0.4	0.0	0.0	0.0	1.2	0.8	0.0	0.3	0.0
MnO	0.00	0.0	0.0	0.2	0.1	0.4	0.0	0.0	0.0
MgO	0.0	0.0	0.00	0.0	0.3	0.0	0.0	1.6	0.0
CaO	0.1	6.0	6.4	9.8	12.5	14.4	3.9	7.8	6.7
Na_2O	13.0	9.4	8.50	5.8	5.1	4.7	10.9	7.4	9.0
K_2O	0.1	0.5	0.6	0.1	0.3	0.2	0.3	0.4	0.3

Table 12 Chemical composition of K-feldspars present in Pokhran and Didwana playas

	Pokhran				Didwana	
Composition	Microcline			Orthoclase	Orthoclase	Adularia
SiO_2	65.5	65.1	64.3	64.6	65.6	65.7
TiO_2	0.4	0.3	0.0	0.7	0.2	0.1
Al_2O_3	18.1	17.7	17.6	18.9	17.9	18.5
FeO	0.0	0.2	0.0	0.0	0.2	0.0
MnO	0.0	0.0	0.0	0.4	0.1	0.2
MgO	0.0	0.0	0.0	0.0	0.2	0.2
CaO	0.3	0.3	0.4	0.3	0.2	0.2
Na_2O	0.8	0.9	0.2	3.1	2.3	1.3
K_2O	14.8	15.3	17.3	11.6	12.9	13.1

Table 13 Chemical compositions of amphiboles of Pokhran and Didwana playas

	Pokhran					Didwana				
Composition	Kaersutite			Gedrite	Hornblende	Tremolite-actinolite			Kaersutite	
SiO_2	42.8	44.7	43.6	38.7	42.3	52.4	49.7	51.7	45.3	46.1
TiO_2	1.4	1.6	1.2	0.2	0.3	0.3	0.8	0.3	0.9	0.9
Al_2O_3	12.7	12.3	15.3	16.5	15.8	8.2	9.2	9.1	9.9	14.3
FeO	19.6	17.1	15.7	24.2	21.4	10.0	10.2	10.0	23.2	15.6
MnO	0.4	0.6	0.0	0.0	0.3	0.2	0.2	0.3	0.8	0.6
MgO	7.4	9.1	8.9	18.7	5.4	14.8	13.9	15.3	6.3	9.2
CaO	12.6	11.4	12.3	0.6	11.2	11.8	14.3	11.0	12.6	9.9
Na_2O	1.4	1.0	1.6	0.0	2.7	0.9	1.1	1.4	1.4	2.6
K_2O	1.7	1.9	1.0	0.8	0.7	0.3	0.3	0.2	1.4	0.5

Table 14 Chemical composition of garnets present in Pokhran and Didwana playas

	Pokhran						Didwana		
Composition	Pyrope-almandine	Almandine			Grossular	Andradite	Almandine	Grossular	Andradite
SiO_2	34.9	37.4	36.5	38.0	37.8	43.4	41.0	38.0	44.4
TiO_2	0.3	0.0	0.0	0.0	0.2	1.1	0.0	0.5	0.8
Al_2O_3	23.1	20.5	20.4	20.4	21.3	14.8	22.3	24.3	14.0
FeO	22.1	37.2	33.4	31.7	14.8	16.1	29.1	9.4	16.9
MnO	0.3	0.8	7.4	1.7	0.5	0.4	0.8	0.2	0.2
MgO	18.6	2.7	1.4	4.3	0.0	8.8	2.2	0.2	8.1
CaO	0.3	1.2	0.8	3.0	24.9	12.6	4.3	27.1	12.5
Na_2O	0.0	0.0	0.0	1.0	0.4	2.2	0.0	0.0	1.5
K_2O	0.2	0.0	0.0	0.0	0.1	0.6	0.1	0.0	0.8

Table 15 Chemical composition of clay minerals from Pokhran and Didwana playas

	Pokhran		Didwana		
	Biotite	Chlorite	Phengite	Illite	Biotite
SiO_2	39.27	30.80	51.00	54.5	39.69
TiO_2	3.53	0.00	1.03	0.33	3.25
Al_2O_3	15.67	23.57	34.33	24.33	15.43
FeO	21.16	25.97	1.36	8.91	20.77
MnO	0.00	0.52	0.00	0.00	0.32
MgO	9.80	18.25	1.53	2.91	10.58
CaO	0.21	0.66	0.00	0.13	0.46
Na_2O	0.00	0.00	0.72	0.00	0.00
K_2O	10.36	0.22	9.88	6.30	9.50
ZrO_2	0.00	0.00	0.00	0.00	0.00

Table 16 Composition of heavy minerals from playa sediments

	Sphene	Zircon	Magnetite	Titano-magnetite	Titano-magnetite	Ilmenite	Rutile	Lawsonite
SiO_2	29.96	35.44	0.48	0.59	1.08	0.26	0.18	39.21
TiO_2	32.32	0.23	0.00	25.28	31.58	54.17	99.23	0.00
Al_2O_3	5.26	0.62	0.30	3.53	1.06	0.22	0.23	29.29
FeO	1.05	1.02	98.03	67.13	61.94	41.99	0.19	5.21
MnO	0.00	0.00	0.00	2.88	3.30	3.05	0.00	0.21
MgO	0.57	0.40	0.20	0.00	0.00	0.00	0.00	0.00
CaO	29.28	0.55	0.15	0.20	0.00	0.19	0.16	26.08
Na_2O	0.57	0.58	0.54	0.00	0.73	0.00	0.00	0.00
K_2O	0.00	0.00	0.31	0.00	0.14	0.00	0.00	0.00
ZrO_2	0.00	58.74	0.00	0.00	0.00	0.00	0.00	0.00

Table17 Composition of epidote and pyroxenes from the Pokhran playa

	Epidote	Epidote-piemontite	Hypersthene	Diopside-augite
SiO_2	39.16	37.15	57.40	45.83
TiO_2	0.13	0.00	0.00	4.04
Al_2O_3	21.32	20.44	0.97	3.40
FeO	14.01	9.88	22.03	15.56
MnO	0.20	15.73	0.86	0.24
MgO	0.00	1.50	17.39	7.20
CaO	24.64	14.96	1.12	21.26
Na_2O	0.00	0.00	0.00	0.95
K_2O	0.00	0.00	0.00	0.17
ZrO_2	0.00	0.00	0.00	0.00

Table 18 major (in mass %) and trace (in ppm) element concentrations in the samples from Sambhar playa surface

Sample	Na_2O	MgO	Al_2O_3	SiO_2	P_2O_5	CaO	K_2O	TiO_2	MnO	Fe_2O_3	Cu	Zn	Br	Rb	Sr	Y	Zr	Ba	La	Ce	Pb
1	1.57	3.54	14.03	48.28	0.22	6.53	2.55	0.62	0.1	5.88	26	56	116	78	301	17	107	219	18	28	14
2	3.89	3.72	14.74	43.82	0.16	5.65	2.55	0.6	0.11	6.71	16	49	110	68	218	12	66	212	17	43	11
3	1.97	3.8	16.3	46.28	0.22	5.62	2.95	0.65	0.12	7.54	38	65	172	102	292	16	85	283	26	50	18
6	2.2	1.63	8.41	67.92	0.07	4.22	1.66	0.36	0.05	2.19	14	30	24	64	214	16	159	317	22	60	9
10	2.38	3.96	12.54	60.56	0.16	3.38	1.92	0.58	0.08	4.21	14	31	192	68	229	13	153	275	28	52	12
12	1.57	3.76	15.32	46.71	0.18	5.88	2.72	0.6	0.11	6.65	21	54	68	81	257	15	89	261	22	53	14
21	1.95	1.8	9.8	74.23	0.11	4.58	1.87	0.71	0.07	2.87	16	34	16	55	192	33	491	246	39	76	12
22	2.11	3.56	13.83	54.99	0.15	6.4	2.45	0.64	0.1	5.58	20	43	153	73	233	17	131	296	23	47	10
24	1.77	2.84	7.99	61.66	0.14	7.68	1.58	0.39	0.05	2.24	17	40	186	75	213	14	125	257	21	55	11
25	2.96	3.33	13.96	39.2	0.15	4.87	2.1	0.52	0.1	5.98	30	61	313	102	252	12	80	258	20	50	11

Table 19 major (in mass %) and trace (in ppm) element concentrations in the samples from Didwana playa surface

Sample	Na_2O	MgO	Al_2O_3	SiO_2	P_2O_5	CaO	K_2O	TiO_2	MnO	Fe_2O_3	Cu	Zn	Br	Rb	Sr	Y	Zr	Ba	La	Ce	Pb
D1	2.72	4.02	12.85	59.37	0.19	5.34	2.59	0.61	0.08	4.79	23	47	70	75	382	20	193	309	38	72	9
D4	2.56	1.77	10.00	73.47	0.14	4.63	1.83	0.54	0.06	2.57	21	32	37	58	378	22	270	309	28	69	9
D6	2.51	1.57	9.77	75.08	0.14	4.63	1.79	0.52	0.05	2.35	18	31	35	62	360	27	328	341	41	89	14
D9	2.34	1.20	8.56	79.48	0.08	4.35	1.63	0.30	0.04	1.33	10	15	68	51	357	14	162	274	26	48	11
D10	2.21	0.92	8.07	81.82	0.10	3.91	1.71	0.28	0.04	1.36	8	17	37	51	294	12	149	303	30	52	7
D12	2.62	1.93	10.18	71.15	0.18	5.38	1.88	0.51	0.05	2.63	13	31	41	63	409	25	274	315	43	81	8
D13	2.40	1.02	8.84	78.42	0.13	4.78	1.55	0.44	0.05	1.69	15	18	30	47	374	21	295	318	47	84	12
D17	2.88	2.53	11.13	65.89	0.16	6.21	2.00	0.55	0.07	3.23	19	32	64	64	371	18	156	269	26	62	8
D19	3.00	1.89	10.21	71.44	0.13	4.97	1.84	0.51	0.06	2.67	16	28	48	61	355	20	220	301	31	70	6
D21	3.10	2.20	10.88	69.88	0.15	5.56	1.98	0.57	0.07	3.05	19	36	38	59	336	16	158	286	30	66	6
D23	2.77	1.74	10.13	71.77	0.12	4.52	1.89	0.46	0.05	2.43	12	33	45	62	371	21	207	306	46	80	11
D24	2.63	1.31	9.61	76.25	0.12	4.64	1.70	0.48	0.05	2.05	15	27	25	58	368	24	264	348	43	79	10
D25	2.52	1.33	9.33	77.31	0.11	4.39	1.78	0.45	0.05	2.07	14	27	40	60	354	21	251	326	27	69	7
D26	2.71	1.68	9.52	73.61	0.12	4.92	1.81	0.44	0.05	2.33	13	32	42	58	384	18	195	300	35	69	11
D27	2.72	1.44	9.54	74.89	0.14	4.74	1.67	0.55	0.06	2.36	13	25	46	56	301	21	265	320	45	71	9
D28	2.35	1.36	9.30	76.27	0.13	4.62	1.74	0.51	0.06	2.28	11	26	49	59	308	22	279	324	47	75	6
D29	2.54	1.52	9.78	73.71	0.18	5.27	1.79	0.55	0.06	2.42	17	36	46	63	381	24	315	338	36	88	10
D30	2.36	1.33	8.92	76.54	0.11	4.66	1.71	0.39	0.05	1.85	12	26	88	66	415	19	215	329	33	62	7
D31	2.48	1.85	9.25	73.10	0.13	5.31	1.78	0.38	0.05	2.03	11	25	75	63	434	16	158	309	31	52	7

Table 20 Concentration of rare eath elements in the Thar playa sediments

Playas	Sample	La	Ce	Pr	Nd	Sm	Eu	Gd	Tb	Dy	Ho	Er	Tm	Yb	Lu
Didwana	D1	32.43	64.95	6.90	23.84	4.96	0.90	3.82	0.50	2.93	0.45	1.44	0.17	1.14	0.15
	D1-5	29.26	59.97	5.92	22.12	4.87	0.94	3.71	0.54	3.24	0.50	1.54	0.18	1.24	0.17
Kuchaman	K3	25.81	51.98	5.20	18.07	4.02	0.76	2.95	0.44	2.56	0.41	1.20	0.15	1.02	0.14
Phulera	P3	26.59	52.59	5.61	19.56	4.06	0.80	3.04	0.43	2.69	0.44	1.31	0.16	1.13	0.15
	P3-7	22.15	43.13	4.84	16.63	3.42	0.65	2.61	0.39	2.34	0.40	1.14	0.15	1.02	0.14
	P3-7*	17.45	45.35	4.51	17.15	2.99	0.48	2.04	0.28	1.84	0.37	1.00	0.15	1.15	0.15
Sambhar	S2	15.09	31.54	3.24	11.44	2.45	0.46	1.90	0.29	1.72	0.29	0.85	0.11	0.73	0.10
	S2-4	16.55	42.04	4.66	16.55	3.38	0.59	2.49	0.36	2.21	0.37	1.11	0.14	0.94	0.13
Bap-Malar	Bap I-4A	39.46	67.11	8.05	28.29	5.23	0.87	3.78	0.53	3.51	0.64	1.72	0.23	1.68	0.22
	Bap I-4D	20.88	46.49	4.90	18.16	3.52	0.63	2.73	0.40	2.63	0.51	1.33	0.19	1.42	0.19
Pokhran	PokI-6A	34.19	72.75	8.52	31.07	6.52	1.07	4.84	0.68	4.98	0.94	2.33	0.35	2.63	0.33
	PokI-6D	16.24	37.68	3.98	14.91	2.88	0.47	2.16	0.30	2.07	0.41	1.01	0.16	1.10	0.15
	PokI-6G	45.83	91.82	10.25	37.73	7.67	1.16	5.72	0.78	5.69	1.08	2.51	0.41	3.02	0.40
	PokI-6L	24.32	53.04	5.72	20.75	4.10	0.69	2.98	0.44	3.10	0.62	1.41	0.23	1.67	0.23
Pachapadra	Pach I-1A	42.32	85.63	9.23	34.04	6.27	1.05	4.51	0.67	4.73	0.90	2.03	0.33	2.29	0.31
	Pach I-1G	42.73	95.68	9.99	36.86	6.70	1.09	4.87	0.71	4.94	0.94	2.27	0.35	2.47	0.33
Thob	Thob I-1	32.92	62.95	7.35	26.20	5.09	0.69	3.27	0.47	3.33	0.62	1.40	0.22	1.59	0.21
That	That I-5A	3.39	6.98	0.73	2.65	0.53	0.06	0.28	0.04	0.30	0.07	0.11	0.02	0.13	0.02
	That I-5B	36.16	72.54	7.81	27.35	5.40	0.90	3.42	0.47	3.32	0.64	1.53	0.22	1.60	0.21

List of tables

List of figures